北京交通大學

硕 士 学 位 论 文

基于深度学习微波和毫米波频段雨衰预测模型

Deep Learning Based Rain Attenuation prediction modeling for Microwave and mmWave Band

作者：

导师：

北京交通大学

2024 年 4 月

学位论文版权使用授权书

本学位论文作者完全了解北京交通大学有关保留、使用学位论文的规定。特授权北京交通大学可以将学位论文的全部或部分内容编入有关数据库进行检索，提供阅览服务，并采用影印、缩印或扫描等复制手段保存、汇编以供查阅和借阅。同意学校向国家有关部门或机构送交论文的复印件和磁盘。学校可以为存在馆际合作关系的兄弟高校用户提供文献传递服务和交换服务。

（保密的学位论文在解密后适用本授权说明）

学位论文作者签名：　　导师签名：

签字日期：　　年　　月　　日　　签字日期：　　年　　月　　日

学校代码：10004　　密级：公开

北京交通大学

硕 士 学 位 论 文

基于深度学习微波和毫米波频段雨衰预测模型

Deep Learning Based Rain Attenuation prediction modeling for Microwave and mmWave Band

作者姓名：　　学　　号：

导师姓名：　　职　　称：

学位类别：工学　　学位级别：硕士

学科专业：信息与通信工程　　研究方向：宽带无线通信

北京交通大学

2024 年 4 月

致谢

Acknowledgement

摘要

为了寻求高速可靠的无线通信系统，研究人员和网络设计人员越来越多地转向微波和毫米波（mmWave）频段。这些较高的频率范围提供了巨大的传输容量和信道能力，这在低频拥塞、带宽需求激增的时代是必不可少的。然而，在这些频率上运行的无线电通信系统的可靠性很容易受到各种气候因素的影响，其中降水是造成损害的主要原因。雨水衰减，尤其是热带气候下 7 GHz 和 10 GHz 的雨水衰减，会导致信号减弱和链路可达性降低，给微波系统的设计带来严峻挑战。

本论文旨在解决埃塞俄比亚对精确雨衰预测的迫切需求，当地的数据驱动设计在很大程度上仍未得到开发。论文对微波和毫米波（mmWave）波段的雨衰减预测建模进行了广泛研究，重点关注深度学习方法。论文进行了全面的文献综述，包括各种研究文章、会议、论文和 ITU-R 报告，以分析现有方法并总结其成果。该研究深入探讨了无线电波传播，研究了大气损伤和传播机制，并深入分析了用于时间序列预测的深度学习技术，包括卷积神经网络（CNN）和循环神经网络（RNN）。

数据收集自埃塞俄比亚的国家计量局（National Metrology Agency of Ethiopia），并以相关研究的微波数据作为补充。随后进行了详细的预处理，以确定设计雨衰减预测深度学习模型的关键参数。该模型利用 ITU-R 建议，特别是 ITU-R P.530、P.618、P.837 和 P.838，得出方程、公式和系数。

论文介绍了一种新方法，利用温带地区的回归系数，将较长积分时间的降雨率累积分布转换为一分钟积分时间。具体衰减采用 ITU-R P.838-3 方法确定，路径衰减根据 ITU-R P.530 模型计算。由此得出的公式包含了降雨率、温度、相对湿度和其他大气条件对信号衰减的影响。

最后，编制了一个涵盖八年时间的综合数据集，用于训练长短期记忆（LSTM）预测模型。该模型经过了严格的测试和验证，证明其能够根据三小时的历史数据预测下一小时的路径衰减。它的表现优于其他深度学习模型，实现了 0.053 的最小平均绝对误差，标志着雨衰减预测领域的重大进步。

关键词：微波毫米波频段；雨衰预测；深度学习；长短期记忆网络；时间序列

ABSTRUCT

In the quest for high-speed and reliable wireless communication systems, researchers and network designers are increasingly turning to the microwave and millimeter wave (mmWave) bands. These higher frequency ranges offer vast transmission capacities and channel capabilities, essential in an era where lower frequencies are congested and demand for bandwidth is soaring. However, the reliability of radio communication systems operating at these frequencies is susceptible to various climatic factors, with precipitation being a predominant cause of impairment. Rain attenuation, particularly over 7 GHz and 10 GHz in tropical climates, leads to signal weakening and reduced link accessibility, presenting a critical challenge in the design of microwave systems.

This thesis addresses the pressing need for precise rain attenuation prediction in the Ethiopian context, where local data-driven design remains largely unexplored. The thesis presents an extensive investigation into rain attenuation prediction modeling for microwave and millimeter wave (mmWave) bands, with a focus on deep learning methodologies. A thorough literature review was conducted, encompassing various research articles, conferences, theses, and ITU-R reports, to analyze existing methodologies and summarize their outcomes. The study delves into radio wave propagation, examining atmospheric impairments and propagation mechanisms, alongside an in-depth analysis of deep learning techniques for time series prediction, including Convolutional Neural Networks (CNNs) and Recurrent Neural Networks (RNNs).

Data was collected from the National Metrology Agency of Ethiopia and supplemented with microwave data from related research. This was followed by detailed preprocessing to define critical parameters for designing a deep learning model for rain attenuation prediction. The model leverages ITU-R recommendations, particularly ITU-R P.530, P.618, P.837, and P.838, to derive equations, formulations, and coefficients.

The thesis introduces a novel approach to convert cumulative distributions of rainfall rates for longer integration times to a one-minute integration time, utilizing regression coefficients for temperate regions. Specific attenuation was determined using the ITU-R P.838-3 method, and path attenuation was calculated based on the ITU-R P.530 model. The resulting formulas incorporate the effects of rainfall rate, temperature, relative

humidity, and other atmospheric conditions on signal attenuation.

Finally, a comprehensive dataset was compiled, covering an eight-year period, to train a Long Short-Term Memory (LSTM) prediction model. The model was rigorously tested and validated, demonstrating its capability to predict path attenuation for the next hour based on three hours of historical data. It outperformed other deep learning models, achieving a minimum mean absolute error of 0.053, marking a significant advancement in the field of rain attenuation prediction.

KEYWORDS： Microwave and mmWave frequency band; Rainfall attenuation prediction; Deep learning; Long short-term memory network (LSTM); Time Series

序言

这篇论文是一项学术追求，始于对面对自然的不可预测性时无线通信的复杂性的好奇。这是对微波和毫米波波段领域的探索，它们是现代追求高速可靠无线通信系统的关键。这项研究的历程植根于降雨衰减带来的挑战，降雨衰减是埃塞俄比亚等热带气候中信号完整性的重要障碍。

这项研究的起源在于认识到电信领域的一个关键差距：需要根据当地数据建立精确的降雨衰减预测模型。主要想法是利用深度学习的潜力来解决这一差距，提供一种更准确地预测降雨衰减的新方法。这项研究的目的超越了学术好奇心；它旨在为在气候条件会严重影响信号传播的地区提高通信系统的可靠性提供实用的解决方案。

这项工作的意义是多方面的。它有助于电信领域的知识体系，特别是在发展中国家的情况下。它还可以作为未来研究的灯塔，有可能影响全球无线通信系统的设计和运行。

本文的方法论以细致的数据收集、预处理和模型设计为特点。它遵循学术严谨的最高标准，利用 ITU-R 的建议推导出构成预测模型支柱的方程和系数。

在编写这篇论文时，遵循了一套文体规则，确保了论文的清晰、连贯和学术完整性。该研究以该领域的专家和对该主题普遍感兴趣的人都可以访问的方式进行介绍。

在整个研究过程中，我们考虑了对相关问题的评论和意见，全面了解了降雨衰减预测的挑战和机遇。

最后，这篇序言介绍了在接下来的几页中展开的发现之旅。这是邀请读者深入研究一项既及时又重要的研究，在这个时代，技术和环境的融合塑造了我们的连接结构。

Preface

This thesis is a scholarly pursuit that began with a curiosity about the intricacies of wireless communication in the face of nature's unpredictability. It is an exploration into the realm of microwave and mmWave bands, which are pivotal in the modern quest for high-speed and reliable wireless communication systems. The journey of this research is rooted in the challenges posed by rain attenuation, a significant barrier to signal integrity in tropical climates like Ethiopia.

The origin of this study lies in the recognition of a critical gap in the field of telecommunications: the need for precise rain attenuation prediction models that are informed by local data. The main idea was to harness the potential of deep learning to address this gap, providing a novel approach to predict rain attenuation more accurately. The purpose of this research extends beyond academic curiosity; it aims to offer practical solutions to enhance the reliability of communication systems in regions where climatic conditions can severely impact signal propagation.

The significance of this work is manifold. It contributes to the body of knowledge in the field of telecommunications, particularly in the context of developing countries. It also serves as a beacon for future research, potentially influencing the design and operation of wireless communication systems worldwide.

The methodology of this thesis is characterized by a meticulous approach to data collection, preprocessing, and model design. It adheres to the highest standards of academic rigor, leveraging ITU-R recommendations to derive equations and coefficients that form the backbone of the predictive model.

In compiling this thesis, a set of stylistic rules were adhered to, ensuring clarity, coherence, and academic integrity. The research is presented in a manner that is accessible to both experts in the field and those with a general interest in the subject matter.

Comments and opinions on related problems have been considered throughout the research process, providing a comprehensive view of the challenges and opportunities in rain attenuation prediction.

In conclusion, this preface serves as an introduction to the journey of discovery that unfolds within the following pages. It is an invitation to the reader to delve into a study that is as timely as it is significant, in an age where the fusion of technology and environment shapes the very fabric of our connectivity.

目录

Table of Contents

致谢 ii
Acknowledgement iii
摘要 iv
ABSTRUCT v
序言 vii
Preface viii
1 Introduction 1
1.1 Background 1
1.2 Statement of The Problem 3
1.3 Objectives 4
1.3.1 General Objective 4
1.3.2 Specific Objectives 4
1.4 Scope and Limitation 4
1.4.1 Scope 4
1.4.2 Limitation 5
1.5 Literature Review 5
1.6 Methodology 7
1.7 Contribution of The Thesis 9
1.8 Organization of the Thesis 9
2 Radio Wave Propagation 11
2.1 The Earth's Atmosphere 11
2.2 Radio Wave Propagation Through Atmosphere 12
2.3 Diffraction 13
2.3.1 Reflection 13
2.3.2 Scattering 14
2.4 Tropospheric Effects on Radio Waves Propagation 15
2.5 Effects of Rainfall, Temperature and Humidity on Radio Waves 16
2.5.1 Effects of Rainfall on Radio Waves 16
2.5.2 Effects of Temperature and Humidity on Radio Waves 17

2.5.3 The Common Effect of Rain, Temprature and humidity 19
2.6 The Link Budget and the Medium Loss 20
2.6.1 The Medium Loss 21
2.7 Summary 22
3 Deep Learning for Time Series Prediction 23
3.1 Introduction 23
3.1.1 Catagorization of Time Series Data 24
3.2 Mathematical Explanation of Time Series Data 24
3.3 Deep Learning vs Conventional Method Time Series Analysis 25
3.4 Time Series Prediction 27
3.5 Summary 29
4 Data Collection, Preprocessing and Modeling 30
4.1 Introduction 30
4.2 Geography and Climate of Ethiopia 30
4.3 Visualization of Collected data 34
4.3.1 Metrological Data 34
4.3.2 Microwave and mmWave link data 36
4.4 ITU-R Rain Attenuation Models 38
4.4.1 ITU-R P.530 Model 38
4.4.2 ITU-R P.618 Model 40
4.4.3 ITU-R P.837 Model 43
4.4.4 ITU-R P.838 Model 45
4.4.5 ITU-R P.839 Model 48
4.5 Data Processing for Rain Attenuation Modeling 48
4.5.1 Determination of Rain Rate $R0.01$ 50
4.5.2 Conversion of 15-min to 1-min Rainfall Rate Distribution 52
4.5.3 Determination of Specific Attenuation 53
4.5.4 Determination of Rainfall Attenuation 55
4.6 Rain Attenutaion Prediction Modeling Using LSTM 57
4.6.1 The Long Short Time Memory (LSTM) Prediction Model 57
4.6.2 LSTM Based Rain Attenuation Prediction Model 60
4.6.3 Model Implementation in Python 60
4.7 Summary 70
5 Result and Discussions 71

5.1 Introduction 71
5.2 Rain Rate Analysis 71
5.3 Analysis of Rainfall Rate $R0.01$ 73
5.4 Conversion of Rain Rate Time Integration 74
5.5 Specific Attenuation Determination and Achieved Result 76
5.6 Rain Attenuation Determination and Achived Results 77
5.7 The LSTM Prediction Model and Achied Results 79
5.8 Summary 87
6 Conclution and Recommendations 88
6.1 Conclusion 88
6.2 Recommendations 88
参考文献 90
References 90
独创性声明 94

图目录

List of Figures

Figure 1-1 Framework of Research Methodology 8
Figure 1-2 Thesis organization 10
Figure 2-1 Common types of radio waves in wireless communication 12
Figure 2-2 Difraction and Reflcation of Radio Wave due to Rain 14
Figure 2-3 Scatering of radio wave signals by rain 15
Figure 2-4 Temperature profile (Temperature vs Height) of Atmospheric layer 18
Figure 2-5 Humidity profile (Specific Humidity vs Height) of Atmospheric layer 19
Figure 3-1 Key areas of time series data involvement 23
Figure 3-2 Developmental trajectories of various technologies 27
Figure 4-1 Map of Ethiopia (source:[74]) 31
Figure 4-2 Annual rainfall distribution and Köppen climate of Ethiopia 33
Figure 4-3 Köppen climate classification in Ethiopia 33
Figure 4-4 15-min rainfall, humidity, and temperature of Addis Ababa city 34
Figure 4-5 15-min rainfall, humidity, and temperature of AlemKetema city 34
Figure 4-6 15-min rainfall, humidity, and temperature of Nekemt city 35
Figure 4-7 15-min rainfall, humidity, and temperature for Mekele city 35
Figure 4-8 15-min rainfall, humidity, and temperature for Combolcha city 35
Figure 4-9 15-min rainfall, humidity, and temperature for DireDewa city 35
Figure 4-10 3D visualization of rain rate(mm/hr) for above cites 36
Figure 4-11 Typical LOS microwave connecting Addis Ababa & Furi 37
Figure 4-12 kH and aH Coefficients for Horizontal Polarization 47
Figure 4-13 8-years rain rate visualization of Addis Ababa 49
Figure 4-14 Chaining Structure of RNN vs LSTM 58
Figure 4-15 LSTM cell architecture with formulas 59
Figure 4-16 Schematic diagram of proposed LSTM model 60
Figure 4-17 Code flowchart of LSTM model 62
Figure 5-1 Rain Rate in mm/hr for Addis Ababa City 72
Figure 5-2 PDF, CDF and CCDF illustration 73
Figure 5-3 $R0.01$ of 15-min integration time for Addis Ababa City 74

Figure 5-4 15-min Rain Rate and 1-min Rain Rate Plotting 75
Figure 5-5 Specific Attenuation at 15-minute and 1-minute time integration..... 76
Figure 5-6 lotting of rain rate dependent effective path length for 15-min and 1-min 78
Figure 5-7 Total path attenuation due to rain for 15-min and 1-min rain rate 78
Figure 5-8 Training data visualization of the LSTM model 80
Figure 5-9 Data visualization for year 2014 81
Figure 5-10 Statistical analysis of observed datasets..... 81
Figure 5-11 Visualization of normalized A0.01(dB)1-min 82
Figure 5-12 Visualization of A0.01(dB)15-min rain attenuation..... 82
Figure 5-13 Visualization of normalized rain rate and temperature parameters..... 83
Figure 5-14 Baseline prediction..... 83
Figure 5-15 Linear model prediction 84
Figure 5-16 CNN Prediction Model 85
Figure 5-17 LSTM-based prediction of rain attenuation A0.01(dB) 86

表格目录

List of Tables

Table 4-1 Annual Rainfall in mm and their Köppen Class of Some Cities 32
Table 4-2 Microwave link profile Addis Ababa to Furi Link Link[42] 37
Table 4-3 cofficient for kH, kV, aH and aV 46
Table 4-4 Sample Processed $R0.01$Data 51
Table 4-5 Sample Processed Data of $R1p$ 53
Table 4-6 kH, kv, aH, and av value of 11 GHz 54
Table 4-7 Sample Processed Specific Attenuation Data 55

1 Introduction

1.1 Background

In-depth investigations into the effects of precipitation on terrestrial communication paths within the microwave and millimeter wavebands have seen a surge in recent years. This surge is largely attributed to the saturation of lower microwave frequencies and the burgeoning demand for communication channels capable of supporting higher data capacities. The microwave and millimeter wave frequency spectrums are increasingly being recognized as critical by service providers and network architects due to their unparalleled ability to carry vast amounts of data. This capability aligns with the escalating requirements of end-users for wireless communication systems that offer robust and rapid data transfer. These frequency bands are anticipated to deliver expansive bandwidths, which are pivotal for the advancement of network performances. Such enhancements are particularly vital in scenarios that demand high-speed data transfer and the seamless streaming of video content, ensuring that end-users experience superior quality of service. However, the propagation of waves, particularly within the microwave and millimeter bands, is subject to a diverse array of environmental influences such as rainfall, which causes scattering, absorbtion or diffraction fading. Diffraction fading arises when the waves encounter multiple pathways due to obstructions in the environment, leading to a complex pattern of interference that can weaken the signal's strength. Collectively, these factors contribute to a degradation of the wave's integrity, manifesting as signal fading, which poses challenges for maintaining the clarity and reliability of communication signals within these specific frequency bands,[1-4]. Within the array of environmental elements that influence signal propagation, rainfall stands out as a significant contributor to signal attenuation, which is the diminishment of signal strength. This attenuation often leads to disruptions in network connectivity, particularly within the microwave and millimeter wave frequency bands. The presence and intensity of rainfall can severely impact the reliability and performance of communication systems operating at these frequencies[5-7]. In temperate climates, radio frequency (RF) communication systems can operate at frequencies up to approximately 10 GHz before experiencing significant degradation due to precipitation. However, in tropical and certain central climates, the threshold for such interference drops to nearly 7 GHz. This is

primarily because the raindrops in these regions are larger compared to those in temperate climates. The size of the raindrops is a critical factor, as larger raindrops can absorb and scatter the RF signals more effectively, leading to what is known as rain fade. This phenomenon results in a critical rate of signal attenuation, which can disrupt communication[8, 9]. Therefore, accurate, and detailed data on rainfall rates are essential in the design of terrestrial line-of-sight communication systems operating at microwave and millimeter wavelengths.

An appropriate parameter for calculating rain attenuation along radio paths is empirically determined through link measurements or predicted from localized precipitation rates, drop-size distribution, and other factors. This empirical approach allows for a more accurate assessment of the impact of rain on signal propagation, which is crucial for designing reliable communication systems in various climates.

The study of atmospheric-induced effects, especially rain-induced effect, on radio wave propagation have been a topic for several decades, such as the studies in [4, 6, 8-14] [15] are some of the earliest studies and the studies in [1, 4, 7, 11, 13, 16-24] are some of the studies that have been their during 2010th. Most of those researches proposed the conventional empirical or physical models which are based on observed data and the fundamental physics of signal interaction with precipitation. Recent studies such as the studies in [25-30] proposed AI-based models.

The conventional models provide a solid foundation for understanding rain attenuation, they often require extensive localized data and may not account for all variables influencing signal degradation. Their predictive accuracy can be limited by the assumptions they make and their inability to adapt to changing environmental conditions[28]. AI-based models on the other hand, particularly those of which implement machine learning and deep learning techniques can process large datasets, identify complex patterns, and improve their predictions over time, bringing a significant advancement in rain attenuation prediction modeling. They are capable of handling non-linear relationships and multiple interacting variables, which are common in atmospheric phenomena. AI-models can also generalize better across different geographic locations and conditions, providing more accurate forecasts even with limited local data[28, 31, 32].

Indeed, while the application of AI models in predicting atmospheric-induced attenuation is a burgeoning field, the number of global research studies utilizing these techniques remains relatively small, especially in tropical countries such as Ethiopia, where rain have

significant impact on signal propagation. The model presented in this research aims to fill this gap by adopting deep learning model, which focus on utilizing local data including rain rate, relative humidity, and temperature to better predict rain attenuation for terrestrial microwave and millimeter bands in the region and assist as a reference for future studies implementing similar models.

In Ethiopia, as in many other countries in Africa, rain rate statistics are poorly documented. Thus, microwave and millimeter wave links are mainly designed based on prediction value. In this sense, accurate prediction of atmospheric factors affecting those link performance is necessary. For this study, rainfall rate, relative humidity and temperature statistics of 8 years have been collected from Ethiopian National Meteorological Agency (ENMA) for 15 main sites in Ethiopia. Those data are recorded in time series fashion of every 15 minutes for the whole period. Microwave and millimeter wave link information of some sites such as Addis Ababa-Furi site, Addis Ababa-Adama west site, Jima-Agaro site has been taken. Rain attenuation values of for those sites has been studied carefully using Recommendation ITU-R P.530, Recommendation ITU-R P.838-3 and other research articles that have been carried on those sites previously and corresponding historical rain attenuation value in dB has generated for the period of 8 years.

1.2 Statement of The Problem

In designing of microwave and mmWave links, the attenuation induced by environmental atmospheric factors have to be analyzed properly so that reliable network between transmitting and receiving end could be achieved[33]. Attenuation effects of primary atmospheric parameters like rain, temperature, and humidity are the main cause of attenuation over those links[34]. The ITU-R database, which is widely used for microwave and mmWave link design, indeed originates from data primarily collected in Temperate regions. This poses a challenge when applying the same parameters to Tropical regions like Ethiopia, where atmospheric conditions differ significantly as the ITU-R parameters may not accurately reflect the local environmental conditions[35, 36]. The need for reliable research based on local data in tropical countries for microwave and millimeter-wave (mmWave) link designing is indeed a significant gap in the field. The gap in AI-assisted research using local data in tropical regions like Ethiopia is a significant issue. While other regions may have advanced in applying AI techniques to atmospheric

studies, tropical regions have not yet fully leveraged local data for AI-based rain attenuation prediction models. This research aims to fill this void by developing deep learning models that utilize local atmospheric data to predict rain attenuation more accurately. Such an approach could lead to a better understanding of the impact of tropical climates on communication systems and provide more reliable data for designing microwave and mmWave links in these regions[37, 38]. By focusing on local data and advanced AI techniques, this research could significantly contribute to the field and help tropical regions catch up with their counterparts in terms of technological advancements in atmospheric research.

1.3 Objectives

1.3.1 General Objective

The general objective of this research is introducing deep learning models in rain attenuation prediction and modeling using local data for microwave and mmWave links and fill the research gap in adopting AI-models in the location of interest.

1.3.2 Specific Objectives

- Investigate the integral effect of rain, temperature, and humidity on signal degradation of microwave and mmWave band.
- Develop a novel AI-assisted rain attenuation prediction model for microwave and mmWave band.
- Develop a software to predict the rain attenuation exceeded for 0.01% of the time for diverse climatic zones.
- Estimating and analyzing the most accurate and exact rain attenuation prediction model for microwave and mmWave band using deep learning technique

1.4 Scope and Limitation

1.4.1 Scope

This thesis works mainly focus on applying deep Learning model in prediction of rain

attenuation over the microwave and mmWave links by utilizing the historically recorded local metrological data and the ITU-R recommendation models, mainly Recommendation ITU-R P.676 & Recommendation ITU-R P.838 in computing the corresponding specific rain attenuation in dB/km and in dB. The thesis also only considers the horizontal polarization of the selected links, where only the horizontal value of the Frequency-dependent coefficients or sometimes called "regression coefficient" has been utilized.

1.4.2 Limitation

This study is limited to only using the actual metrological data such that the rain rate in mm/15-min, temperature in °C/15-min and relative humidity collected from the Ethiopian National Meteorological Agency (ENMA). Historical received signal level (RSL) value in dB for each selected links should have to be obtained for the deep learning model for better accuracy but those data have not been available. Mathematically generated attenuation value in dB has been utilized instead, where there might be some inaccuracy in the data utilized by the deep learning algorithm.

1.5 Literature Review

Historically, Rain attenuation prediction modeling for microwave and mmWave frequency band has been studied by several authors. Several prediction models have proposed by different authors. The study in [39] presents a comprehensive review on computational intelligence-based techniques for analysis and prediction of rain attenuation and proposed a machine learning-based model which utilizes regression analysis to determine the values of the regression coefficients κ and α for various frequencies, which are traditionally challenging to calculate. The proposed model requires only the frequency in GHz and the rain rate in mm/h as inputs and has demonstrated an impressive accuracy of 97%. The paper in [29] highlights the limitations of traditional empirical, statistical, and fade slope models, which require statistical measurements of rain characteristics and are not easily generalizable, proposes a deep learning-based architecture to achieve accurate predictions for both near and long-term rain fade events using satellite and radar imagery data and link power measurements. The study demonstrates that the model outperforms existing machine learning algorithms and suggests that radar data is more effective for short-term predictions, while satellite data is

better for long-term forecasts. The research in [30] proposes a probabilistic model using a Deep Neural Network (DNN) to predict rain attenuation. The model is built upon data from the ITU-R and uses rainfall data from Oyo State, Nigeria, spanning seven years. The DNN model aims to eliminate the need for complex mathematical models and instead uses rainfall features to predict attenuation. The results show an RMSE of 0.21 and a Loss of 0.021 at 100 epochs, with a Pearson's linear correlation of 0.7172, indicating a strong similarity between predicted and observed values. The model efficiency index n_t shows a value of 0.1744, providing near acceptable results, and concluding that the DNN model predicts rain attenuation more effectively compared to the ITU-R model. Another study by S. N. Livieratos and P. G. Cottis, in [25], published in IEEE Access, introduces a novel prediction method for rain attenuation on terrestrial millimeter wave links. The proposed method combines Supervised Machine Learning (SML) with Gaussian Processes (GPs) for regression, utilizing a dataset from the ITU-R databank that includes 12 predictors such as path length, operation frequency, wave polarization, and rain rate levels. Initially, the SML algorithm's predictions were not more accurate than the ITU-R model. However, after incorporating the ITU-R model's estimates as an additional predictor, the enhanced SML algorithm significantly improved its predictive accuracy. The study concludes that the enhanced SML method outperforms existing models and is globally applicable, with potential for further refinement for specific locations and conditions through tailored training datasets. The study in [40] also presents an AI model that predicts and mitigates rain-induced attenuation in satellite communications. The model employs three AI algorithms and a novel 3D antenna design, focusing on optimizing channel quality in the UAE. It utilizes a new database of rain-induced attenuation, analyzing various parameters for different modulation schemes. The study concludes with a smart antenna design using frequency diversity to mitigate rain fade, showing significant variation in rain-induced attenuation based on rainfall rate and frequency, and demonstrating the model's predictive capabilities for enhancing satellite communication reliability. A research in [41] proposed a Long-Short Term Memory (LSTM) network method, a deep learning algorithm adept at handling time-series data, for predicting rain attenuation events in satellite communications. To overcome the absence of a rainfall database, the authors created a synthetic rain attenuation database following the ITU-R's guidelines. The LSTM model was trained with this data, and the best model achieved an accuracy of 91.88%, outperforming the external best model's accuracy of 87.99%. This method shows promise for enhancing satellite network performance by predicting rain attenuation events. A

research work in [26] by M. M. N. Ahuna, T. J. Afullo, and A. A. Alonge explores the use of a Backpropagation Neural Network (BPNN) to predict rain attenuation for satellite communication links. The BPNN was trained on rainfall data collected from 2013 to 2016 at the University of KwaZulu-Natal, Durban, using a disdrometer with a 30-second sampling time. The model was validated with data representing all four seasons from January 2017 to May 2018. The results showed that the BPNN could predict rain attenuation with a high degree of accuracy, as indicated by a correlation coefficient of 0.8298. The model's predictions were closely aligned with actual measurements and the ITU-R model for rain rates up to 0.01% of an average year. Additionally, the study confirmed the model's portability by successfully applying it to rainfall data from Butare, Rwanda, suggesting its adaptability to different geographical climates

In conclusion, the exploration of deep learning-based rain attenuation prediction models for microwave and millimeter-wave (mmWave) bands has revealed significant advancements in the field. The studies reviewed demonstrate the efficacy of various deep learning architectures, such as Backpropagation Neural Networks (BPNN) and Long-Short Term Memory (LSTM) networks, in accurately forecasting rain-induced signal attenuation. These models, trained on extensive datasets from diverse geographical locations, have shown a high degree of accuracy and adaptability, outperforming traditional prediction methods and the ITU-R model in some cases. The integration of AI algorithms with detailed rain rate databases and the consideration of wet antenna effects have further enhanced the precision of these models. The collective findings underscore the potential of deep learning techniques to revolutionize the prediction and mitigation of rain attenuation, thereby bolstering the reliability of satellite and terrestrial communication systems operating within the microwave and mmWave frequency bands.

1.6 Methodology

This study has made the ITU-R rain attenuation models as it's fundamental concept. Eventhough, those models are statistical or empirical nature, they play a great role in determining the formulation of atmospheric induced rain attenuation, specifically, rain attenuation. The methodology of this study is presented as follow;

- The study first conducts an indepth explorations about rain attenuation prediction modeling in the background and literature review section in orderto clearly undertstand the purpose of the research and familiarize with available related research

works and then identify the necessary data.

- The study then furthure explains conceptual understandings of radio wave propagations and deep learning technology in detail.
- Metrological data collection from Ethiopian national meteorological agency (ENMA) and microwave link profile from related previous study using similar data (from [42]).
- An indepth analysis of existing ITU-R rain attenuation models were conducted.
- Then the statistical data analysis, preprocessing and modelling using MS-Excel, OrigioPro, Matlab and Python using jupernotebook were performed.
- LSTM based rain attenuation prediction model was developed to predict the rain attenuation using the preprocessed data.

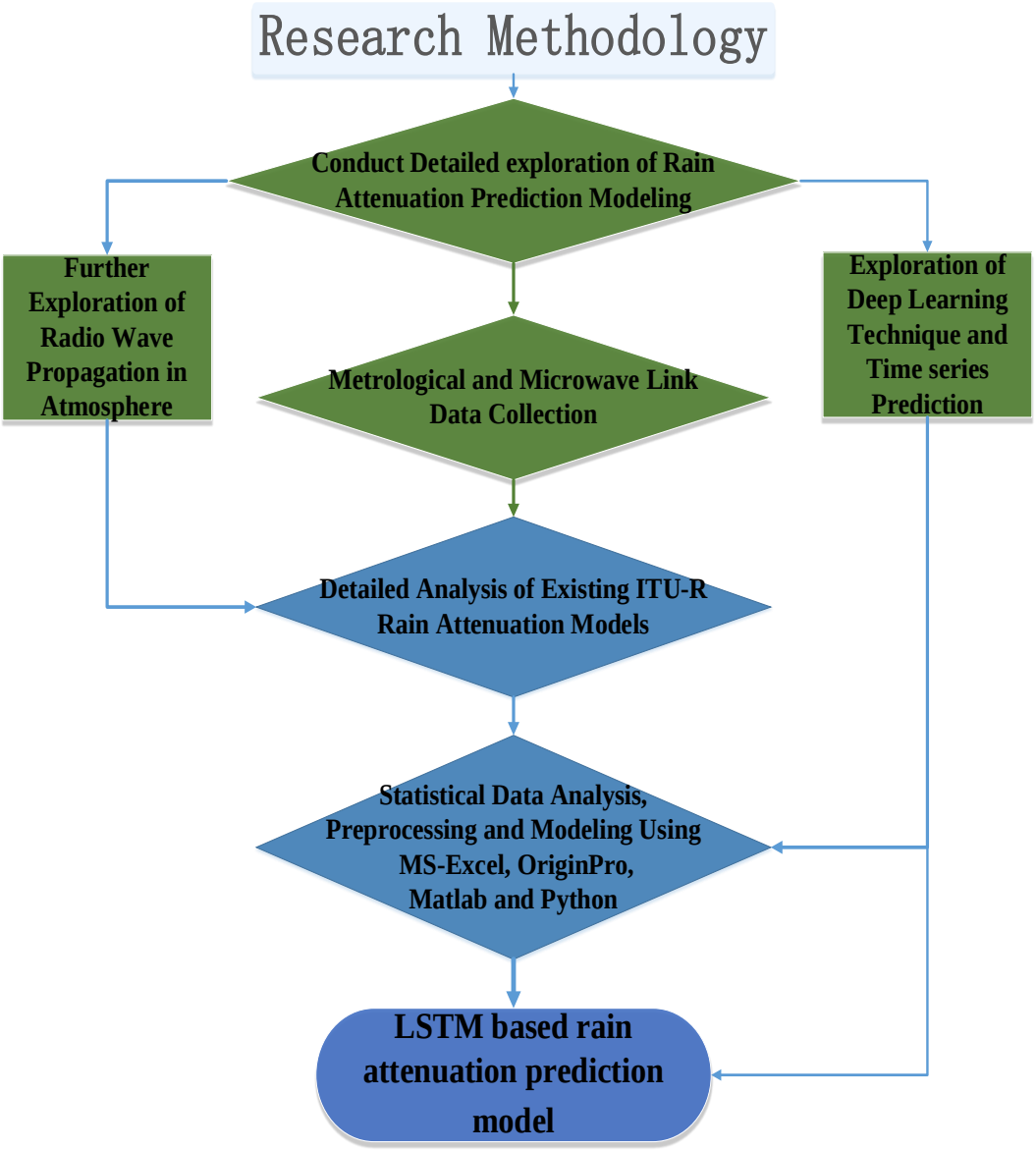

Figure 1-1 Framework of Research Methodology

1.7 Contribution of The Thesis

Rain attenuation poses a significant hurdle for wireless communication systems operating at higher frequencies, such as microwave and millimeter wave bands. This challenge is exacerbated by the escalating demand for wireless data capacity, driving mobile providers to anticipate surges in mobile traffic year after year. Therefore, the development of a reliable model capable of accurately predicting attenuation caused by rain and other climatic conditions is imperative for wireless link designers.

This thesis offers contributions across various fronts. With the rise of AI tools like deep learning, which excel in analyzing and predicting variable time series events such as stock market trends, weather patterns, and signal processing, there's a ripe opportunity to leverage these technologies for rain attenuation prediction. By introducing a novel AI-assisted rain attenuation prediction model, this research aims to enhance the accuracy and efficacy of such forecasts.

Understanding atmospheric impairments, particularly the impact of rain attenuation, is paramount for microwave link designers. The proposed deep learning approach to rain-induced attenuation prediction holds promise for superior results compared to traditional models. Consequently, the outcomes of this study can be utilized as crucial inputs for designing and deploying microwave links in specific locations, aiding in optimizing network performance.

Moreover, this thesis serves as a valuable resource for researchers and students in the field of microwave and millimeter wave communications. It provides a comprehensive reference point for those embarking on related research endeavors and offers insights for further refinement and development of the proposed prediction model. By fostering knowledge exchange and advancement in this domain, the thesis contributes to the ongoing evolution of wireless communication technologies

1.8 Organization of the Thesis

This thesis is composed of six chapters, such that the Introduction, Radio Wave Propagation, Deep Learning for Time Series Prediction, Data Collection, Preprocessing and Modeling, Reuslt and Discussion, and Conclusion. The organization of this thesis is presented in pictorial diagram in figure 1-2.

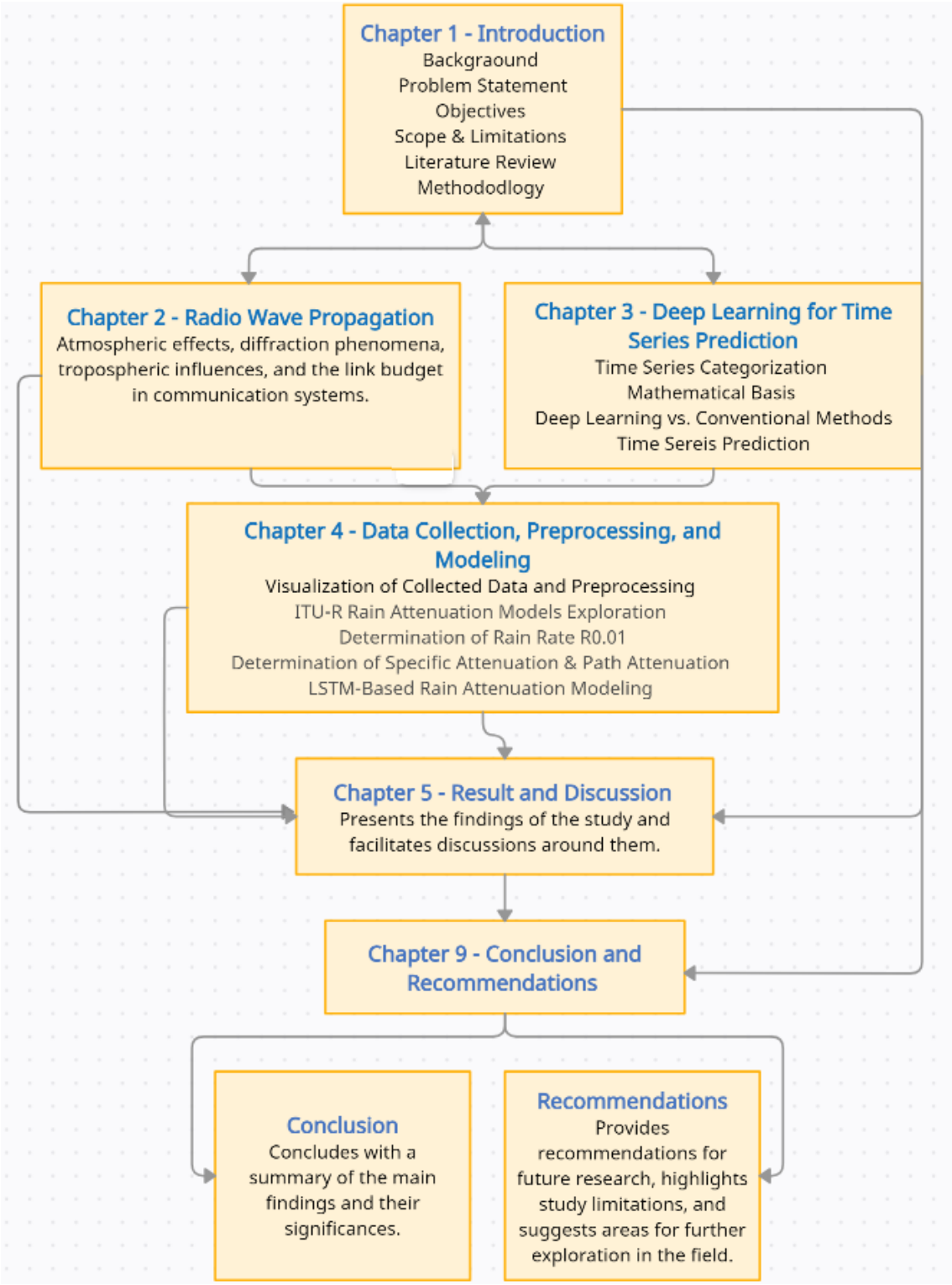

Figure 1-2 Thesis organization

2 Radio Wave Propagation

Radio waves, as a form of electromagnetic radiation, travel through space and the Earth's atmosphere, connecting transmitters and receivers in telecommunication systems. Understanding the effects of various conditions on radio propagation is crucial for designing reliable communication networks. At its core lies the fascinating behavior of electromagnetic waves, weaving their way through the Earth's atmosphere to facilitate seamless communication across vast distances. This chapter is designed to overview the the intricate mechanisms that govern the propagation of radio waves, exploring the diverse phenomena that influence their journey from transmitter to receiver.

2.1 The Earth's Atmosphere

The Earth's atmosphere, particularly the troposphere, plays a crucial role in the propagation of radio waves. This lowest atmospheric layer, extending from the Earth's surface to about 10 km at the poles and 17 km at the equator, is where weather phenomena occur and is characterized by its proximity to the ground and the direct influence of the natural environment[43]. The troposphere contains much of the atmospheric mass, including water vapor, making it the densest layer. Due to its density and composition, the troposphere has a significant impact on radio wave propagation, especially at frequencies above 7 and 10 GHz, where the effects of precipitation and other climatological factors become more pronounced. As radio waves travel through this turbulent layer, they are subject to reflection, refraction, and scattering, which can affect signal strength and reliability[44].

In the troposphere, the temperature decreases with altitude, influencing cloud formation and precipitation. Rainfall is most intense at the elevation of maximum precipitation (EMP), above which it diminishes. Relative humidity, the ratio of water vapor to the air's moisture capacity at a given temperature, affects rainfall; high relative humidity can lead to condensation and precipitation. These atmospheric dynamics, including temperature gradients and moisture content, are crucial for understanding weather patterns and predicting climate behavior. The stratosphere, above the troposphere, has a temperature increase with altitude due to UV radiation absorption by ozone, which affects the overall climate system but not weather directly[45].

2.2 Radio Wave Propagation Through Atmosphere

The transmission of electromagnetic waves through the atmosphere relies on a multitude of physical mechanisms, each influencing the propagation characteristics in unique ways. These methods encompass diverse phenomena such as point-to-point propagation, free-space transmission, diffraction, reflection, waveguiding, and scattering. In free-space propagation, the attenuation of signals stems primarily from the scattering of energy as it disperses from the transmitting source over increasing distances. Both distance and frequency play pivotal roles in determining the extent of attenuation in free space. Beyond free-space losses, additional sources of attenuation include atmospheric gas absorption, vegetation interference, diffraction losses, and hydrometer effects, among others. Reflection, scattering, diffraction, and free-space propagation represent the principal contributors to attenuation in free space, delineating the complex interplay between electromagnetic waves and the atmospheric environment. Understanding these mechanisms is imperative for devising strategies to mitigate signal degradation and optimize the reliability of wireless communication systems[46, 47].

Radio waves traverse through space in diverse manners, presenting unique characteristics that captivate the attention of designers in numerous wireless communication systems. These propagating waves encompass various classifications, including direct (or free space), ground (or surface), tropospheric, and ionospheric. Figure 2.2 provides visual representation of these wave types.

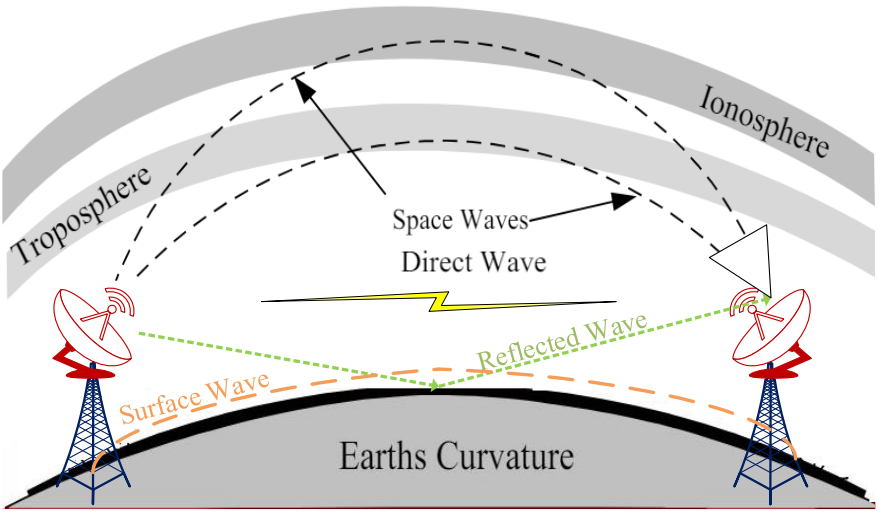

Figure 2-1 Common types of radio waves in wireless communication

2.3 Diffraction

Diffraction occurs when obstacles impede the direct path of signal propagation in the atmosphere between a source and receiver antenna[48]. When the dimensions of these obstacles are significant relative to the wavelength of the signal, they give rise to secondary waves. Despite being diffracted, these waves can still reach the receiving antenna, influencing the line-of-sight communication link[49]. Different frequencies exhibit varied diffraction characteristics: below 1GHz, attenuation increases with obstruction size, while above 1GHz, attenuation escalates more rapidly, potentially destabilizing the connection. The size of the obstruction dictates the total attenuation caused by diffraction, impacting the transmitted energy. Microwave link designers aim to ensure sufficient clearance to minimize loss due to obstacles between the links. Huygen's principle and Fresnel's zone theory are fundamental tools used to determine adequate clearance and manage diffraction caused by obstructions. The attenuation resulting from diffraction at an edge can be described by a frequency-dependent relation, typically expressed as $10\,log(f)$. Notably, attenuation due to diffraction becomes significantly pronounced at frequencies exceeding 15GHz. The following mathematical formula provides further insight into the attenuation arising from diffraction within terrestrial line-of-sight links:

$$\upsilon = \mathrm{h}\sqrt{\frac{2}{\lambda}\left(\frac{1}{\mathrm{d}_1}+\frac{1}{\mathrm{d}_2}\right)} \qquad 2.1$$

Here, d1 and d2 represent the distances from the edge point to the signal transmitter and the receiver, respectively. The parameter h denotes the height of the obstructing obstacle extending above the direct line between the two endpoints. Based on designers' experience, it's advisable to ensure a clearance equivalent to 60% of the first Fresnel zone plus an additional 3 meters to mitigate diffraction and scattering effects caused by obstructing objects within microwave links. Notably, greater clearance necessitates more antenna towers, which entails both economic and technical implications that must be carefully considered during the design phase[50].

2.3.1 Reflection

Reflection occurs when a wave encounters a surface of considerable size, exhibiting

minimal irregularities relative to the wavelength[48, 51]. Specular reflection and diffuse reflection are two fundamental phenomena in the context of electromagnetic wave propagation, especially in the field of radio frequency (RF) and microwave or mmWave communications. Specular reflection occurs when waves reflect off a smooth surface, where the angle of incidence is equal to the angle of reflection. This type of reflection is described by the Fresnel equations, which relate the electric field of the reflected wave to that of the incident wave, taking into account the material's properties such as conductivity (σ), permittivity (ε), and complex permittivity (ε'). These equations are crucial for understanding how electromagnetic waves interact with different materials, especially at high frequencies like 60 GHz. Diffuse reflection, on the other hand, happens when waves encounter a rough surface with irregularities. Unlike specular reflection, the reflected waves scatter in many directions. The Rayleigh criterion is used to determine whether a reflection is specular or diffuse by comparing the height of the surface irregularities (h) to the wavelength of the incident wave and considering the angle of incidence[52].

The diffraction and reflection phenomenon of radio wave propagating through lign of sight can be seen in the figure 2.3.

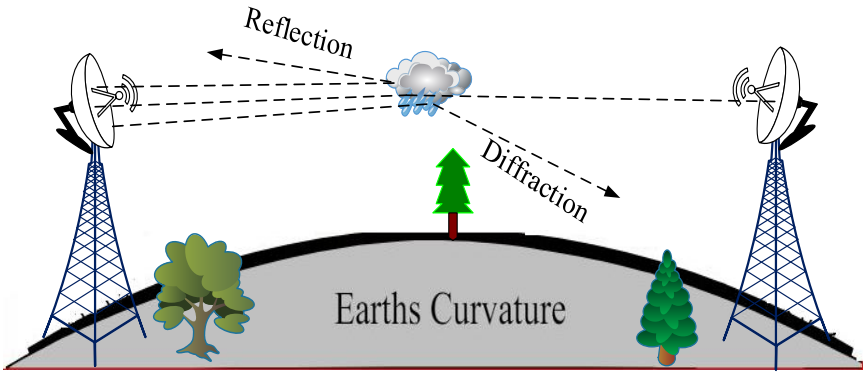

Figure 2-2 Difraction and Reflcation of Radio Wave due to Rain

2.3.2 Scattering

Scattering is a fundamental phenomenon in radio wave propagation, particularly when a signal encounters a rough surface with dimensions smaller or comparable to the wavelength of the incident wave, leading to the energy of the signal being dispersed in various directions. As the number of wavelengths increases, so does the computational complexity[48].

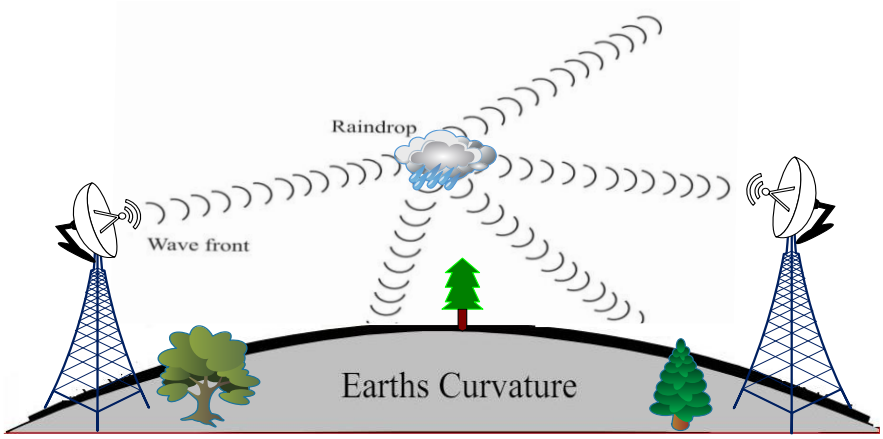

Figure 2-3 Scatering of radio wave signals by rain

There are two main types of scattering: Elastic scattering, where the kinetic energy of particles or waves is conserved after interaction with another particle, direction of the radio waves is altered due to the interaction and can be predicted and calculated using theoretical models like the Fresnel equations[52]. Inelastic scattering, where the kinetic energy of a particle or wave is not conserved after an interaction with another particle, often leading to a change in frequency or energy of the scattered wave.

2.4 Tropospheric Effects on Radio Waves Propagation

The troposphere layer of the atmosphere has a significant impact on terrestrial radio wave propagation including[53]: -

- Attenuation: Radio waves can be absorbed or scattered by atmospheric gases (mainly oxygen and water vapor) and hydrometeors (like rain, fog, hail, snow, and clouds), leading to signal weakening.
- Beam Path Alteration: The radio beam path can bend due to changes in the refractive index along the path, which is influenced by atmospheric conditions such as temperature and humidity.
- Enhanced Propagation: Atmospheric conditions can create ducts that guide radio waves, allowing them to travel further than they would in a vacuum.
- Signal Fluctuations: Multiple signal paths caused by reflections, diffraction, and scattering can lead to fluctuations in the amplitude of the received signal.
- Tropospheric Scattering: Irregularities in the troposphere can scatter radio waves, enabling them to reach great distances, be used for tropo-scatter communication links. The most critical tropospheric effect on microwave and millimeter wave (mmWave)

propagation is attenuation due to atmospheric gases, mainly oxygen and water vapor. This frequency-dependent attenuation is particularly significant at mmWave frequencies, where the atmosphere can induce additional losses to signal power. Precipitation, such as rain, also contributes to attenuation and is especially impactful for terrestrial microwave and mmWave links operating at frequencies higher than 10 GH[48, 54]. Temperature and humidity have a significant effect, where higher humidity levels tend to weaken signal strength, while higher temperatures can enhance it[55]. Understanding these effects is essential for designing and optimizing communication systems that operate in these frequency bands.

2.5 Effects of Rainfall, Temperature and Humidity on Radio Waves

2.5.1 Effects of Rainfall on Radio Waves

Rainfall is a dynamic natural occurrence that differs in intensity and frequency across different locations and over time. In meteorology, various types of rainfall are characterized by their formation or phase as they reach the ground. Rainfall can occur in three primary ways[56]; Convective rainfall, stratiform rainfall and Orographic rainfall. Convective rainfall tends to be intense and brief compared to stratiform rainfall. Stratiform rain is caused by frontal weather systems converging into areas of low pressure, the situation when warm air meets cool air. Orographic rainfall happens when moist air is pushed upwards over elevated terrain, leading to condensation on slopes, such as mountains.

Rainfall events can ben represented and studied by the fundamental unit called rain cells. There have been many studies into the size and shape of rain cells using radars long-term time series measurements made from rain gauges with a time resolution such as 1 minute, which are used to estimate rain cell sizes using the synthetic storm technique. Rain cells are used to improve the effectiveness of propagation models, especially for systems with multiple paths, when predicting attenuation due to rain. The prediction of signal fade can greatly improve the effectiveness of fade mitigation techniques, and help maintain high-quality communication services.

At frequencies above a certain threshold, rainfall-induced attenuation becomes a critical factor limiting the performance of microwave and millimeter-wave propagation. The transmission of electromagnetic waves in the microwave and millimeter bands

experiences significant disruptions from rain rate and raindrop size, causing attenuation, depolarization, and noise. Vertical-looking radiometers measure vertical path attenuation caused by rain, while line-of-sight links measure horizontal path attenuation, and satellite links measure slant path attenuation. Rainfall rates as modest as 2 mm/hr can induce mmWave attenuation reaching up to 2.55 dB/km, escalating to 20 dB/km in instances of heavy rainfall. Such figures may elevate notably in tropical areas characterized by exceptionally high rainfall rates, substantial raindrop sizes, and heightened intensity[57].

2.5.2 Effects of Temperature and Humidity on Radio Waves

Temperature and humidity have significant effects on radio wave propagation, especially in the troposphere, which is the lowest part of the atmosphere where most weather phenomena occur.

Temperature is a measure of the average kinetic energy of air molecules. As we go higher in the atmosphere, the temperature generally decreases, which means the kinetic energy of the air molecules also decreases. This decrease in temperature with elevation is a normal condition in the troposphere. However, under certain atmospheric conditions known as temperature inversions, this typical temperature profile can be inverted. A temperature inversion occurs when a layer of cooler air is trapped near the ground by a layer of warmer air above. This can happen, for example, during the evening or at night when the ground cools down rapidly after sunset, cooling the air close to it. The presence of a temperature inversion affects the density and refractive index of the air. The refractive index is a measure of how much a wave is bent, or refracted, when it enters a medium. In the case of a temperature inversion, the refractive index gradient can cause radio waves to bend back towards the Earth rather than spreading out into space. This bending of radio waves due to the refractive index gradient is known as refraction. The cooler air near the ground is denser than the warmer air above it during an inversion. This density difference creates a boundary layer in the atmosphere that can refract radio waves. The sudden change in densities when a radio wave enters the warm air above the duct causes the wave to be refracted back toward Earth. This refraction can enhance the range of radio waves, allowing them to travel beyond the normal line-of-sight distance. It's particularly noticeable for VHF and UHF bands, where the waves can be refracted well beyond the normal radio horizon distance during temperature inversions[58].

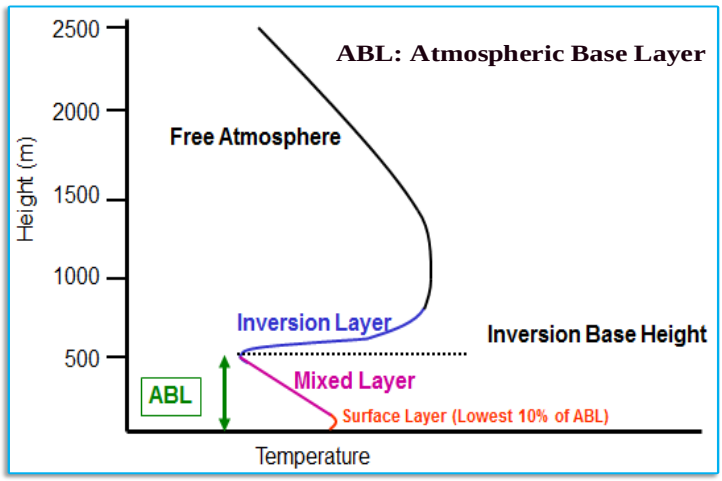

Figure 2-4 Temperature profile (Temperature vs Height) of Atmospheric layer

Humidity refers to the amount of water vapor present in the air. It's an important factor in radio wave propagation because water molecules can absorb electromagnetic energy. When humidity levels are high, there are more water molecules in the air to absorb this energy, which can lead to increased attenuation or weakening of radio signals as they travel through the atmosphere. Vapor pressure is the pressure exerted by water vapor in the air. It's directly proportional to the number of water molecules in each volume. Higher vapor pressure means more water vapor is present, which can lead to greater absorption and attenuation of radio waves. This is particularly relevant for frequencies that are close to the resonant frequencies of water vapor. Saturation vapor pressure is the maximum pressure that water vapor can exert at a given temperature; it's the point at which the air is "saturated" with water vapor and cannot hold any more without condensation occurring. This is important because it represents the upper limit of water vapor content in the air at a particular temperature. As the temperature increases, the saturation vapor pressure also increases, allowing the air to hold more water vapor before reaching the point of condensation.

The presence of water vapor in the atmosphere impacts radio waves in several ways. Firstly, it alters the refractive index of air, causing radio waves to bend or refract as they pass through regions with varying humidity, affecting their trajectory. Secondly, humidity influences diffraction, the bending of waves around obstacles, potentially leading to signal fading or shadow zones where signal strength decreases. Lastly, water vapor can scatter radio waves, redirecting their energy in multiple directions, resulting in multipath interference and signal fading as signals arrive at the receiver from various paths.

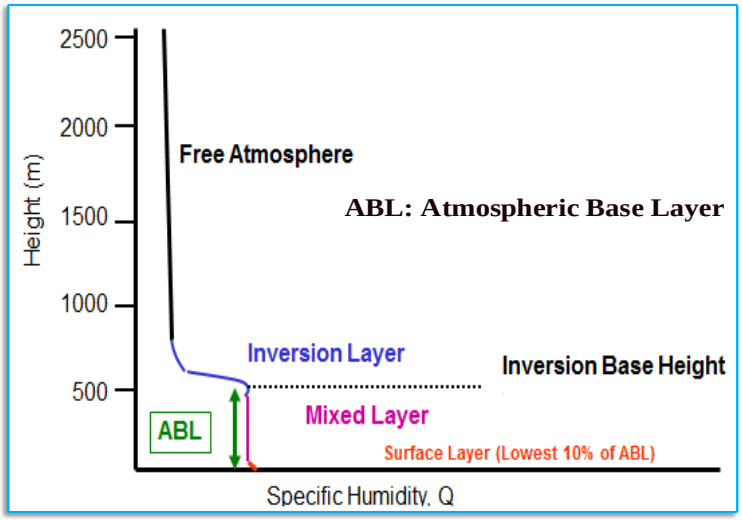

Figure 2-5 Humidity profile (Specific Humidity vs Height) of Atmospheric layer

2.5.3 The Common Effect of Rain, Temprature and humidity

Rain, temperature, and humidity collectively exert significant influence on radio wave propagation, affecting signal strength, reliability, and quality in various ways. Rain plays the most disruptive role, acting like tiny sponges that absorb radio waves and scattering them in unpredictable directions. The heavier the rain, the more it disrupts the signal, especially at higher frequencies where raindrops become more effective at attenuation. Temperature fluctuations can also be a party crasher. While generally higher temperatures weaken the signal, there can be exceptions. Under specific atmospheric conditions, temperature inversions can act like a mirage, bending the radio wave and extending its reach. Humidity, ever-present in the air, throws another wrench into the mix. Water vapor molecules have a taste for radio waves, particularly at frequencies close to their own resonant frequency. The more humid the air, the more the signal is absorbed, leaving it weaker at the receiver. But the problems don't stop there. Rain can also cause the signal strength to fluctuate wildly, making it difficult to receive the information clearly. Similarly, humidity variations can act like a mischievous wind, bending the radio wave in unexpected directions and causing issues with the signal's arrival angle. These effects become even more critical at higher frequencies, where radio waves are more susceptible to disruptions from environmental factors.

2.6 The Link Budget and the Medium Loss

The link budget stands as a fundamental concept in the design of any radio system, regardless of its purpose, be it communication, navigation, remote sensing, surveillance, or interference management[59]. The fundamental equation that governs the propagation of radio waves in free space from a transmitter to a receiver is the Friis transmission equation given as:

$$p_r = \frac{P_t G_t G_r \lambda^2}{(4\pi D^2)} \qquad 2.2$$

Where p_r is received power, P_t is transmitted power, G_t and G_r are the transmitting and receiving antenna gain, λ is the wavelength of the radio waves and D is the path length.

However, the outdoor environment is not free space. Instead, it experiences different natural phenomenon, which affects the propagation of radio waves and cause medium loses. In this case, the medium effect can be included by a correction factor F such that the Friis transmission equation can be modified as:

$$p_r = \frac{P_t G_t G_r \lambda^2}{(4\pi D^2)} |F|^2 \qquad 2.3$$

Given that the received power (P) is proportional to the square of the electric field, we can express the factor F as the numeric ratio (Eo/Em) of the actual electric field (Em) resulting from the presence of the medium to the pseudo-electric field (Eo) in free space.

The link budget equation isn't derived from a single complex concept, but rather follows the fundamental principle of power balance in a communication system. It's essentially an accounting of all the power gains and losses experienced by a signal as it travels from the transmitter to the receiver.

Transmit Power (dBm): This represents the raw power emitted by the transmitter.

Gains (dB): These terms account for amplifications in the system, like gains from transmitting and receiving antennas that focus the signal.

Losses (dB): These terms represent reductions in signal strength due to various factors:

Path Loss: The inherent weakening of a signal as it travels through the transmission medium itself.

Feedline Losses: The power loss specifically due to the cable that carries the signal between the transmitter/receiver and the antenna.

Other Losses: Any additional factors that reduce signal strength, like atmospheric attenuation or connector losses.

Losses can be seen as either free space path loss (L_0) or medium losses (L_p). The free space loss refers to the attenuation of radio frequency (RF) signals as they propagate through free space without encountering any significant obstacles or objects and can be expressed as:

$$L_0 = 10\log\frac{4\pi D^2}{\lambda} \qquad 2.4$$

ITU-R explains free space path loss in more detail in [60] and set up calculation methods in [61].

Medium loss, which occurs due to interactions between the RF signal and the propagation medium itself and is related to F factors can be formulated as:

$$L_p = -10\log|F|^2 \qquad 2.5$$

In the realm of radio wave propagation, the medium typically acts as a diminisher of signal strength and a distorting agent for phase. This is indicated by the fact that the factor F is typically of a magnitude less than one. Consequently, it's common for L_p to assume a positive value.

Thus, the link budget equation is a summation of transmitted power, the transmitter and receiver gains and the losses, having in mind that losses are a reduction from the total received power. It can be written as:

$$p_{r=}P_t+G_t+G_r - L_0 - L_p \qquad 2.6$$

It's important to recognize that in the link budget equation, all parameters except the medium loss (L_p) are fixed values determined by the configuration of the radio system in question. Medium Loss (L_p) is a stochastic variable, subject to variation. Its magnitude holds significant influence as it essentially sets the system limit for a radio system.

2.6.1 The Medium Loss

Medium Loss (L_p) is influenced by numerous factors, including frequency, geometry, environment, and other complex variables. Therefore, accurately assessing Medium Loss

(L_p) is crucial in evaluating the performance of radio systems across various applications such as communications, navigation, remote sensing, surveillance, and electronic warfare.

There are many effects which contribute to Lp. For frequencies above 10GHz, several factors contribute to medium loss (Lp):

(a) Rain-induced absorption and scattering of electromagnetic waves lead to signal attenuation.

(b) Rain causes signal depolarization, while other hydrometeors cause attenuation and depolarization.

(c) Absorption in atmospheric gases and emission noise from absorbing media add to the loss.

(d) Loss occurs due to beam divergence of earth-station antennas and atmospheric refraction.

(e) Effective antenna gain decreases due to phase decorrelation across the antenna aperture caused by refractive-index irregularities.

(f) Beam-bending from large-scale refractive index changes causes slow fading, while small-scale variations result in rapid fading (scintillation) and angle of arrival variations.

(g) Bandwidth limitations arise from multiple scattering or multipath effects, particularly in high-capacity digital systems.

2.7 Summary

This chapter explores radio wave propagation, crucial for modern communication systems. It focuses on understanding electromagnetic wave behavior in the Earth's atmosphere, with an emphasis on the troposphere's role. The chapter discusses mechanisms affecting radio wave propagation such as diffraction, reflection, refraction, scattering due to atmospheric factors and their impact on signal reliability. It also examines how atmospheric conditions influence signal strength and fluctuations. Critical factors such as rainfall, temperature, and humidity are explored, with a focus on their impact on signal degradation. The chapter concludes by discussing the link budget and medium loss, highlighting the multitude of factors contributing to signal degradation, including rain-induced effects, atmospheric absorption, antenna characteristics, and environmental factors. Generally, the chapter provides valuable insights for communication system design and optimization.

3 Deep Learning for Time Series Prediction

3.1 Introduction

Deep learning neural networks possess the capacity to autonomously acquire intricate mappings from inputs to outputs, accommodating numerous inputs and outputs. These capabilities hold significant potential for time series forecasting, especially in scenarios characterized by intricate nonlinear dependencies, diverse input variables, and multi-step prediction tasks. These functionalities, coupled with the advancements in modern neural networks, offer promising prospects, such as the automated feature extraction facilitated by convolutional neural networks and the inherent support for sequential data in recurrent neural networks.

Time series modeling has held a prominent position within academic research over time, serving as a fundamental component in numerous applications, with particular significance in domains such as climate modeling[62], signal processing[63], medicine[64], commercial decision making[65] and more. A time series represents a sequential arrangement of data points ordered by time, typically illustrating the evolution of a particular phenomenon over a defined period. Time series forecasting involves the prediction of future values within such a sequence, enabling the formulation and implementation of informed decision-making strategies.

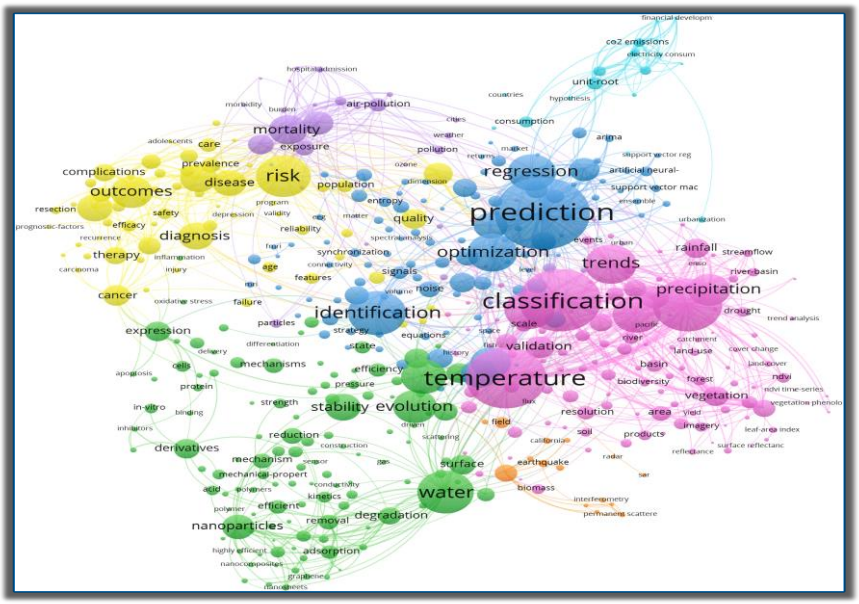
prediction
classification
temperature
regression
optimization
trends
precipitation
identification
mortality
risk
disease
outcomes
diagnosis
therapy
cancer
expression
derivatives
nanoparticles
water
stability
evolution
surface
validation
rainfall
unit-root
air-pollution
consumption
complications
exposure
care
prevalence
population
quality
signals
features
mechanisms
reduction
mechanism
degradation
removal
adsorption
efficiency
pressure
resolution
area
vegetation
imagery
products
soil
earthquake
biomass
basin
forest
biodiversity
streamflow
river-basin
drought
ndvi
arima
artificial-neural-
support vector mac
ensemble
urbanization
events
urban
synchronization
connectivity
noise
failure
particles
strategy
equations
state
scale
space
over
land-use
cover change
land-cover
ndvi time-series
vegetation phenolo
leaf-area index
surface reflectanc
reflectance
radar
sar
interferometry
permanens scattere
scattering
field
drain
construction
sensor
gas
conductivity
kinetics
polymers
acid
efficient
polymer
highly efficient
nanocomposites
graphene
nanosheets
in-vitro
binding
inhibitors
apoptosis
cells
protein
strength
delivery
differentiation
mechanical-propert
carcinoma
injury
inflammation
oxidative stress
prognostic-factors
resection
recurrence
efficacy
safety
depression
program
reliability
spectroscopy
matter
entropy
dimension
ozone
pollution
weather
return
market
cities
countries
hypothesis
co2 emissions
electricity consum
financial-developm
hospitalization
mortality
burden
adolescents
support vector reg
trend analysis
drought
catchment
paddy
rice
cotton
wheat
maize
corn
soybean
potato
tomato
grape
olive
banana
coffee
tea
sugarcane
cassava
yield
crop
irrigation
fertilizer
pesticide
herbicide
fungicide
insecticide
pest
weed
disease
plant
leaf
root
stem
seed
fruit
flower
pollen
nectar
chlorophyll
photosynthesis
respiration
transpiration
stomata
chlorophyll
carotenoid
anthocyanin
flavonoid
tannin
lignin
cellulose
hemicellulose
starch
sugar
glucose
fructose
sucrose
lactose
maltose
galactose
mannose
xylose
arabinose
ribose
deoxyribose
nucleotide
nucleic acid
dna
rna
mrna
trna
rrna
gene
genome
chromosome
allele
mutation
transcription
translation
protein
enzyme
hormone
receptor
ligand
antibody
antigen
vaccine
immunity
immune
inflammation
cytokine
chemokine
interleukin
tumor
cancer
carcinoma
metastasis
chemotherapy
radiotherapy
surgery
biopsy
histology
pathology
diagnosis
prognosis
survival
recurrence
remission
relapse
metastasis
malignant
benign
tumor
cell
tissue
organ
blood
serum
plasma
urine
saliva
sweat
feces
excretion
secretion
metabolism
catabolism
anabolism
homeostasis
hypertension
hypertension
diabetes
obesity
cardiovascular
heart
lung
liver
kidney
brain
spinal cord
nerve
neuron
synapse
neurotransmitter
dopamine
serotonin
acetylcholine
glutamate
gamma-aminobutyric acid
glycine
histamine
epinephrine
norepinephrine
melatonin
cortisol
testosterone
estrogen
progesterone
insulin
glucagon
thyroid
parathyroid
adrenal
pituitary
hypothalamus
pineal
gonad
ovary
testis
uterus
vagina
penis
prostate
breast
mammary
menstrual
menopause
pregnancy
fetus
placenta
amniotic
umbilical
cord
embryo
zygote
blastocyst
morula
gastrula
neurula
organogenesis
fertilization
ovulation
spermatogenesis
oogenesis
meiosis
mitosis
chromosome
centromere
telomere
kinetochore
spindle
microtubule
actin
myosin
kinesin
dynein
cytoskeleton
cytoplasm
nucleus
nucleolus
ribosome
endoplasmic reticulum
golgi apparatus
mitochondrion
chloroplast
vacuole
lysosome
peroxisome
glyoxysome
cell membrane
cell wall
extracellular matrix
collagen
elastin
fibronectin
laminin
proteoglycan
glycosaminoglycan
hyaluronic acid
chondroitin sulfate
heparan sulfate
keratan sulfate
dermatan sulfate
heparin
heparinoid
glycoprotein
lipoprotein
phospholipid
sphingolipid
glycolipid
cholesterol
triglyceride
fatty acid
saturated fatty acid
unsaturated fatty acid
monounsaturated fatty acid
polyunsaturated fatty acid
omega-3 fatty acid
omega-6 fatty acid
omega-9 fatty acid
trans fatty acid
cis fatty acid
hydrogenation
saponification
esterification
transesterification
glycerol
monoglyceride
diglyceride
triglycerides
phosphatidylcholine
phosphatidylethanolamine
phosphatidylserine
phosphatidylinositol
phosphatidylglycerol
phosphatidic acid
cardiolipin
sphingomyelin
ceramide
cerebroside
ganglioside
sulfatide
globoside
lactosylceramide
glucosylceramide
galactosylceramide
sphingosine
sphinganine
dihydrosphingosine
phytosphingosine
sphingosine-1-phosphate
ceramide-1-phosphate
sphingosine-1-phosphate
lysophosphatidic acid
lysophosphatidylcholine
lysophosphatidylethanolamine
lysophosphatidylserine
lysophosphatidylinositol
lysophosphatidylglycerol
lysophosphatidylserine
lysophosphatidylcholine
lysophosphatidylethanolam

3.1.1 Catagorization of Time Series Data

Time series can be categorized into five distinct types based on various data characteristics[66]:

1. **Variables:** Depending on the number of variables involved, time series are either *univariate* or *multivariate*. Univariate time series feature a single variable, like electrocardiogram (ECG) data used in [67] to predict heart disease. Conversely, multivariate time series involve multiple variables, such as weather and climate data utilized in [68] to analyze their impact on animal populations.
2. **Continuity:** Time series can be further classified as *either discrete* or *continuous*.
3. **Stability:** The stability of a time series distinguishes it as either *stationary* or *non-stationary*. A stationary time series remains unchanged over time, displaying random fluctuations around a constant value within a bounded range, without discernible trends or periodic patterns. Real-life examples of non-stationary time series abound, like wind intensity.
4. **Distribution:** Time series can be categorized based on their distribution as *Gaussian* or *non-Gaussian*.
5. **Chaos:** Chaotic time series are influenced by their initial conditions, where even slight changes in the system's starting state can lead to critical or inflection points, significantly impacting system performance.

3.2 Mathematical Explanation of Time Series Data

To elucidate time series and its methodologies more effectively, the explanation below introduces some definitions related to time series.

Definition 1: Univariate Time Series; can be denoted as $s = t_1, t_2, \dots, t_L$, represents an ordered set of length L.

Definition 2: A multivariate time series; can be denoted as $X = (x_1, x_2, \dots, x_T)$, consists of a sequence vector where each element x_i is a univariate time series with varying lengths. X comprises T variables, with the ith variable represented as x_i.

Definition 3: Subsequence; given a time sequence s with length L, a subsequence $s_{\text{sub}} = s[m, m+n-1]$ has a length $n < L$. The starting point of the subsequence is at position m in s, and the endpoint is at position $m+n-1$, denoted as $s_{\text{sub}} = t_m, \dots, t_{m+n-1}$, where $1 \le m \le L-n+1$.

Definition 4: Similarity Degree; for two time series b and s (assuming $|b| \leq |s|$), the similarity degree between them, denoted as $\mathrm{Sim}(b, s)$, is computed as $\min\{\mathrm{dist}(b, s_i)\}$, where s_i is any subsequence of s satisfying $|b| = |s_i|$.

Definition 5: Shapelet; a shapelet is a subsequence of a time series s with strong discriminative ability. Specifically, a shapelet is represented as $p = (b, \delta, c)$, where b, δ, and c denote the subsequence, threshold, and class label, respectively. If an unknown time series satisfies the condition $\mathrm{Sim}(p, s) \leq \delta$, it can be categorized into class c.

Definition 6: Euclidean Distance; eculidean distance is a commonly used distance measurement to quantify the similarity between two distinct time series. For sequences b and c both with length L, the Euclidean distance is calculated as

$$\mathrm{dist}_{\mathrm{euclidean}} = \sqrt{\sum_{i=1}^{L} (b_i - c_i)^2}$$

Definition 7: Dynamic Time Warping (DTW); DTW is another widely adopted distance measurement method. Unlike the Euclidean distance, DTW can compute the minimum distance between two sequences with different lengths. While the principle is not elaborated here due to its extensive application, the calculation is given as $\mathrm{dist}_{\mathrm{DTW}} = \mathrm{DTW}(s, b)$.

In tasks involving time series classification and prediction, the fundamental and extensively utilized algorithms include 1NN-DTW (1 nearest neighbor dynamic time warping), as well as autoregressive (AR) and moving average (MA) models. The 1NN-DTW model employs DTW for distance measurement and utilizes the simple yet effective 1NN algorithm to identify the nearest training sample for the current instance, assigning the same class label as the nearest training sample. This model does not necessitate parameter training and demonstrates high accuracy.

3.3 Deep Learning vs Conventional Method Time Series Analysis

While conventional approaches have emphasized parametric models guided by domain knowledge, such as autoregressive (AR)[69], exponential smoothing[70], or structural time series models[71], contemporary machine learning techniques offer a pathway to comprehend temporal dynamics purely through data-driven means. The surge in data accessibility and computational capabilities in recent years has elevated machine

learning to an indispensable component of the next wave of time series forecasting methodologies. Some of the limitation of traditional methods include: -

- ✧ Limited ability to capture complex patterns: Traditional methods assume linear relationships between variables and may struggle to capture non-linear patterns or long-term dependencies in the data.
- ✧ Lack of scalability: Traditional methods may not scale well to large datasets or high-dimensional time series data.
- ✧ Manual feature engineering: Traditional methods often require manual feature engineering to extract relevant information from the data, which can be time-consuming and may not capture all relevant patterns.

Deep learning techniques, on the other hand, offer several advantages for time series prediction:

- ✧ Handling High-Dimensional Data: Deep learning models are well-suited for high-dimensional datasets, which are common in time series data. They can process and extract useful features from large amounts of input data without extensive manual feature engineering[72].
- ✧ Learning Complex Patterns: These models can learn and model complex nonlinear relationships that are often present in time series data. This is particularly useful for capturing intricate patterns, trends, and anomalies[72].
- ✧ Long-Term Dependencies: With architectures like Recurrent Neural Networks (RNNs) and Long Short-Term Memory networks (LSTMs), deep learning models can remember information for long periods, which is essential for predicting future values based on past observations[72].
- ✧ Flexibility and Adaptability: Deep learning models can be adapted to various types of time series prediction problems, making them versatile tools across different domains and applications[72].
- ✧ Automatic Feature Extraction: These models are capable of automatic feature extraction, which means they can identify relevant features from raw data, reducing the need for domain expertise and manual intervention[72].
- ✧ Improved Accuracy: Deep learning models often outperform traditional statistical models in terms of prediction accuracy, especially when dealing with large and complex datasets[72].
- ✧ End-to-End Learning: Deep learning allows for end-to-end learning, where raw data can be input directly into the model, and the model can learn to make predictions as

output, simplifying the modeling pipeline[72].

3.4 Time Series Prediction

Time series forcasting entails creating and employing a predictive model on data exhibiting a sequential arrangement of observations. While time series prediction techniques have undergone extensive development over time, the exponential growth in data volume has posed significant challenges to conventional methods and has notably impacted their efficiency. Over the years, these methods have evolved from basic linear and nonlinear regression models rooted in traditional statistics to encompass machine learning approaches such as neural networks and support vector machines. Additionally, alternative prediction techniques tailored to specific characteristics of time series data have emerged based on diverse theoretical frameworks. For instance, fuzzy cognitive maps offer a means to address data uncertainty while maintaining interpretability. To tackle the issue of insufficient labeled data in practical applications, transfer learning methods present a viable solution. Looking ahead, two primary avenues for future research become apparent: firstly, addressing the escalating scale of time series data, and secondly, identifying the most appropriate model selection for a particular problem. Figure 3.2 outlines the developmental trajectories of various technical pathways alongside the algorithms they yield.

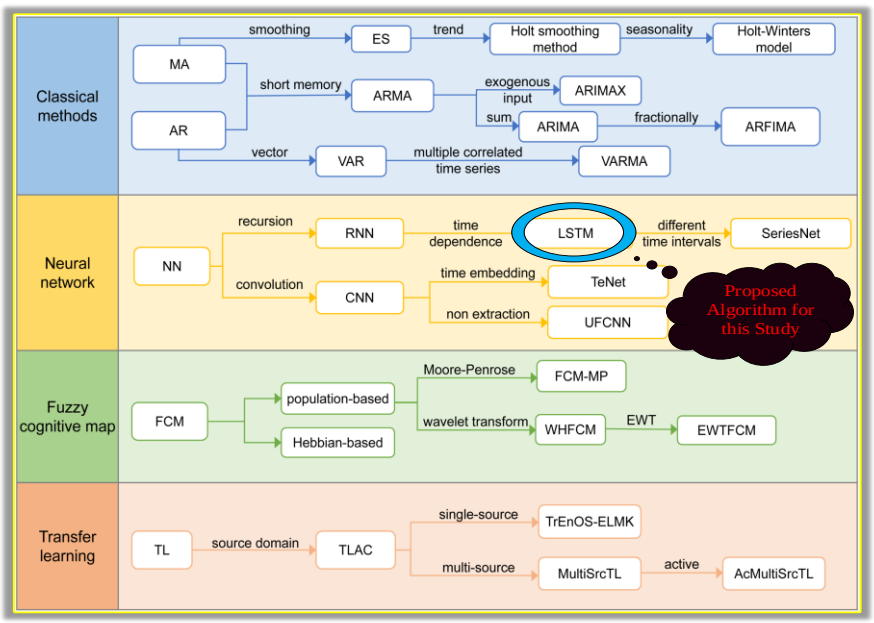

Figure 3-2 Developmental trajectories of various technologies

Classical methods for time series prediction primarily involve determining model parameters based on stationary, non-stationary, or multivariate time series. For stationary series, pioneers like Slutzky and Yule introduced the moving average (MA) and autoregressive (AR) models, respectively. The ARMA model, proposed by Box and Jenkins, extended these concepts to short memory models. Non-stationary series, characterized by trends, find solutions in the autoregressive integrated moving average (ARIMA) model, although its limitation lies in capturing nonlinear patterns. Models like ARFIMA and ARIMAX offer alternatives for long memory dependence and incorporating exogenous inputs, respectively. Exponential smoothing (ES) methods and Holt-Winters models provide options for series with or without trend and seasonality.

For multivariate time series, the vector autoregressive (VAR) model extends AR to dynamic multivariate data, while VARMA considers cross-correlations. These models improve prediction accuracy by accounting for inter-sequence influences. Neural networks, notably artificial neural networks (ANNs), provide a flexible, nonlinear approach to time series prediction, offering improved accuracy without the need for predefined model forms. Recurrent neural networks (RNNs) and their variant, long short-term memory (LSTM), excel in capturing long-term dependencies and have become popular for time series analysis. Convolutional neural networks (CNNs), on the other hand, utilize filters to extract features from local data subsets, offering an efficient alternative to RNNs. Hybrid models combining linear and nonlinear methods are also explored for enhanced prediction quality.

Fuzzy cognitive map (FCM) emerges as a dynamic system modeling tool, adept at dealing with uncertain data while maintaining interpretability. FCM-based time series prediction leverages population-based and Hebbian-based learning algorithms. Transfer learning addresses the challenge of insufficient labeled data by transferring knowledge from related tasks. TLAC and OS-ELMK combine transfer learning with other techniques to improve prediction accuracy. Multi-source transfer learning and deep transfer learning further enhance model performance by leveraging knowledge from multiple source domains. Though relatively less explored in time series prediction, transfer learning offers promise in leveraging knowledge from related datasets to overcome data scarcity challenges.

3.5 Summary

The chapter introduces the application of deep learning techniques for time series prediction, highlighting their potential to handle complex nonlinear dependencies, diverse input variables, and multi-step prediction tasks. It begins by discussing the significance of time series forecasting across various domains and presents five categorizations of time series data based on different characteristics.

Definitions related to time series data are provided to facilitate understanding, including univariate and multivariate time series, subsequences, similarity degree, shapelets, Euclidean distance, and Dynamic Time Warping (DTW). Key algorithms used in time series classification and prediction, such as 1NN-DTW, autoregressive (AR), and moving average (MA) models, are also explained.

The chapter compares deep learning approaches to conventional methods, emphasizing the advantages of deep learning in handling high-dimensional data, learning complex patterns, capturing long-term dependencies, and automatic feature extraction. It outlines the limitations of traditional methods and highlights the capabilities of deep learning models.

The discussion concludes by addressing the challenges faced by traditional methods due to the exponential growth of data volume and presents the evolution of time series prediction methods from linear and nonlinear regression models to machine learning approaches like neural networks. Alternative techniques such as fuzzy cognitive maps and transfer learning are explored to address specific challenges in time series prediction, paving the way for future research directions. Figure 3.2 illustrates the developmental trajectories of various technologies in time series prediction.

4 Data Collection, Preprocessing and Modeling

4.1 Introduction

This chapter provides the data collection of the study, preprocessing of the collected data and the modeling of rain attenuation prediction for microwave and mmWave frequency bands. An extensive and detailed work is presented in each section and subsection of the chapter by explaining the theretical concept supporting with data and graphical illustrations, which help readers to comprehend the thesis easily and properly. The chapter first intrduces the geography and climate of the study area in details followed by data sources and visualization of collected data. Both the metrological data and the microwave and mmWave data have been described properly and visualized graphically. Additionally, the ITU-R rain attenuation models, the major constituent of this study, are presented in detail. Furthermore, the data processing section provides readers with statistical analysis of the study by utilizing the ITU-R models in determining the rain rate, $R_{0.01}$, the convertion process of 15-minute rain rate to 1-minute rain rate and determination of specific attenuation, effective path length and total path attenuation of the selected microwave link. Finally, LSTM-based rain attenuation prediction model is designed and simulated using the preprocessed data to predict the signal power loss due to rain on the target microwave link. The proposed LSTM-based model appears to be advantageous in rain attenuation prediction with its capability of capturing long-term dependencies in time series data, it's ability of handling the irregular rainfall pattern with irregular time intervals. Moreover, LSTM's memory cell state allows it to retain information across lengthy sequences, enhancing prediction accuracy and robustness to missing data and noisy inputs. Lastly, LSTM's adaptability enables it to adjust to changing conditions, such as varying rainfall intensities or seasonal patterns, further improving its predictive performance in dynamic environments.

4.2 Geography and Climate of Ethiopia

Geographically, Ethiopia occupies the Horn of Africa, spanning latitudes from approximately 3°N to 15°N and longitudes from around 33°E to 48°E. Its elevation ranges from about 100 meters below sea level in the Danakil Depression to over 4,000 meters

above sea level in the Ethiopian Highlands. The country shares borders with Eritrea to the north, Djibouti and Somalia to the east, Sudan and South Sudan to the west, and Kenya to the south. Ethiopia is primarily characterized by plateaus, with the Great Rift Valley dividing the western and eastern highlands. The highlands gradually slope down towards the lowlands of Sudan to the west and Somalia to the east[73].

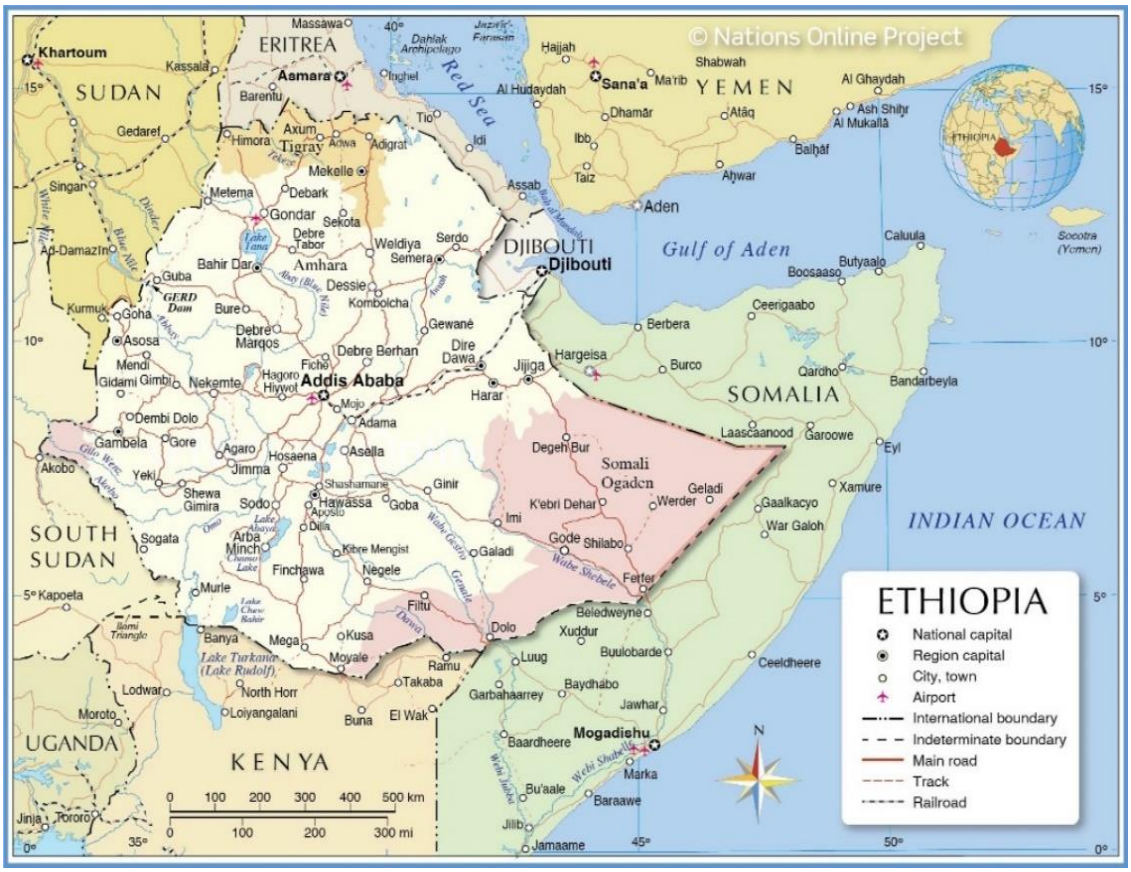

Figure 4-1 Map of Ethiopia (source:[74])

The climate in the Ethiopian highlands is characterized as temperate, while the lowlands experience arid conditions[75]. Climatic variations over Ethiopia are influenced by unique geographical features. The classification system developed by Köppen in 1931, based on elevation, proves valuable in understanding these variations[76]. Consequently, Ethiopia's climate can be broadly categorized into three main classes: Class A includes climates (As, Aw, Am) found in the lowlands, ranging from semi-humid to semi-arid, surrounding the highlands; Class B comprises hot-arid (BWh), hot-semi arid (BSh), and BSk climates prevalent in the Afar-Triangle and the Somali Region; and Class C consists of warm temperate (Cwb, Cfb) and cool mountainous (Cwc) climates in the highlands, characterized by semi-humid to humid conditions. The following table provides some

cities of Ethiopia with their latitude and longitude coordination, annual rainfall in mm and their Köppen climate class.

Table 4-1 Annual Rainfall in mm and their Köppen Class of Some Cities

Cities	Lat. (°N)	Long. (ºE)	Annual Rainfall(mm)	Köppen Class of Cities
Addis Ababa	9.02	38.45	1165	Cwb
Adama	8.33	39.17	922.81	Aw
Ambo	8.95	37.93	968.7	Cwb
Debre Markos	10.32	37.73	1380	Cwb
Bahir Dar	11.35	37.23	1480	Cwb
Metehara	8.89	39.91	571	Aw
Jimma	7.40	36.49	1414	Cfb
Nekemt	9.08	36.55	1998	Cwb
Mekelle	13.28	39.32	601	Bsh
Axum	14.12	38.72	104.53	Bsh
Alem Ketema	10.05	38.99	1104.35	Cwb
Mehalmeda	10.30	39.65	865.42	Cwb
Combolcha	11.09	39.74	1139	Cwb
Dire Dawa	9.58	42.32	729.8	BSh
Awash Arba	9.10	40.32	456	Aw

Ethiopia's climate and rainfall patterns are highly varied, influenced by its diverse topography. The annual rainfall ranges from less than 300 mm in the lowlands to over 2,000 mm in the highlands. The Köppen climate classification spans from Cwb in the highlands, Aw in the midlands, to BWh in the desert areas. This diversity impacts rain attenuation, which is a critical factor for communication systems, especially in regions with heavy rainfall. Cities like Nekemt, Bahir Dar, Addis Ababa, Debre Markoss e.t.c, with high annual rainfall will have more signal attenuation, while drier cities like Dire Dawa will have less, though occasional heavy rains must still be accounted for in communication infrastructure planning. This variability necessitates tailored approaches to communication network design across Ethiopia.

Annual rainfall distribution and Köppen climate classification of major cities in Ethiopia Can be visualized in figure 4.2. The main study location of this thesis is Addis

Ababa city, Capital of Ethiopia.

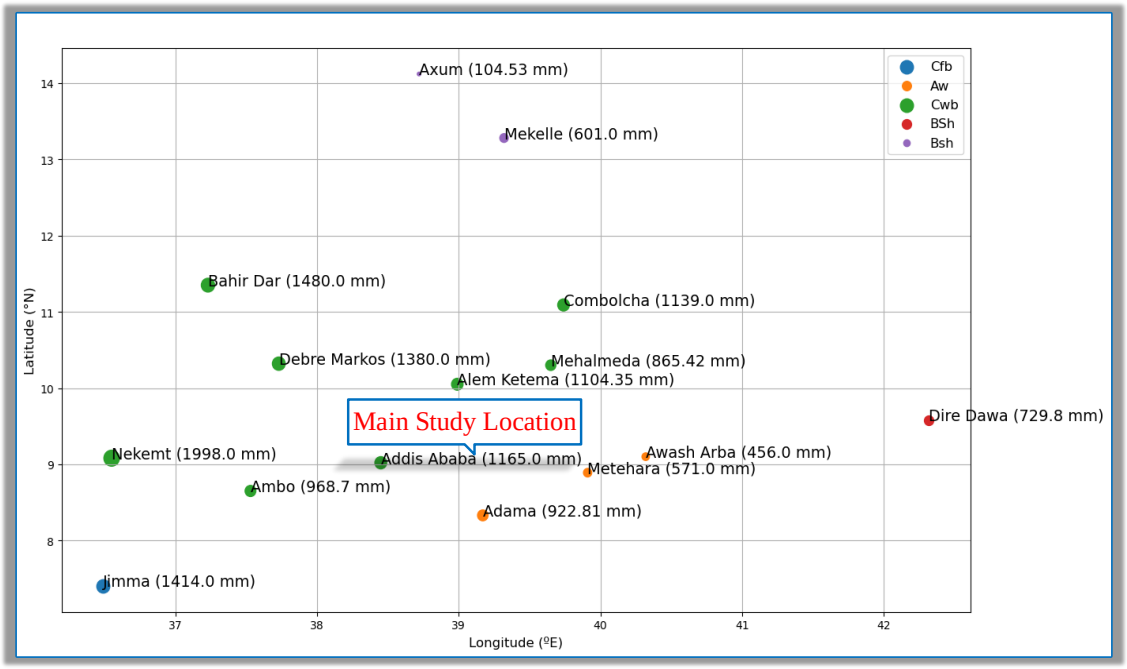

Figure 4-2 Annual rainfall distribution and Köppen climate of Ethiopia

Based on the Köppen Class graph below, one can tell that Ethiopia's weather is dominantly warm temperate climate with a dry winter and rainy summar overall falling in the Cwb class. It is th subtropical highland climate or temperate oceanic climate with dry winters; coldest month averaging above 0°C(32°F), all months with average temperatures below 22°C(71.6 °F), and at least four months averaging above 10°C (50°F).

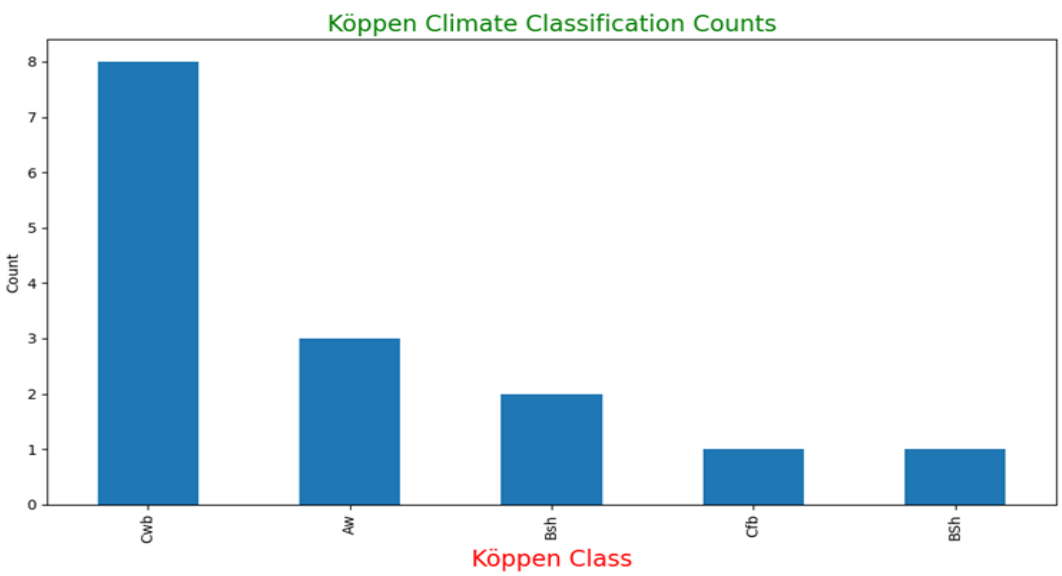

Figure 4-3 Köppen climate classification in Ethiopia

4.3 Visualization of Collected data

4.3.1 Metrological Data

In accordance with the recommendation of ITU-R rain attenuation forecast procedures, coordinate estimation performed at the place of interest is the most effective method for determining total precipitation dispersion. For various places in Ethiopia, a trustworthy source of long-term rainfall measurements is needed to ease the use of the suggested rain rate distribution models. Various devices are available to record rainfall for this purpose. The Ethiopian National Meteorological Authority (NMA) gathers rainfall data in two ways: it utilizes automated rain gauges to record rainfall intensity every fifteen minutes, and it employs networks of rain gauges to measure rainfall intensity every twenty-four hours. The gauges satisfy the requirements of the World Meteorological Organization. This study utilizes the data from July 11, 2014, to June 16, 2022. The data includes precipitation(mm), temperature(°C) and relative humidity(%). It can be visualized in the following figures for some major cities.

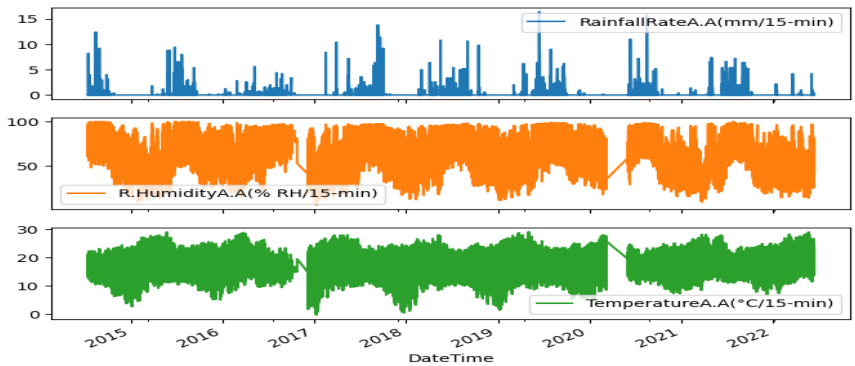

Figure 4-4 15-min rainfall, humidity, and temperature of Addis Ababa city

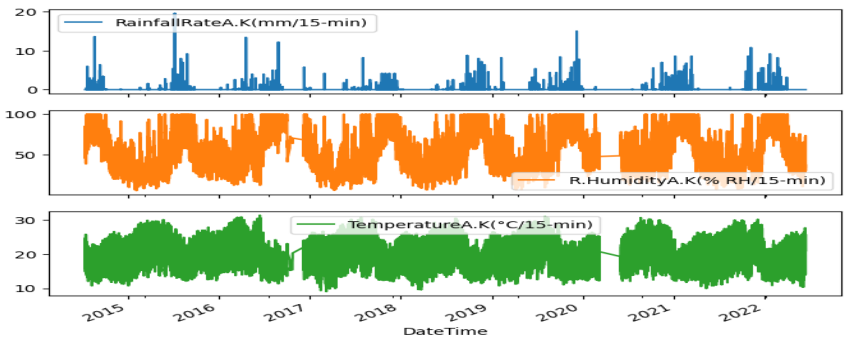

Figure 4-5 15-min rainfall, humidity, and temperature of AlemKetema city

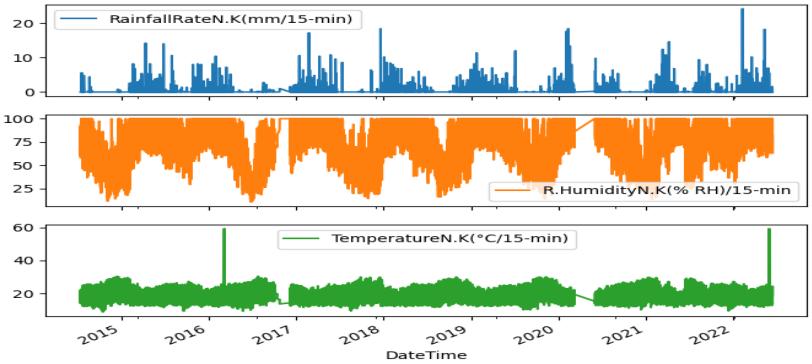

Figure 4-6 15-min rainfall, humidity, and temperature of Nekemt city

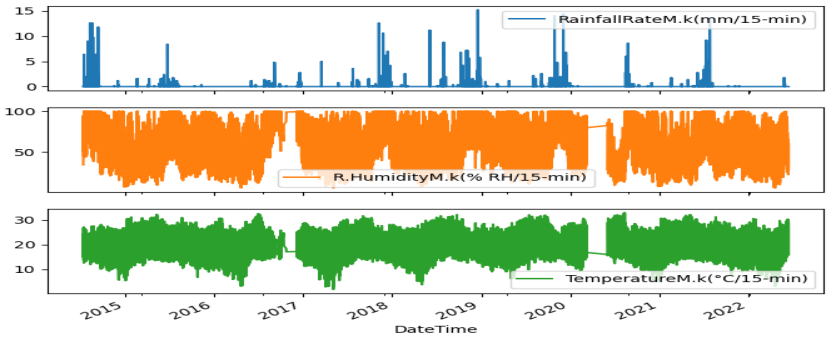

Figure 4-7 15-min rainfall, humidity, and temperature for Mekele city

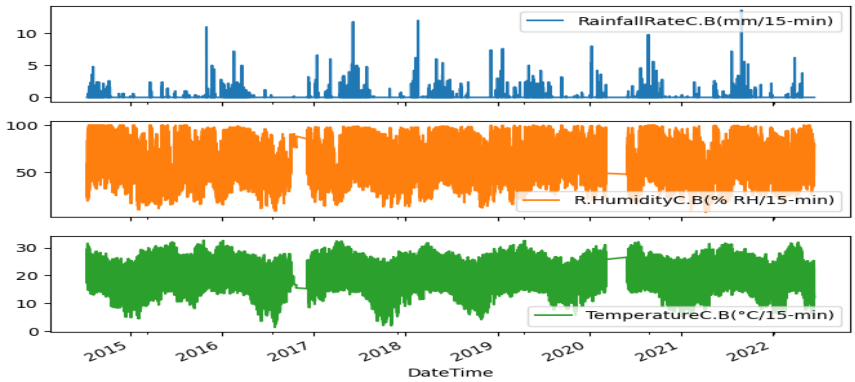

Figure 4-8 15-min rainfall, humidity, and temperature for Combolcha city

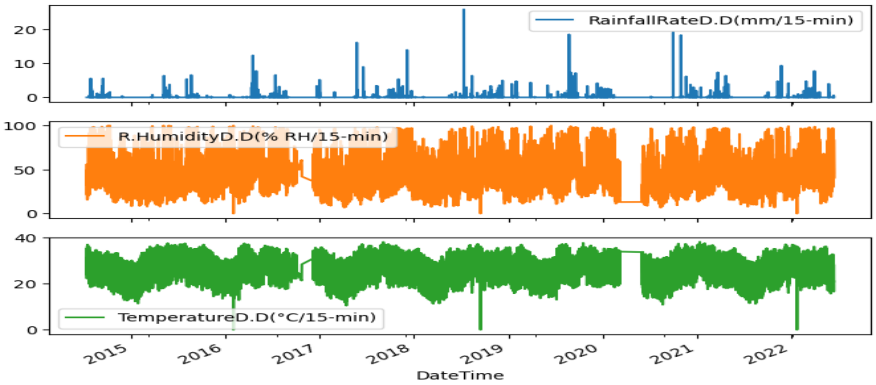

Figure 4-9 15-min rainfall, humidity, and temperature for DireDewa city

Rainfall rate of the selected cities has been furthure processed as this study focus more on rain effects on the signal propagation in the line-of-sight communication links. The precipitation data for those cities has been changed to mm/hr by multiplying by and its statistics has been further analyzied using using softwares like Microsoft excel and origionPro. This can be seen in the figure bellow;

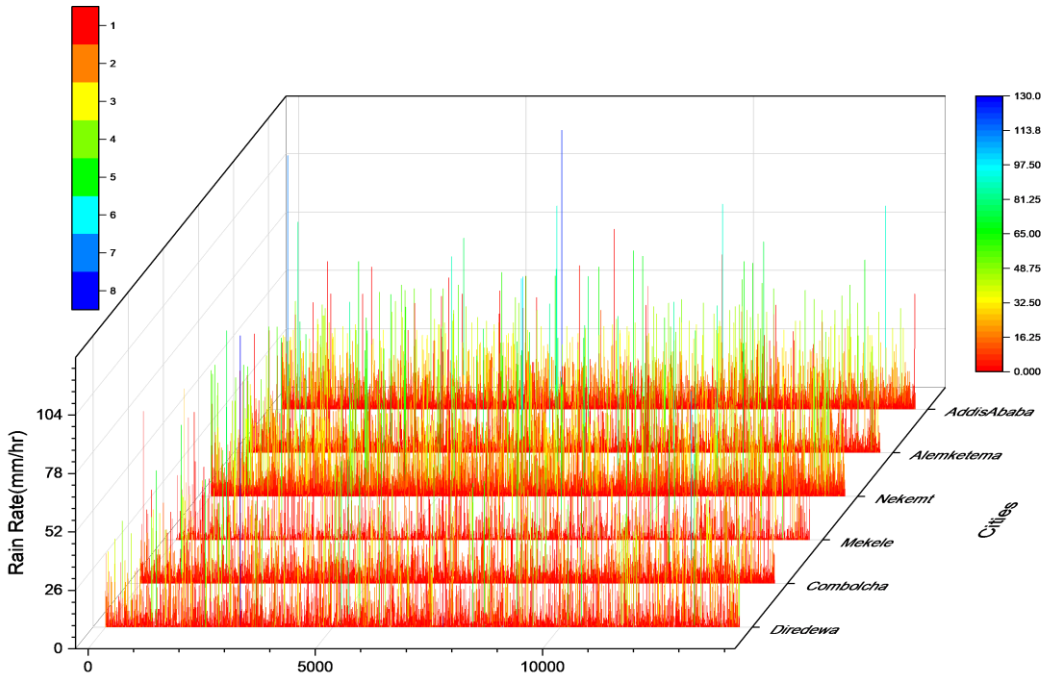

Figure 4-10 3D visualization of rain rate(mm/hr) for above cites

4.3.2 Microwave and mmWave link data

Microwave and millimeter wave technologies are widely used in communication, radar, sensors, and other fields, but signal attenuation can occur in rainy days, affecting communication quality and system performance. Therefore, studying the attenuation prediction model of microwave and millimeter wave rain is of great significance. Microwave and millimeter wave technologies are widely used in communication, radar, sensors, and other fields, but signal attenuation can occur in rainy days, affecting communication quality and system performance. Therefore, studying the attenuation prediction model of microwave and millimeter wave rain is of great significance. This study explores the conventional and the latest AI rain attenuation prediction methods.

mmWave links are not commericially implemented in Ethiopia except that only in 5G testing sites at some part of Addis Ababa. Whereas, microwave links are widly used

in many application scinartios in telecommunication, radio broadcasting, and TV broadcasting. Therefore, this research focuses in utilizing microwave links as primary input data in studying the rain induced attenuation. The microwave link that this research uses is the link that strechs from Addis Ababa to Mount Furi, where two main radio broadcasting stations exists. The link is visualized in the figure below using ms Viso.

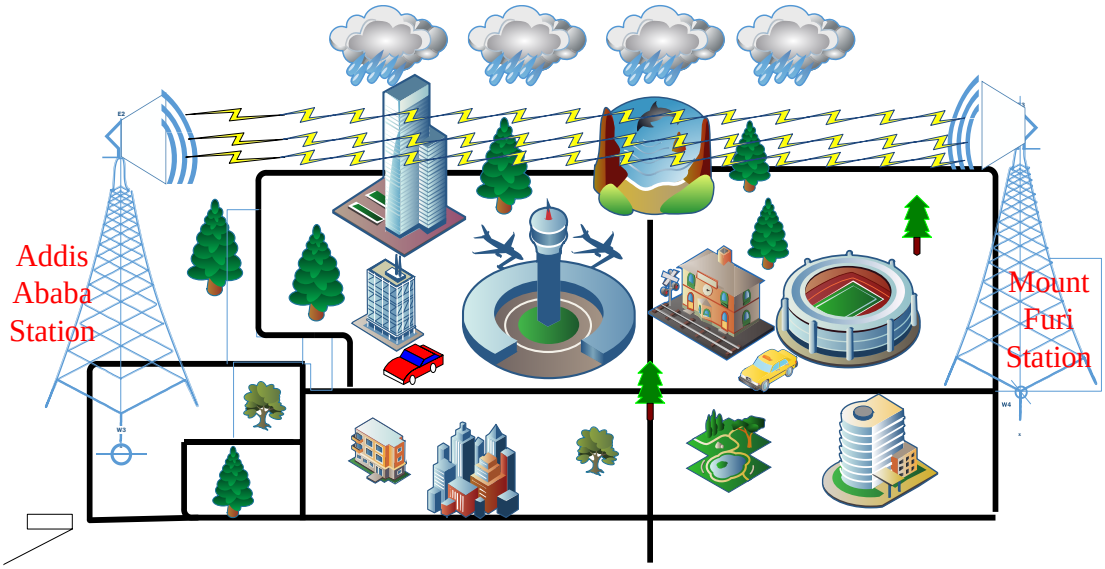

Figure 4-11 Typical LOS microwave connecting Addis Ababa & Furi

The terrestrial Line-of-Sight between Addis Ababa at an azimuthal angle of 203.920 with an altitude of 2401 m above sea level and Furi at an azimuthal angle of 23.910 with altitude of 2842 m above sea level. The link is vertically polarized at operating frequency of 11 GHz. The link profile is displayed in the table below.

Table 4-2 Microwave link profile Addis Ababa to Furi Link Link[42]

Parameters	Addis Ababa (Tx)	Mount Furi (Rx)
Elevation (m)	2842	2401
Latitude	08.52582°N	09.01067°N
Longitude	38.41125°E	38.44504°E
Antenna gain (dBi)	42	42
Atenna helght (m)	10	10
Frequency (GH)	11	11
True azimuth (°)	23.92	203.93
Vertical angle (°)	-1.59	1.48
Link length (km)	16.42	

4.4 ITU-R Rain Attenuation Models

Rain attenuation is a critical aspect of designing microwave communication systems, particularly for frequencies above 10 GHz where rain can significantly impact signal propagation. The specific calculation of rain attenuation typically involves the use of empirical models such as the ITU-R models. Those ITU-R models includes ITU-R P.530, ITU-R P.618[78], ITU-R P.837[79], ITU-R P.838[15] and ITU-R P.311[80], and they provide necessary information in calculating and predicting rain caused signal attenuation. Each of them involves modeling how electromagnetic waves interact with the atmosphere under different conditions. Prediction of rain attenuation should be carried out on a properly processed input data to achieve amicable result. Data processing of this study mainly focus on utilizing ITU-R models that are relevant to the indicated topic. First, summarization of some some of those models as follow;

4.4.1 ITU-R P.530 Model

The ITU-R P.530 recommendation provides propagation data and prediction methods required for the design of terrestrial line-of-sight (LOS) systems. It's a comprehensive document that outlines the factors affecting radio wave propagation in the atmosphere and offers models to predict the performance of microwave links under various environmental conditions. It assists in designing LOS communication links, especially for microwave and millimeter-wave systems and covers frequencies from 30 MHz to 100 GHz and considers both point-to-point and point-to-multipoint links. This model covers the propagation phenomenons such as:

- Free-Space Loss: The basic loss of signal strength over distance in a vacuum.
- Atmospheric Absorption: Losses due to gases in the atmosphere, primarily oxygen and water vapor.
- Multipath Fading: Variations in signal strength caused by interference between multiple paths.
- Rain Attenuation: Signal degradation due to precipitation.
- Refraction: Bending of radio waves as they pass through the atmosphere with varying density.
- Diffraction: Bending of waves around obstacles and the spreading of waves past openings.

Long-term rain attenuation statistics are crucial for designing reliable communication systems, particularly those relying on satellite or microwave links. These statistics describe how often signal attenuation due to rain occurs over a long period. The ITU-R P.530 the following simple technique may be used for estimating the long-term statistics of rain attenuation:

Step 1: Obtain the rain rate R0.01 exceeded for 0.01% of the time (with an integration time of 1 min). If this information is not available from local sources of long-term measurements, an estimate can be obtained from the information given in Recommendation ITU-R P.837.

Step 2: Compute the specific attenuation, γ_R(dB/km) for the frequency, polarization, and rain rate of interest using Recommendation ITU-R P.838.

Step 3: Compute the effective path length, $d_{eff}(km)$, of the link by multiplying the actual path length d by a distance factor r. An estimate of this factor is given by:

$$r = \frac{1}{0.477 d^{0.633} R_{0.01}^{0.073\alpha} f^{0.123} - 10.579(1-exp(-0.024d))} \quad 4.1$$

where f (GHz) is the frequency and α is the exponent in the specific attenuation model from Step 2. The effective path length is then can be formulated as:

$$d_{eff}(km) = d(\text{km})r \quad 4.2$$

Step 4: An estimate of the path attenuation exceeded for 0.01% of the time is given by:

$$A_{0.01}(dB) = \gamma_R(dB/km) d_{eff}(km) \quad 4.3$$

Step 5: The attenuation exceeded for other percentages of time p in the range 0.001% to 1% may be deduced from the following power law:

$$\frac{Ap}{A_{0.01}} = C_1 p^{-(C_2 + C_3 \log_{10} p)} \quad 4.4$$

$$c_1 = (0.07^{c_0})\left[0.12^{(1-c_0)}\right] \quad 4.5$$

$$C_2 = 0.855C_0 + 0.54(1 - C_0) \quad 4.6$$

$$C_3 = 0.139C_0 + 0.043(1 - C_0) \quad 4.7$$

where:

$$C_0 = \begin{cases} 0 \cdot 12 + 0.4[log_{10}(f|10)^{0.8}] & f \geq 10GH_Z \\ 0 \cdot 12 & f < 10GH_Z \end{cases} \quad 4.8$$

Step 6: If worst-month statistics are desired, calculate the annual time percentages p corresponding to the worst-month time percentages pw using climate information specified in Recommendation ITU-R P.841. The values of A exceeded for percentages of the time p on an annual basis will be exceeded for the corresponding percentages of time pw on a worst-month basis. The prediction procedure outlined above is valid in all parts of the world at least forfrequencies up to 100 GHz and path lengths up to 60 km.

4.4.2 ITU-R P.618 Model

The ITU-R P.618 series of recommendations focused on predicting how radio signals propagate between Earth and space through the atmosphere. This is important for designing reliable satellite communication systems, as the signal strength can be affected by factors like rain, water vapor, and atmospheric gases.

Calculating long-term rain attenuation statistics from point rainfall rate involves statistical analysis of rainfall data to predict the impact of rain on signal attenuation, particularly for satellite and microwave communication systems. The ITU-R P.618 model provides a method for this, which can be adapted to specific regions based on available rainfall data. The model predicts rain attenuation over a range of frequencies up to 55 GHz using statistical methods based on long-term rainfall data. It considers the specific location's climate, the elevation angle of the satellite link, and the frequency of operation. This model addresses several propagation phenomena, including:

- Rain Attenuation: Predicting signal loss due to rainfall, which is particularly significant for frequencies above 10 GHz.
- Gaseous Attenuation: Accounting for signal absorption by atmospheric gases, primarily water vapor and oxygen.
- Scintillation: Estimating the rapid fluctuations in signal amplitude and phase caused by irregularities in the refractive index structure of the atmosphere.
- Depolarization: Assessing the alteration of the polarization state of the signal due to atmospheric conditions

The ITU-R P.618 Model provides mathematical formulas and empirical methods to estimate these effects. The methods consider various factors such as:

- Frequency: The operating frequency of the Earth-space link.

- Elevation Angle: The angle between the Earth station's line of sight to the satellite and the plane tangent to the Earth's surface.
- Latitude: The geographical location of the Earth station, which influences factors like rain height and gaseous attenuation.
- Rainfall Rate: The intensity of rainfall, which is a critical factor for predicting rain attenuation.

The ITU-R P.618 recommends the following steps in the calculation method of long-term rain attenuation statistics from point rainfall rate.

Step 1: Determine the rain height, h_R, as given in Recommendation ITU-R P.839

Step 2: For $\theta \geq 5^0$ compute the slant-path length, L_S, below the rain height from:

$$L_S = \frac{(h_R - h_S)}{\sin\theta} \quad km \tag{4.9}$$

For $\theta < 5^0$, the following equation is used:

$$L_S = \frac{2(h_R - h_S)}{sin^2\theta + 2\frac{(h_R - h_S)^{\frac{1}{2}}}{R_e} + sin\,\theta} \quad \text{km} \tag{4.10}$$

If $h_R - h_S$ is less than or equal to zero, the predicted rain attenuation for any time percentage is zero and the following steps are not required.

Step 3: Calculate the horizontal projection, L_G, of the slant-path length from:

$$L_G = \cos\theta\, L_s \;\; km \tag{4.11}$$

Step 4: Obtain the rainfall rate, $R_{0.01}$, exceeded for 0.01% of an average year (with an integration time of 1 min). If this long-term statistic cannot be obtained from local data sources, an estimate can be obtained from the maps of rainfall rate given in Recommendation ITU-R P.837. If $R_{0.01}$ is equal to zero, the predicted rain attenuation is zero for any time percentage and the following steps are not required.

Step 5: Obtain the specific attenuation, γ_R, using the frequency-dependent coefficients given in Recommendation ITU-R P.838 and the rainfall rate, $R_{0.01}$, determined from Step 4, by using:

$$\gamma_R = k(R_{0.01})^{\alpha} \quad dB/km \tag{4.12}$$

Step 6: Calculate the horizontal reduction factor, $r_{0.01}$, for 0.01% of the time:

$$r_{0.01} = \frac{1}{1+0.78\sqrt{\frac{L_G \gamma_R}{f}} - 0.38\left(1-e^{-2L_G}\right)} \qquad 4.13$$

Step 7: Calculate the vertical adjustment factor, $v_{0.01}$, for 0.01% of the time:

$$\xi = tan^{-1}\left(\frac{h_R - h_s}{L_G r_{0.01}}\right) \quad degrees$$

For $\xi > \theta$, $L_R = \frac{L_G - r_{0.01}}{cos\,\theta}$ km , Else, $L_R = \frac{(h_R - h_s)}{sin\,\theta}$ km

If $|\varphi| < 36^0$, $\chi = 36 - |\varphi|$ $degrees$, Else, $\chi = 0$ $degrees$

$$v_{0.01} = \frac{1}{1+\sqrt{\sin\theta}\left(31\left(1-e^{-(\theta)/(1+x)}\right)\frac{\sqrt{L_R \gamma_R}}{f^2} - 0.45\right)}$$

Step 8: The effective path length is:

$$L_E = L_R v_{0.01}\ km \qquad 4.14$$

Step 9: The predicted attenuation exceeded for 0.01% of an average year is obtained from:

$$A_{0.01} = \gamma_R L_E \qquad dB \qquad 4.15$$

Step 10: The estimated attenuation to be exceeded for other percentages of an average year, in the range 0.001% to 5%, is determined from the attenuation to be exceeded for 0.01% for an average year:

$$If\ P \geq 1\%\ or\ |\varphi| \geq 36^0: \quad \beta = 0$$

$$If\ P < 1\%\ \ and\ \ |\varphi| < 36^0\ \ and\ \ \theta \geq 25^0 \quad \beta = -0.005(|\varphi| - 36)$$

$$Otherwise: \qquad \beta = -0.005(|\varphi| - 36) + 1.8 - 4.25\,sin\,\theta$$

$$Ap = A_{0\cdot 0,1}\left(\frac{P}{0.01}\right)^{-0.655+0.033\,ln(p)-0.045\,ln(A_{0.01})-\beta(1-p)\,sin\,\theta} \qquad dB \qquad 4.16$$

This method provides an estimate of the extended statistical influence of rain-induced attenuation. When comparing observed statistics to the forecast, it's crucial to account for the substantial year-to-year variations in rainfall rate statistics. Thus, ITU-R plays a great role in this regard.

4.4.3 ITU-R P.837 Model

The ITU-R P.837 model provides detailed statistical characteristics of precipitation for use in propagation modeling, which is essential for the design and analysis of radio communication systems. Rainfall rate data measured over a one-minute integration period is necessary for forecasting rain attenuation in both terrestrial connections (as specified in Recommendation ITU-R P.530) and Earth-space links (outlined in Recommendation ITU-R P.618). In the cases where dependable long-term local rainfall rate data is unavailable, a prediction method can be employed to estimate the rainfall rate surpassing a specified average annual probability of exceedance for a given location and integration time of one minute. This prediction method relies on two key factors: a) total monthly rainfall data, and b) monthly mean surface temperature data, as outlined in Recommendation ITU-R P.1510.

Calculations can be made for Link Availability (%) for all frequency bands, to consider link budgets, transmit power, receive sensitivity, antenna gain, target availability and other factors. When reliable long-term local rainfall rate data is not available, the ITU-R P.837-7 Annex 1 provides the following 8 steps in determining the rainfall rate of R0.01in a statistical method by considering: Input parameters as:

p: Desired annual probability of exceedance (%)

Lat: Latitude of the desired location (degrees, N)

Lon: Longitude of the desired location (degrees, E)

Output parameter as:

R_p: Rainfall rate exceeded for the desired probability of exceedance (mm/h).

Step 1: For each month of the year, define the month number, ii, and the number of days in each month, N_{ii}, as follows:

Month	Jan	Feb	Mar	Apr	May	Jun	Jul	Aug	Sep	Oct	Nov	Dec
ii	01	02	03	04	05	06	07	08	09	10	11	12
N_{ii}	31	28.25	31	30	31	30	31	31	30	31	30	31

Step 2: For each month number ii, determine monthly mean surface temperatures, $T_{ii}(k)$ at the desired location (Lat, Lon) from reliable long-term local data. If reliable long-term local data is not available, the monthly mean surface temperatures, $T_{ii}(k)$, at the desired location (Lat, Lon) can be obtained from the digital maps of monthly mean surface temperature in Recommendation ITU-R P.1510[81].

Step 3: For each month number ii, determine the monthly mean total rainfall,

$MT_{ii}(mm)$, at the desired location (Lat, Lon) from reliable long-term data. If reliable long-term local data is not available, the monthly mean total rainfall at the desired location (Lat, Lon) can be determined from the digital maps of monthly mean total rainfall, $MT_{ii}(mm)$, provided as an integral part of this Recommendation as follows:

a) determine the four grid points (Lat_1, Lon_1), (Lat_2, Lon_2), (Lat_3, Lon_3) *and* (Lat_4, Lon_4) surrounding the desired location;

b) determine the monthly mean total rainfall, $MT_{ii,1}$, $MT_{ii,2}$, $MT_{ii,3}$ and $MT_{ii,4}$ at the four surrounding grid points of the maps provided with this recommendation;

c) determine MT_{ii} at the desired location by performing a bi-linear interpolation using the four surrounding grid points as described in Annex 1 Paragraph 1b of Recommendation ITU-R P.1144[82].

Step 4: For each month number, ii, convert $T_{ii}(k)$ to t_{ii}(°C).

Step 5: For each month number, ii, calculate r_{ii} as follows:

$$r_{ii} = \begin{cases} 0.5874e^{0.0883\times t_{ii}} & for\ t_{ii} \geq 0° \\ 0.587 & for\ t_{ii} < 0°C \end{cases} \quad \text{(mm/hr)} \qquad 4.17$$

Step 6a: For each month number, ii, calculate the monthly probability of rain as follows:

$$P_{o_{ii}} = 100\frac{MT_{ii}}{24\times N_{ii}\times r_{ii}} \quad (\%) \qquad 4.18$$

Step 6b: For each month number ii, if $P_{o_{ii}} > 70$, set

$$\begin{cases} P_{o_{ii}} = 70 \\ r_{ii} = \dfrac{100}{70}\times\dfrac{MT_{ii}}{N_{ii}}_{o_{ii}} \end{cases}$$

Step 7: Calculate the annual probability of rain, $P_{o_{annual}} = P(R > 0)$ as follows:

$$P_{o_{annual}} = \frac{\sum_{ii=1}^{12} p_{o_{ii}}\times N_{ii}}{365.25} \quad (\%) \qquad 4.19$$

Step 8: If the desired rainfall rate probability of exceedance, p, is greater than $P_{o_{annual}}$, the rainfall rate at the desired rainfall rate probability of exceedance, R_p is 0 mm/hr.

If the desired rainfall rate probability of exceedance, p is less than or equal to $P_{o_{annual}}$, the rainfall rate should be adjusted as R_{ref}, until the absolute value of the relative error between the annual rainfall rate probability of exceedance, P(R>R_{ref}), and

the desired rainfall rate probability of exceedance, p, is less than 0.001%.

When aiming for a 0.01% average annual probability of exceedance and considering factors like memory usage and computational complexity, employing a pre-calculated map of $R_{0.01}$ can serve as a viable solution without significant compromise in accuracy. This approach enables the estimation of rainfall rates at any specified location on Earth's surface by employing bilinear interpolation as outlined in Annex 1 Paragraph 1b of Recommendation ITU-R P.1144. Notably, the discrepancy between this method and full rainfall rate prediction is minimal across most of Earth's surface: The absolute difference remains below 0.3 mm/hr for over 99.9% of the surface. Likewise, it stays under 1 mm/hr for over 99.99% of the surface.

4.4.4 ITU-R P.838 Model

Recommendation ITU-R P.838 is a document that provides a method to calculate the specific attenuation for rain for use in prediction methods for terrestrial microwave links. Specific attenuation is the amount of signal loss due to rain along a path. The method uses a power-law relationship between the specific attenuation and the rain rate, which depends on the frequency of the microwave signal. The Recommendation also provides tables and graphs of the coefficients for the power-law relationship for different frequencies and polarization angles.

The specific attenuation γ_R (dB/km) is obtained from the rain rate $R_{0.01}$ (mm/hr) using the power-law relationship:

$$\gamma_R \left(\frac{dB}{km}\right) = kR_{0.01}{}^{\alpha} \tag{4.20}$$

Where values for the coefficients κ and α are determined as functions of frequency, f(GHz), in the range from 1 to 1 000 GHz, from the following equations, which have been developed from curve-fitting to power-law coefficients derived from scattering calculations:

$$log_{10}\, k = \sum_{j=1}^{4} \left(a_j\, exp\left[-\left(\frac{log_{10} f - b_j}{c_j} \right)^2 \right] \right) + m_k\, log_{10} f + c_k \tag{4.21}$$

$$\alpha = \sum_{j=1}^{5} \left(a_j \, exp\left[-\left(\frac{log_{10} f - b_j}{c_j} \right)^2 \right] \right) + m_k \, log_{10} f + c_k \qquad 4.22$$

where: f: frequency (GHz)

k: either k_H or k_V

α: either a_H or a_V

All the values of constants of the coefficients k_H, k_V, a_H and a_V are given in the tables below:

Table 4-3 cofficient for k_H, k_V, a_H and a_V

k_H					
j	a_j	b_j	c_j	m_k	c_k
1	–5.33980	–0.10008	1.13098	–0.18961	0.71147
2	–0.35351	1.26970	0.45400		
3	–0.23789	0.86036	0.15354		
4	–0.94158	0.64552	0.16817		
k_V					
1	–3.80595	0.56934	0.81061	–0.16398	0.63297
2	–3.44965	–0.22911	0.51059		
3	–0.39902	0.73042	0.11899		
4	0.50167	1.07319	0.27195		
a_H					
j	a_j	b_j	c_j	*ma*	*ca*
1	–0.14318	1.82442	–0.55187	0.67849	–1.95537
2	0.29591	0.77564	0.19822		
3	0.32177	0.63773	0.13164		
4	–5.37610	–0.96230	1.47828		
5	16.1721	–3.29980	3.43990		
a_V					
1	–0.07771	2.33840	-0. 76284	– 0.053739	0.83433
2	0.56727	0.95545	0.54039		
3	–0.20238	1.14520	0.26809		
4	–48.2991	0.791669	0.116226		
5	48.5833	0.791459	0.116479		

ITU-R P.838 also recommends that for linear and circular polarization, and for all path geometries, the regression coefficients (κ and α) can be calculated from the values given by equations (4.21) and (4.22) using the following equations:

$$k = [k_H + k_v + (k_H - k_v)\cos^2\theta\cos 2\tau] / 2 \quad 4.23$$

$$\alpha = [k_H a_H + k_v a_v + (k_H a_H - k_v a_v)\cos^2\theta\cos 2\tau] / 2k \quad 4.24$$

where θ is the path elevation angle and τ is the polarization tilt angle relative to the horizontal polarization ($\tau = 45°$ for circular polarization).

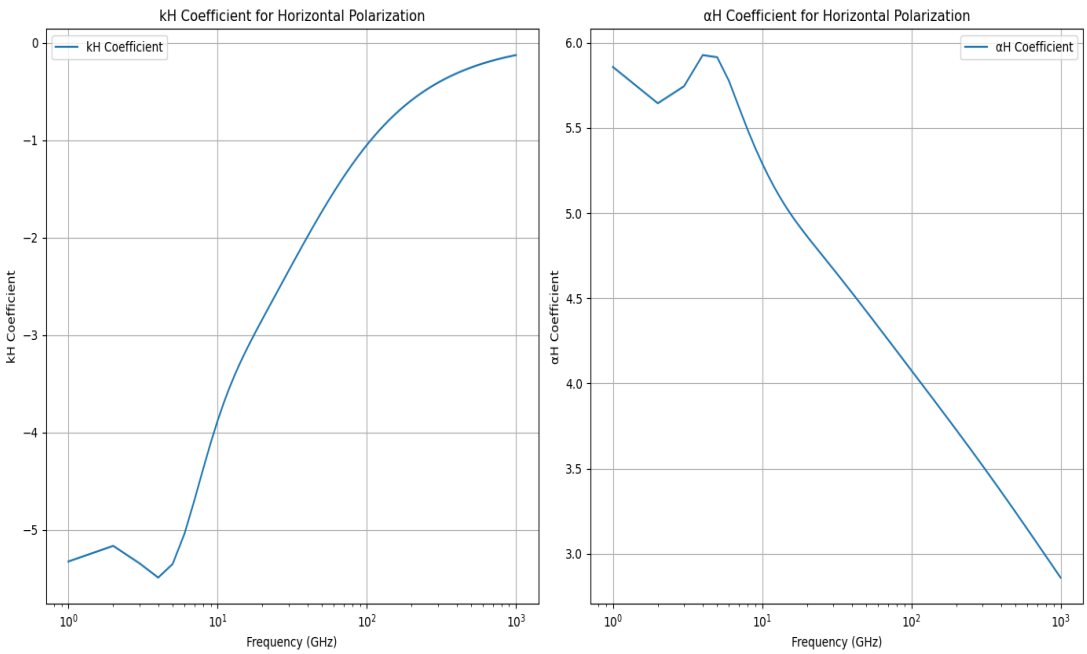

Figure 4-12 k_H *and* a_H Coefficients for Horizontal Polarization

The k_H and a_H coefficients for horizontal polarization are crucial for understanding rain attenuation in radio communication systems. The k_H coefficient, depicted on a logarithmic frequency scale, starts negative, increases with frequency, and plateaus near zero around 100 GHz, indicating increasing specific attenuation due to rain that stabilizes at higher frequencies. Conversely, the a_H coefficient starts just above 3, peaks over 5.5 around 10 GHz—marking the most significant rain impact on signal attenuation—then sharply declines below 3 by 100 GHz. These trends are vital for engineers to design and optimize communication systems to withstand frequency-specific environmental conditions.

The frequency-dependent coefficients, k_H, k_v, a_H, and a_v, that are used for

estimating specific rain attenuation are crucial in predicting signal loss due to rain in communication systems. These coefficients vary with frequency and are determined based on scattering calculations. The ITU-R P.838 provides the value of those cofficients for frequency ranging from 1GHz to 100GHz and are presented in a table in Annex 3.

4.4.5 ITU-R P.839 Model

ITU-R P.839 model provides a method to predict the rain height for propagation prediction. It is used in conjunction with other propagation models to predict the attenuation and delay of radio waves due to rain. The rain height is the height above mean sea level where the rain intensity is maximum. The rain height is important for the design of terrestrial line-of-sight systems, especially in the microwave frequency range, where rain attenuation can be significant.

The recommendation outlines how to calculate the rain height based on geographic latitude. This is important because the height at which rain occurs can significantly affect the attenuation of radio signals as they pass through the atmosphere. The model considers the fact that rain does not occur at a uniform height across the globe; for example, rain typically occurs at higher altitudes near the equator than it does at higher latitudes.

The average yearly height of rain, denoted as h_R, can be determined using the 0° C isotherm height, h_0, by adding 36 kilometers to it as:

$$h_R = h_0 + 36\text{km} \tag{4.25}$$

In regions lacking specific data, the average annual 0° C isotherm height above sea level, h_0, is a crucial component of this Recommendation. The provided data spans longitudes from 0° to 360° and latitudes from +90° to -90°. If the desired location does not align with the provided grid points, the mean annual 0° C isotherm height above sea level for that location should be calculated using bilinear interpolation based on the nearest four grid points' values.

4.5 Data Processing for Rain Attenuation Modeling

The performance of wireless networks operating in microwave and millimeter-wave bands is often hindered by rainfall intensity, prompting radio engineers to incorporate rainfall attenuation into overall link budgets for consistent performance. This involves

determining the point rain rate R0.01 (in mm/h), indicative of the rainfall rate exceeded for 0.01% of an average year, typically measured over one-minute intervals. Obtaining such data can be challenging in regions like Africa and Ethiopia, where one-minute rainfall measurements are scarce, but many meteorological agencies archive data from rain gauges at longer intervals, such as hourly or daily. In the absence of one-minute data, credible rain rate climatological models offer a means to convert rainfall data from longer integration times to shorter ones, but this research intendes to use the 15-min actual data directely rather than applying conversion models where there may be a loss of data. The model here relay solely on the data quality because the model completely depends on historical events to accutrately predict the future events. This can ensure reliability and precision in designing wireless communication systems in microwave and millimeter-wave bands in areas with limited one-minute rainfall data availability.

For validation of this study, precipitation data has been properly analysed for Addis Ababa city where the microwave link this study is performed. The rain rate data for this city has been filtered and sorted using Microsoft excel to determine the rain rate distribution for Addis Ababa city. The actual 15-min precipitation in mm has been multiplied by 4 to change it to mm/hr unit. The converted 15-min rain rate data in mm/hr for the period 8 years the selected city can be visualized in the graph below;

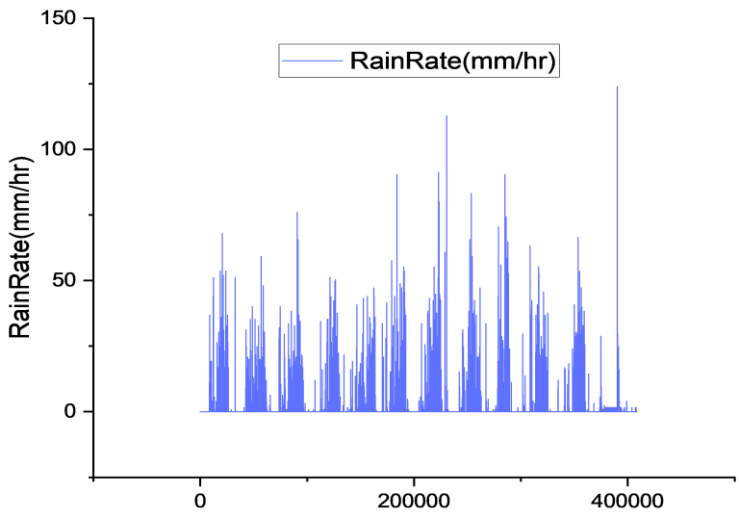

Figure 4-13 8-years rain rate visualization of Addis Ababa

4.5.1 Determination of Rain Rate $R_{0.01}$

ITU-R P.837-7 proposes a method of determining the rainfall rate that surpasses a specific average annual probability of occurrence at a given location. This method uses digital maps of monthly total rainfall and monthly mean surface temperature to calculate the rainfall rate that surpasses a specified average annual probability of occurrence at a given location on the Earth's surface.

Implementing ITU-R models using Python offers numerous advantages. Python's open-source nature and large community make these models widely accessible, fostering collaboration and knowledge-sharing among researchers and practitioners. Python's simplicity and readability simplify the implementation process, enabling rapid development and prototyping of applications. Integration with popular scientific libraries like NumPy and SciPy facilitates data analysis and visualization, enhancing the utility of ITU-R models. Python's interactive capabilities, particularly in environments like Jupyter Notebooks, enable users to explore and experiment with models interactively. Additionally, Python's scalability ensures that ITU-R models can be applied to a wide range of scenarios, from small-scale simulations to large-scale analyses, meeting diverse research and industry needs. The computation of ITU-R P.837-7 in python can be drawn a simple high-level algorithm as follow;

Algorithm 1: ITU-R P.837-7

```
Start;
Preparation;
Import Libraries:
    numpy
    astropy
    scipy
    itur models and utilities
    Define Classes and Methods;
Data Loading;
    Load Interpolator Data;
    Load Monthly Mean Surface Temperature Data;
    Load Monthly Mean Total Rainfall Data;
Modelling;
```

Calculate Monthly Mean Surface Temperature;
Convert Temperature from Kelvin to Celsius;
Determine Monthly Mean Total Rainfall;
Use Mt Function with Interpolator;
Calculate Probability of Rain for Each Month;
Calculate rii with Temperature Data;
Calculate P0ii (Monthly Probability of Rain);
Update rii and P0ii if P0ii >70
Compute Annual Probability of Rain (P0annual);
Compute Rainfall Rate Exceeded for a Certain Percentile;
Check if Percentile is 0.01, Return R001 Value;
Use Bisect Method for Given Percentile;

Results;

Return Annual Probability of Rain;
Return Rainfall Rate Exceeded for a Certain Percentile;

End;

The above algorithm has been used to compute the probability of excedence for the data for addis ababa city. Eventhough, the study focusses mainly on the behaiviour of rain fall, it also covers temperature and relative humidity data processing and analysis as those environmental variables also contribute significant amount of signal power degradation. Thus, the pdf, cdf and ccdf of those data has been furthure analysied using Microsoft excel data analysis tool to clearly seen the features of each data. Sample of this proceesed data can be visualized in the table below;

Table 4-4 Sample Processed $R_{0.01}$ Data

DateTime+E10E1/	Precipitatic	RainRate(n	rank	Probability of Exceedance(%)
11/2/2018 11:45	28.2	112.8	1	3.83E-06
8/15/2018 3:15	22.8	91.2	2	7.66E-06
7/7/2017 18:15	22.6	90.4	3.5	1.34E-05
8/16/2020 16:15	22.6	90.4	3.5	1.34E-05
6/29/2019 16:45	20.8	83.2	5	1.91E-05
8/22/2018 3:45	20	80	6	2.30E-05
8/6/2014 16:15	19	76	7	2.68E-05
8/28/2020 14:45	18.6	74.4	8	3.06E-05
6/14/2020 13:45	17.6	70.4	9	3.45E-05

4.5.2 Conversion of 15-min to 1-min Rainfall Rate Distribution

Converting rain-rate cumulative distributions from any integration time, T, to one minute presents a practical alternative in cases where local one-minute data, either in time series or cumulative distribution functions, are unavailable for microwave system design. Analysis of converting rainfall cumulative distributions derived from time series with integration times differing from the recommended one-minute interval has been a topic of study since the 1980s[83, 84].

The cumulative distribution of rainfall rate for a one-minute integration time can be derived by converting cumulative distributions with longer integration times using the following relationship:

$$R_1(p) = a(R_t(p))^b \qquad 4.26$$

Where:

$R_1(p)$ is the rainfall rates with 1-minute integration time and $(R_t(p)$ is t-minute integration time exceeded with equal probability, p, and t is the integration time in minutes (15-minutes as for this study).

a and b are the regression coefficients for conversions from 15 min to 1 min in temprate region and are available in the Table 2 of [83] for 5-min to 1-min, 10-min to 1-min, 20-min to 1-min, 30-min to 1-min and 60-min to 1-min. a and b are given as global coefficient and can be calculated using the following formula;

$$a = 0.0002t^2 - 0.0189t + 1.136 \qquad 4.27$$

$$b = 0.0063t + 1.10366 \qquad 4.28$$

From the Köppen climate classification of Ethiopia shown in Figure 4.4, the climate zone of Addis Ababa city is humid subtropical climate with Cwb Köppen class and falls under the temprate region of [83]. a and b are not available for conversion of 15-min to 1-min in the table. Hence, the are calculated using equation 4.27 and 4.28 by replacing t with 15. The numerical value has been gotten as $a = 0.8525$ and $b = 1.19816$. The correlation coefficient, ρ, has been neglected for this calculation.

Using equation 4.26 – 28, $R_1(p)$ for Addis Ababa city has been processed and sample data can be visualized in the table below;

Table 4-5 Sample Processed Data of $R_1(p)$

DateTime	Precipitation(mm)	RainRate(mm/hr)	rank	R0.01(mm/hr)	Rt(p)(mm/hr)	a	b	R1(p)(mm/hr)
11/2/2018 11:45	28.2	112.8	1	3.83E-06	3.83E-06	0.8525	1.19816	2.76E-07
8/15/2018 3:15	22.8	91.2	2	7.66E-06	7.66E-06	0.8525	1.19816	6.33E-07
7/7/2017 18:15	22.6	90.4	3.5	1.34E-05	1.34E-05	0.8525	1.19816	1.24E-06
8/16/2020 16:15	22.6	90.4	3.5	1.34E-05	1.34E-05	0.8525	1.19816	1.24E-06
6/29/2019 16:45	20.8	83.2	5	1.91E-05	1.91E-05	0.8525	1.19816	1.90E-06
8/22/2018 3:45	20	80	6	2.30E-05	2.30E-05	0.8525	1.19816	2.36E-06
8/6/2014 16:15	19	76	7	2.68E-05	2.68E-05	0.8525	1.19816	2.84E-06
8/28/2020 14:45	18.6	74.4	8	3.06E-05	3.06E-05	0.8525	1.19816	3.33E-06
6/14/2020 13:45	17.6	70.4	9	3.45E-05	3.45E-05	0.8525	1.19816	3.83E-06

4.5.3 Determination of Specific Attenuation

Specific attenuation serves as the primary measure in calculating rain attenuation for both terrestrial and slant paths, expressed as the attenuation per unit distance (dB/km). It holds significant importance in the formulation of predictive rain attenuation models.

The approach to forecasting rain attenuation relies on the correlation between specific attenuation and rain rate, which is determined by modeling factors such as rain shape, size, temperature, and terminal velocity of raindrops. Rain attenuation is computed by integrating specific attenuation over the propagation path. The computation of specific attenuation necessitates a cumulative distribution of one-minute rain rates[15, 85]. ITU-R P. 838-3 suggests a method called power-law equation, available in 4.20 for specific attenuation (γ) caused by rain for radio links operating within frequencies up to 1000 GHz. It utilizes input data such as rainfall rate (R) evaluated over a one-minute integration period, along with parameters like link frequency, polarization, and elevation angle.

The power-law expression for rain-specific attenuation is highly convenient and widely applied in computing rain attenuation statistics. Specific attenuation, representing the attenuation per unit distance, plays a crucial role in these calculations. Typically, such parameters are determined by assessing the electromagnetic power that is scattered and absorbed by raindrops along the path traversed by the wave.

Equation 4.23 and 4.24 needs the k and α value calculated from the rain rate and the link profile parameters. The variables to calculate k and α includes k_H, k_v, a_H, a_v θ and τ. ITU-R P. 838-3 has provided the value of k_H, k_v, a_H, and a_v for frequency ranging from 1GHz to 1000 GHz. The frequency band that this study is interested in

is $f = 11\text{GHz}$. The k_H, k_v, a_H, and a_v value for this frequency band is presented in the table below:

Table 4-6 k_H, k_v, a_H, and a_v value of 11 GHz

f	k_H	k_v	a_H	a_v
11GHz	0.01772	1.2140	0.01731	1.1617

Whereas, the value of θ and τ need to be determined from the knowledge of the microwave link profile. θ is the elevation angle the link and can be determined using the following formula;

$$\theta = tan^{-1}(\frac{R_x\, height - T_x\, height}{d}) \quad 4.29$$

Where $R_x\, height$ and $T_x\, height$ are receiver and transmitter height of the microwave link in meters and d is the link length in km.

From Table 4.2, the elevation of T_x and R_x above sea level is given as 2842m and 2401m. The link length $d = 16.42$ km. The antenna hight is also given as 10m for both T_x and R_x. $T_x\, height$ and $R_x\, height$ should the sum of the elevation above sea level and the antenna height. Thus,

$T_x\, height = 2842m + 10m = 2852m$, and $R_x\, height = 2401m + 10m = 2411m$.

Thus,

$$\theta = tan^{-1}(\frac{2411-2852}{16420}) = -1.54 \quad 4.30$$

The polarization tilt, denoted by τ, refers to the angle between the electric field vector of the transmitted microwave signal and the vertical axis. For a vertical polarization microwave link, the electric field vector is aligned vertically. Therefore, the polarization tilt, τ, for a vertical polarization microwave link is 0 degrees since there is no tilt away from the vertical axis.

Thus,

$$\tau = 0 \quad 4.31$$

Using the equation 4.23, the regression coefficient, k, can be calculated as:

$k = [k_H + k_v + (k_H - k_v)\, cos^2\, \theta\, cos\, 2\tau]/2$

$k = [\, 0.01772 + 1.2140 + (0.01772 - 1.2140)\, cos^2(-1.54)\, cos\, 2(0)]/2$

$$k \approx 0.02 \qquad 4.32$$

Using the equation 4.24, the regression coefficient, α, can be calculated as:

$$\alpha = [k_H a_H + k_v a_v + (k_H a_H - k_v a_v)\cos^2\theta \cos 2\tau] / 2k$$

$$\alpha = [0.01772 * 0.01731 + 1.2140 * 1.1617 + (0.01772 * 0.01731 - 1.2140 * 1.1617)\cos^2\theta \cos 2\tau]/2k$$

$$\alpha \approx 0.25 \qquad 4.33$$

Thus, the regression coefficients for the desired microwave link have been calculated and approximated to values given above.

As proposed by the ITU-R P. 838-3, applying the power low equation to calculate the specific attenuation is the most appropriate method as agreed by many researchers. The power low equation, which is given in equation 4.20, has been used to calculate the specific attenuation for the desired microwave link as follow;

$$\gamma_R \left({}^{dB}/_{km}\right) = kR_{0.01}{}^{\alpha}$$

$$\gamma_R \left({}^{dB}/_{km}\right) = 0.02\, R_{0.01}{}^{0.25} \qquad 4.34$$

Sample Processed data can be seen in the table below;

Table 4-7 Sample Processed Specific Attenuation Data

rank	R0.01(mm/hr)	Rt(p)(mm/hr)	a	b	R1(p)(mm/hr)	κ	α	γR (dB/km)
1	3.83E-06	3.83E-06	0.853	1.1982	2.76E-07	2.00E-02	2.50E-01	8.85E-04
2	7.66E-06	7.66E-06	0.853	1.1982	6.33E-07	2.00E-02	2.50E-01	1.05E-03
3.5	1.34E-05	1.34E-05	0.853	1.1982	1.24E-06	2.00E-02	2.50E-01	1.21E-03
3.5	1.34E-05	1.34E-05	0.853	1.1982	1.24E-06	2.00E-02	2.50E-01	1.21E-03
5	1.91E-05	1.91E-05	0.853	1.1982	1.90E-06	2.00E-02	2.50E-01	1.32E-03
6	2.30E-05	2.30E-05	0.853	1.1982	2.36E-06	2.00E-02	2.50E-01	1.38E-03
7	2.68E-05	2.68E-05	0.853	1.1982	2.84E-06	2.00E-02	2.50E-01	1.44E-03
8	3.06E-05	3.06E-05	0.853	1.1982	3.33E-06	2.00E-02	2.50E-01	1.49E-03
9	3.45E-05	3.45E-05	0.853	1.1982	3.83E-06	2.00E-02	2.50E-01	1.53E-03

4.5.4 Determination of Rainfall Attenuation

Rainfall-induced attenuation at frequencies exceeding 10 GHz is particularly significant for terrestrial point to point or point to multipoint links and ground-to-space radio links, particularly in tropical regions where rainfall intensity is high. In conjunction

with rain rate measurement campaigns, acquiring data on signal attenuation is essential for comparison with existing prediction models. Rain attenuation along a terrestrial path is determined by multiplying specific attenuation (measured in dB/km) by the effective propagation path length (in kilometers)[12].

The ITU-R P.530 model[86] presents a straightforward method for estimating the prolonged statistical characteristics of rain attenuation. The path attenuation is derived via this technique;

$$A(dB) = \gamma_R \left({}^{dB}/_{km}\right) \times \mathrm{d}_{eff}(km) \qquad 4.35$$

The effective path length, $\mathrm{d}_{eff}(km)$, is the multiplicative result of the actual path length, d(km) and the distance factor, r, as expressed in equation 4.2. Equation 4.1 provides the formula to determine the the distance factor. The actual distance, d(km) for the microwave link that this study considers is 16.42 km as given in table 4.2, and the distance factor can then be calculated as follow;

The frequency band $f = 11 \times 10^9\ Hz,\ d = 16.42km = 16420m,\ \alpha = 0.25$

$$r = \frac{1}{0.477(16420)^{0.633} R_{0.01}^{0.073(0.25)} (11\times10^9)^{0.123} - 10.579(1-exp(-0.024(16420)))}$$

$$r = \frac{1}{3818.99 R_{0.01}^{0.018} - 10.579} \qquad 4.36$$

The $R_{0.01}$ value have been computed in previous section for the historical data. The effective path length can be defined as;

$$d_{eff}(km) = d(km)r$$

$$d_{eff}(km) = \frac{16.42}{3818.99 R_{0.01}^{0.018} - 10.579}\ km \qquad 4.37$$

Because effective path length is rain rate dependant value, it has been computed for both 15-min rain rate distribution and 1-min rain rate distribution. This can be visualized in the graph below;

By incorporating this formula in the excel file for this historical data, the total rain attenuation for the historical data can be derived from equation 4.34 and 4.37 as follow;

$$A_{0.01}(dB) = \gamma_R \left({}^{dB}/_{km}\right) \times \mathrm{d}_{eff}(km)$$

$$= 0.02\, R_{0.01}{}^{0.25} \times \frac{16.42}{3818.99 R_{0.01}^{0.018} - 10.579} \text{ dB}$$

$$A_{0.01} = \frac{0.33 R_{0.01}{}^{0.25}}{3818.99 R_{0.01}^{0.018} - 10.579} \text{ dB} \qquad 4.38$$

Using equation 4.38, historical data of rain attenuation of the microwave link introduced in section 4.2.2 has been processed, which later then be used as input data the proposed LSTM algorithm. This is done, because, there is no historical rain attenuation data localy as the rain rate data were abotained. If there were historical attenuation data in dB alongside with the rain rate data, it would have been much easier to directly emplemen the deep learning algorithm as those algorithms can learn the data behaviour and predict the future event using history.

4.6 Rain Attenutaion Prediction Modeling Using LSTM

AI Techniques have not been utilized widely in modeling of rain attenuation prediction until present day. Much of the studies conducted previously focus on using traditional stastistical, empreical or physical modelling methods to predict the rain causes either terrestrial links or satellite links. This is because the very unlinear nature of the rainfall and lack of designated measurement of attenuation data due to rain on communication links. AI models on the other hand, can perform prediction of future event with excellent accuracy and precision. Even though, rain attenuation data from local station is not available, this study has developed a way of calculating the rain attenuation using the ITU-R models as it has been covered in previous section. In this section of the study, deep learning method of rain attenuation, LSTM model, will be discussed in detail.

4.6.1 The Long Short Time Memory (LSTM) Prediction Model

In 1997, Sepp Hochreiter and Jürgen Schmidhuber introduced Long Short-Term Memory (LSTM). By employing constant error carousel (CEC) units, LSTM addresses issues like exploding and vanishing gradients. The initial iteration of the LSTM block comprised cells, along with input and output gates. Renowned for its architecture, LSTM stands out as a specific kind of recurrent neural network, finding diverse applications not feasible with standard RNNs. Unlike traditional RNNs, which suffer from the vanishing gradient problem due to their limited capacity to retain past state information, LSTM

effectively mitigates this issue.

LSTM was designed specifically to address the challenge of handling long-term dependencies, inherently capable of retaining information over extended periods by default. Unlike traditional RNNs, which feature repetitive chain modules within the neural network, typically represented by simple structures like the tanH layer, LSTM employs an analogous chaining structure. This approach deviates from the single-layer neural network paradigm and contributes to LSTM's effectiveness in managing long-term dependencies.

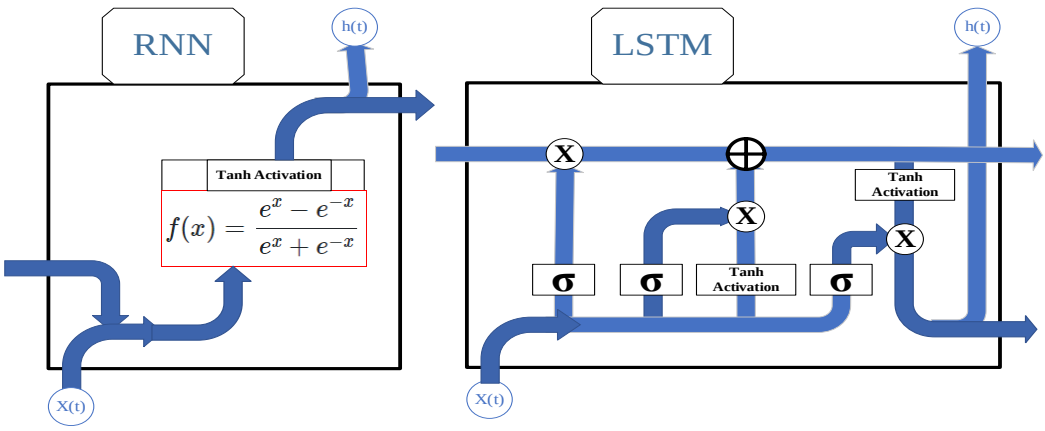

Figure 4-14 Chaining Structure of RNN vs LSTM

In comparison to RNNs, LSTM incorporates an additional component known as memory, which includes:

- A forget gate (f), represented by a neural network with sigmoid activation
- A candidate layer (C), which comprises a neural network with tanH activation
- An input gate (I), implemented as a neural network with sigmoid activation
- An output gate (O), structured as a neural network with sigmoid activation
- The hidden state (h)
- The memory cell (C)

LSTM model can be explained in the following four steps and can visualized in the figure 4.17.

Step 1: To predict future sequences, it is necessary to utilize the cell state to retain pertinent information from past inputs, ensuring accurate predictions. Then the incoming data can be linked to previous patterns in the time-series data. This process can be formulated as forget gate equation as follow;

$$f_t = \sigma\left(W_f \times [h_{t-1}, x_t] + b_f\right) \qquad 4.39$$

Step 2: Determining crucial information for storage involves two stages. The first input gate layer, employing a sigmoid layer, decides which values to update. Subsequently, a tanH layer generates a vector for new candidate values, termed which is combined with the input gate's decision to update the state. This phenomenon can be formulated as candidate gate equations as follow;

$$\left.\begin{aligned} i_t &= \sigma(W_i \times [h_{t-1}, x_t] + b_i) \\ \overline{C_t} &= \tanh\,(W_c \times [h_{t-1}, x_t] + b_c) \end{aligned}\right\} \qquad 4.40$$

Step 3: Updating the old cell state to the new cell state, involves multiplying the old state by the forget gate discarding unnecessary elements. Then, the product of the input gate and the candidate gate creates the new candidate value, adjusted by the update decisions. This can be given as the cell state information given as follow;

$$C_t = f_t \times C_{t-1} + i_t \times \overline{C_t}) \qquad 4.41$$

Step 4: Determining the output state involves filtering the cell state. The first sigmoid layer decides which part of the cell state's output to produce, followed by applying the tanH function to the cell state and multiplying it by the sigmoid gate's output. This process enables the generation of output based on the decision-making mechanism and it can be formulated as follow;

$$\left.\begin{aligned} O_t &= \sigma(W_o \times [h_{t-1}, x_t] + b_o) \\ h_t &= O_t \times \tanh(C_t) \end{aligned}\right\} \qquad 4.42$$

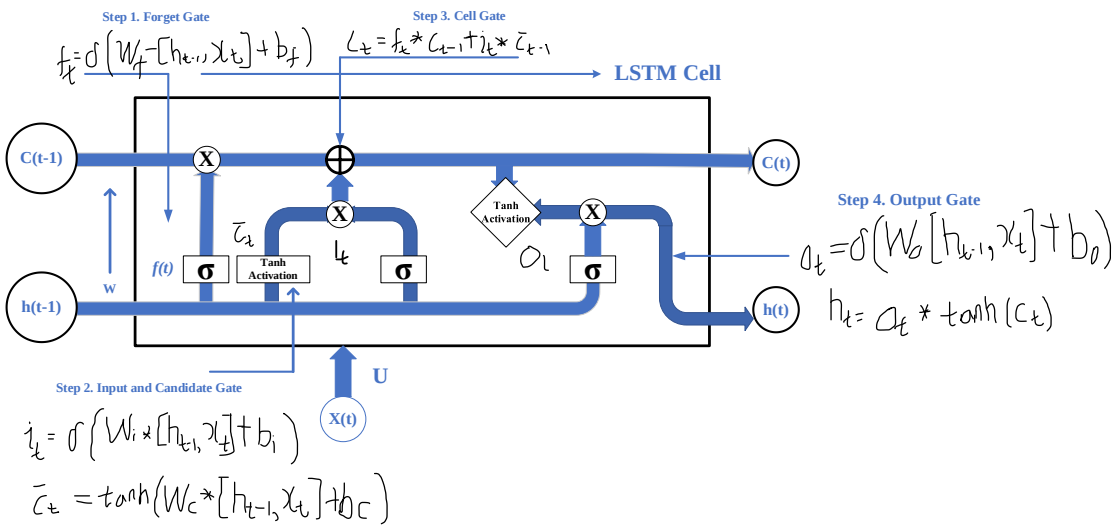

Figure 4-15 LSTM cell architecture with formulas

4.6.2 LSTM Based Rain Attenuation Prediction Model

Rain attenuation poses a significant challenge for terrestrial or satellite communications, affecting link availability. To address this issue, researchers have developed various methods, including complex mathematical models and data-driven approaches. One such intriguing approach is the Long-Short Term Memory (LSTM) network, a deep learning algorithm based on artificial recurrent neural networks.

This study proposes a method of rain attenuation prediction using LSTM model. The model proposed here have 7 input features and output feature. The input output schematic diagram of proposed LSTM model can be seen below;

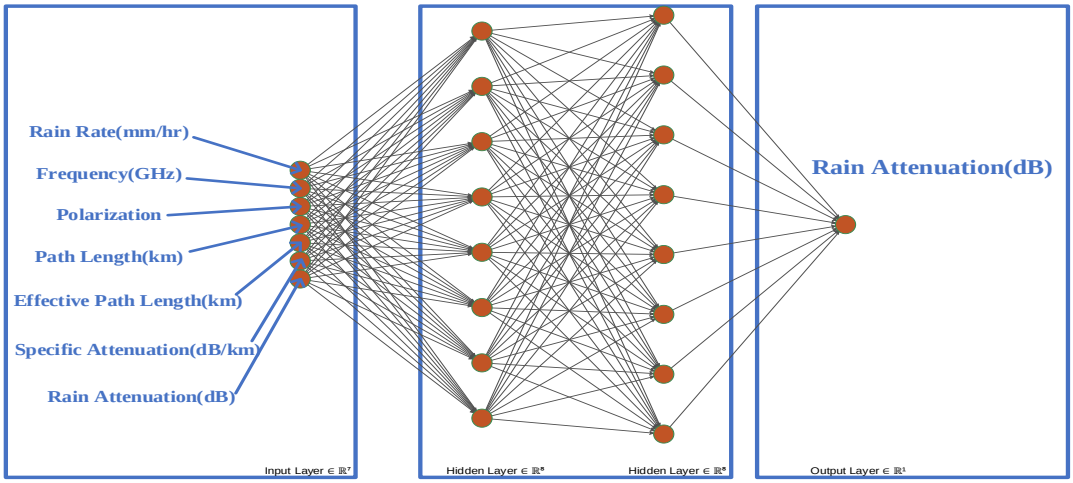

Figure 4-16 Schematic diagram of proposed LSTM model

The LSTM model designed here has four layers; an input layer, two hidden layers and an output layer. The input layer has the 7 inputs; Rain Rate(mm/hr), Frequency (GHz), Polarization, Path Lebgth(km), Effective Path Length(km), Specific Attenuation(dB/km) and Rain Attenuation(dB). The two hidden layers have 8 nodes and lastely the output layer has one output feature, Rain Attenuation(dB).

4.6.3 Model Implementation in Python

The python implementation of the model strats by importing a set of essential libraries for data manipulation, visualization, and deep learning tasks. The `os` library is used for interacting with the operating system, while `datetime` handles date and time data. `IPython` and `IPython.display` provide utilities for interactive computing and displaying outputs, respectively. `matplotlib` and `seaborn` are employed for data visualization, with

`matplotlib.pyplot` providing plotting functionality and `seaborn` offering enhanced statistical graphics. `numpy` is utilized for numerical computing tasks, and `pandas` is employed for data manipulation, particularly for handling tabular data structures. The `tensorflow` library is imported for deep learning tasks, serving as a comprehensive framework for building and training the neural networks of LSTM mode.

```
import os
import datetime

import IPython
import IPython.display
import matplotlib as mpl
import matplotlib.pyplot as plt
import numpy as np
import pandas as pd
import seaborn as sns
import tensorflow as tf
```

The df.describe().transpose() statement generates summary statistics for each numerical column in the DataFrame df, such as count, mean, standard deviation, minimum, quartiles, and maximum values. The describe() method computes these statistics, while the transpose() function flips the orientation of the result, making it more readable by displaying the statistics as columns and the variables as rows.This can be seen as below;

	count	mean	std	min	25%	50%	75%	max
RainRate(mm/hr)	43523	0.121591	1.370636	0	0	0	0	65.6
Temperature(°C)	43523	16.76177	4.537377	-0.3	13.5	16.2	20.3	29.1
R.Humidity(%RH)	43523	62.01187	22.33559	5.7	43.5	62.5	81.9	100
R0.01(mm/hr)15-min	43523	0.500028	0.088322	4.21E-05	0.516145	0.516145	0.516145	0.516145
S.A0.01(dB/km)15-min	43523	0.016671	0.001818	0.00161	0.017	0.017	0.017	0.017
Deff(km)15-min	43523	0.00437	5.69E-05	0.00436	0.00436	0.00436	0.00436	0.00517
A0.01(dB)15-min	43523	7.26E-05	7.55E-06	8.33E-06	0.000074	0.000074	0.000074	0.000074
R0.01(mm/hr)1-min	43523	0.373761	0.067064	4.88E-06	0.386	0.386	0.386	0.386
S.A0.01(dB/km) 1-min	43523	0.015462	0.001867	0.00094	0.0158	0.0158	0.0158	0.0158
Deff(km)1-min	43523	0.004402	6.74E-05	0.00439	0.00439	0.00439	0.00439	0.00538
A0.01(dB)1-min	43523	6.77E-05	7.83E-06	5.05E-06	6.91E-05	6.91E-05	6.91E-05	6.91E-05
Day sin	43523	-0.00066	0.707133	-1	-0.70711	-1.1E-13	0.707107	1
Day cos	43523	-0.00034	0.707096	-1	-0.70711	-7E-14	0.707107	1
Year sin	43523	0.000695	0.698709	-1	-0.69009	-0.00065	0.69238	1
Year cos	43523	0.009328	0.715361	-1	-0.71356	0.016503	0.73169	1

Code flowcharts are an easy way to get the mind map of any code of a specific task. The full code flowchart has been drawn and presented below to better help readers to understand the code and the model as well.

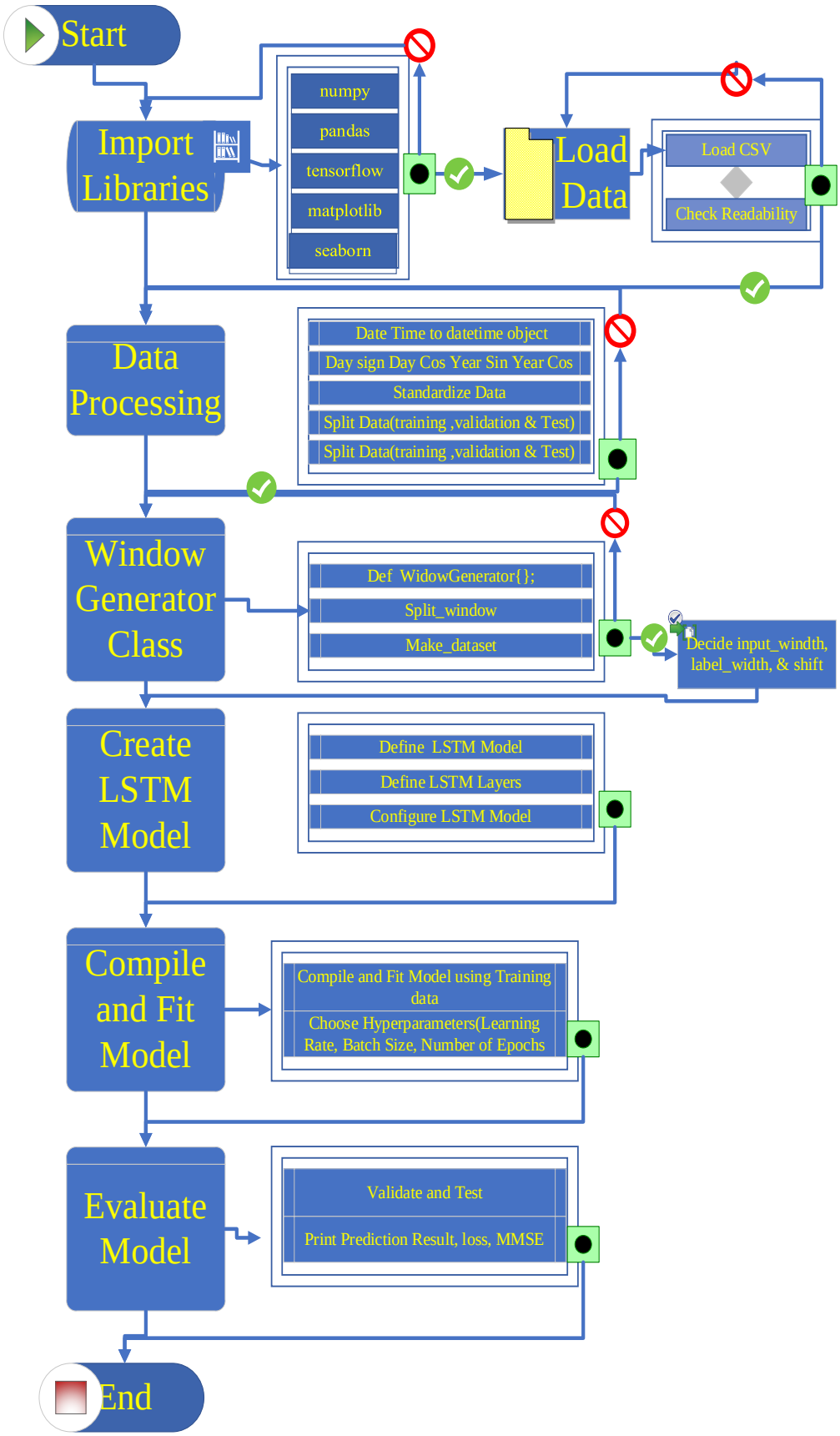

Figure 4-17 Code flowchart of LSTM model

Figure 4.15 Code flowchart of LSTM model

This matplotlib function helps in configuring the visual aspects of plots created with matplotlib. The figure size and grid lines are set to ensure that all plots have a consistent appearance, making the data visualization process more standardized and the results easier to interpret. This has been seat using the following statement;

```
mpl.rcParams['figure.figsize'] = (8, 6)
mpl.rcParams['axes.grid'] = False
```

The dataset is loaded from a specified CSV file path into a pandas DataFrame. This DataFrame serves as the primary data structure for subsequent operations. The path points to a file containing time series data related to rain attenuation, which is likely a collection of measurements over time.

The data preprocessing involves selecting a subset of the data and converting date and time information into a format suitable for analysis. The DateTime column is transformed into a series of timestamp values, which are more amenable to feature engineering and time series forecasting models.

```
df = pd.read_csv(csv_path)
# Slice [start:stop:step], starting from index 5 take every 6th record.
df = df[5::6]
date_time = pd.to_datetime(df.pop('DateTime'), format='%m/%d/%Y %H:%M')
```

The feature engineering section of the code gives a command that creates new features from the timestamp data to capture cyclical patterns within the day and across the year. These features, such as 'Day sin' and 'Year cos', help the model recognize and leverage periodicity in the data, which is especially useful in time series forecasting where seasonality may play a significant role. This can bee coded as follow;

```
day = 24*60*60
year = (365.2425)*day

df['Day sin'] = np.sin(timestamp_s * (2 * np.pi / day))
df['Day cos'] = np.cos(timestamp_s * (2 * np.pi / day))
df['Year sin'] = np.sin(timestamp_s * (2 * np.pi / year))
df['Year cos'] = np.cos(timestamp_s * (2 * np.pi / year))
```

The next step of the code development for LSTM model is the data splitting process. The dataset is split into three distinct sets: training, validation, and test. The training set comprises **70%** of the data and is used to train the machine learning model. The validation set makes up **20%** and is utilized for tuning the model's hyperparameters and preventing overfitting. The remaining **10%** is designated as the test set, which is used to evaluate the model's performance on new, unseen data. This specific division strategy is intentional and avoids random shuffling for two key reasons. First, it allows for the creation of sequential data windows, which are vital for time series forecasting models that rely on the order of data points. Second, it ensures that the model's evaluation is based on the most recent data, reflecting a more realistic scenario where the model is tested on future data following its training period. This approach aligns with real-world applications where models are deployed to make predictions on data that comes sequentially after the training phase.

```
column_indices = {name: i for i, name in enumerate(df.columns)}

n = len(df)
train_df = df[0:int(n*0.7)]
val_df = df[int(n*0.7):int(n*0.9)]
test_df = df[int(n*0.9):]

num_features = df.shape[1]
```

Normalization is applied to the data to scale the feature values. This helps in speeding up the training process and improving the model's performance as it ensures that all features contribute equally to the model's learning.

```
train_mean = train_df.mean()
train_std = train_df.std()

train_df = (train_df - train_mean) / train_std
val_df = (val_df - train_mean) / train_std
test_df = (test_df - train_mean) / train_std
```

The WindowGenerator class is an ingeniously crafted tool within the time series forecasting framework, designed to streamline the creation of input and label windows for models like LSTMs. This class meticulously segments the dataset into windows of consecutive samples, which are essential for the model to learn temporal patterns and make predictions. The windows are defined by their width, indicating the amount of

historical data considered, and the time offset, dictating the prediction horizon. By incorporating features as inputs, labels, or both, the WindowGenerator facilitates various model architectures and prediction tasks, from single-output to multi-output and from single-time-step to multi-time-step forecasts. This versatile approach to data windowing is crucial for models to capture the inherent dependencies in time series data, ensuring that the model can be trained effectively to make accurate forecasts, whether it's predicting 24 hours into the future or another specified timeframe. The class's flexibility allows it to adapt to different models and tasks, making it a cornerstone of the time series analysis process. The WindowGenerator class is defined as follow;

```
class WindowGenerator():
  def __init__(self, input_width, label_width, shift,
               train_df=train_df, val_df=val_df, test_df=test_df,
               label_columns=None):
    # Store the raw data.
    self.train_df = train_df
    self.val_df = val_df
    self.test_df = test_df

    # Work out the label column indices.
    self.label_columns = label_columns
    if label_columns is not None:
      self.label_columns_indices = {name: i for i, name in
                                    enumerate(label_columns)}
    self.column_indices = {name: i for i, name in
                           enumerate(train_df.columns)}

    # Work out the window parameters.
    self.input_width = input_width
    self.label_width = label_width
    self.shift = shift

    self.total_window_size = input_width + shift

    self.input_slice = slice(0, input_width)
    self.input_indices = np.arange(self.total_window_size)[self.input_slice]

    self.label_start = self.total_window_size - self.label_width
    self.labels_slice = slice(self.label_start, None)
    self.label_indices = np.arange(self.total_window_size)[self.labels_slice]

  def __repr__(self):
    return '\n'.join([
        f'Total window size: {self.total_window_size}',
        f'Input indices: {self.input_indices}',
        f'Label indices: {self.label_indices}',
        f'Label column name(s): {self.label_columns}'])
```

Instances of the WindowGenerator class are created with specific configurations for the input and label windows. Methods are defined within the class to handle the splitting of data into windows, plotting of the results, and creating TensorFlow datasets ready for model training. The WindowGenerator class, coupled with its split_window method, forms a comprehensive system for preparing time series data for LSTM models. Instances of this class are configured with specific parameters that define the size and structure of input and label windows, essential for capturing temporal dependencies within the data. The split_window method takes a sequence of consecutive data points and deftly partitions them into inputs and labels, adhering to the class's configuration. It ensures that features designated as labels are correctly aligned and stacked, while also meticulously setting the shapes of the resulting tensors to maintain consistency and facilitate inspection. This harmonious integration of window generation and data splitting is vital for training robust time series models, allowing them to learn from historical data and make accurate predictions about future events, whether it's forecasting rain rates or other time-dependent variables. The WindowGenerator thus serves as a cornerstone in the modeling process, ensuring data integrity and model readiness for a variety of forecasting tasks. The split_window function is defined as follow;

```
def split_window(self, features):
  # Slice the features to get the inputs
  inputs = features[:, self.input_slice, :]
  # Slice the features to get the labels
  labels = features[:, self.labels_slice, :]
  # If specific columns are designated as labels, stack them together
  if self.label_columns is not None:
    labels = tf.stack(
        [labels[:, :, self.column_indices[name]] for name in self.label_columns],
        axis=-1)

  # Manually set the shapes of the inputs and labels
  inputs.set_shape([None, self.input_width, None])
  labels.set_shape([None, self.label_width, None])

  return inputs, labels
```

The make_dataset method within the WindowGenerator class is a streamlined process that transforms a time series DataFrame into a tf.data.Dataset composed of (input_window, label_window) pairs, ready for training LSTM models. It begins by converting the DataFrame into a NumPy array, ensuring compatibility with TensorFlow's

operations. Utilizing the timeseries_dataset_from_array function, it crafts a dataset where each sequence is a window of data points determined by the total_window_size. These sequences are shuffled to promote model generalization and batched for efficient training. The split_window method is then applied to each sequence, dividing it into input and label windows, which is a critical step for supervised learning. This method encapsulates the complexity of data preparation, providing a clean and efficient pathway to generate datasets that are primed for feeding into time series forecasting models.

```
def make_dataset(self, data):
  data = np.array(data, dtype=np.float32)
  ds = tf.keras.utils.timeseries_dataset_from_array(
      data=data,
      targets=None,
      sequence_length=self.total_window_size,
      sequence_stride=1,
      shuffle=True,
      batch_size=32,)

  ds = ds.map(self.split_window)

  return ds

WindowGenerator.make_dataset = make_dataset
```

The WindowGenerator class within the TensorFlow framework elegantly encapsulates the functionality needed to manage and access time series data for machine learning models. By defining properties like train, val, test, and example, it offers a seamless interface to the corresponding datasets, ensuring they are readily available as tf.data.Datasets. The example property is particularly ingenious, caching an example batch from the training data for quick and efficient access, which is invaluable for visualization and debugging. This design not only streamlines the data preparation process but also exemplifies the principles of object-oriented programming, where encapsulation and abstraction lead to more maintainable and reusable code. With these properties, the WindowGenerator serves as a robust foundation for developing sophisticated LSTM models capable of capturing complex temporal patterns in data. This functionality of the WindowGenerator object giving access to the tf.data.Dataset objects to easily iterate over the data has been designed as follow;

```
@property
def train(self):
  return self.make_dataset(self.train_df)

@property
def val(self):
  return self.make_dataset(self.val_df)

@property
def test(self):
  return self.make_dataset(self.test_df)

@property
def example(self):
  """Get and cache an example batch of `inputs, labels` for plotting."""
  result = getattr(self, '_example', None)
  if result is None:
    # No example batch was found, so get one from the `.train` dataset
    result = next(iter(self.train))
    # And cache it for next time
    self._example = result
  return result

WindowGenerator.train = train
WindowGenerator.val = val
WindowGenerator.test = test
WindowGenerator.example = example
```

The LSTM model for rain attenuation prediction is a specialized form of a Recurrent Neural Network (RNN), adept at handling time series data like weather patterns. RNNs, and by extension LSTMs, process data sequentially, maintaining an internal state to capture temporal dependencies across time steps. The LSTM layer, defined in TensorFlow as `tf.keras.layers.LSTM`, is particularly beneficial for this task due to its ability to remember long-term patterns and disregard irrelevant information, a feature crucial for predicting phenomena such as rain attenuation which depends on historical weather trends. An important constructor argument for all Keras RNN layers, such as tf.keras.layers.LSTM, is the return_sequences argument. This setting can configure the layer in one of two ways: The `return_sequences` parameter of the LSTM layer plays a pivotal role. If is's set to `False`, it primes the model with historical data before making a single prediction at the final time step. Conversely, setting it to `True` allows the model

to output predictions at every time step, which is essential for generating a continuous forecast or when constructing deeper networks with multiple RNN layers. This flexibility makes LSTMs highly effective for modeling and predicting complex sequential problems where the timing and order of events are key, such as in predicting the attenuation of rain over time. This model is programed as follow;

```
lstm_model = tf.keras.models.Sequential([
    # LSTM layer with 32 units.
    #'return_sequences=True' ensures that the LSTM outputs a sequence,
    # which is necessary if you're stacking LSTM layers or need
    # the full sequence for output.
    tf.keras.layers.LSTM(32, return_sequences=True),
    # Dense layer with a single unit for output.
    #This is typically used for regression tasks
    # or binary classification when the output is a single value.
    tf.keras.layers.Dense(units=1)
])
```

The next and the final process the model compilation and training placeholder function process. The LSTM model is compiled and trained using a placeholder function compile_and_fit, which is taken from tensorflow. The code is below;

```
history = compile_and_fit(lstm_model, wide_window)

IPython.display.clear_output()
val_performance['LSTM'] = lstm_model.evaluate(wide_window.val, return_dict=True)
performance['LSTM'] = lstm_model.evaluate(wide_window.test, verbose=0, return_dict=True)
```

In the context of machine learning, particularly when working with LSTM (Long Short-Term Memory) models for time series forecasting, the process of model compilation and training is a critical step. The placeholder compile_and_fit function encapsulates this process. It takes the lstm_model and a data window object, wide_window, as arguments. The function is responsible for setting up the model with the appropriate optimizer and loss function, and then fitting the model to the training data encapsulated by wide_window. After training, the IPython.display.clear_output() function clears the output of the training process to maintain a clean workspace. The model's performance is then evaluated on both validation and test datasets, with the results stored in val_performance and performance dictionaries, respectively. This allows for a clear comparison of the LSTM model's effectiveness in predicting future data points based on historical time series data. The return_dict=True parameter ensures that the evaluation metrics are returned as a dictionary for easy access and interpretation.

4.7 Summary

This chapter presents a comprehensive study on the data collection, preprocessing, and modeling of rain attenuation prediction for these frequency bands, with a focus on the geographical and climatic context of Ethiopia.

The chapter begins with an introduction to the challenges of predicting rain attenuation and the necessity for accurate data collection and preprocessing. It emphasizes the importance of understanding the geography and climate of Ethiopia, as these factors greatly influence rain patterns and, consequently, signal attenuation. The highlands and lowlands of Ethiopia present unique meteorological data, which is meticulously collected and visualized to aid in the development of predictive models.

A detailed examination of the ITU-R rain attenuation models is provided, highlighting their significance in the design of microwave communication systems. These models, including ITU-R P.530, ITU-R P.618, ITU-R P.837, ITU-R P.838, and ITU-R P.839, offer methods for calculating specific attenuation, effective path length, and total path attenuation. They serve as the foundation for the statistical analysis of rain rate and the determination of specific attenuation, which are crucial for the accurate prediction of rain attenuation.

The chapter then delves into the data processing for rain attenuation modeling. It discusses the conversion of 15-minute rain rate data to 1-minute intervals and the determination of the point rain rate (R0.01), which is essential for designing robust communication systems. The study leverages actual 15-minute data directly, avoiding potential data loss from conversion models, and validates its approach by analyzing precipitation data for Addis Ababa.

The culmination of this chapter is the introduction of a novel deep learning method for rain attenuation prediction, the Long Short-Term Memory (LSTM) model. LSTM's ability to capture long-term dependencies and handle irregular rainfall patterns makes it an excellent tool for modeling rain attenuation. The chapter provides an in-depth discussion on the LSTM model, its architecture, and its advantages over traditional statistical methods. Finally, the chapter presents the implementation of the LSTM model in Python, utilizing a range of libraries for data manipulation, visualization, and deep learning tasks. The Python implementation showcases the practical application of LSTM for rain attenuation prediction, demonstrating its potential to enhance the accuracy and reliability of communication systems in the face of environmental challenges.

5 Result and Discussions

5.1 Introduction

This chapter unveils the empirical findings of the study on "Deep Learning based rain attenuation prediction modeling for microwave and mmWave band," a pivotal step towards enhancing the reliability of communication systems in adverse weather conditions. The research embarked on a journey to collect, preprocess, and model data with the aim of predicting rain attenuation, a notorious impediment to signal clarity in microwave and mmWave communications.

The results presented herein are the culmination of rigorous data analysis and innovative application of Long Short-Term Memory (LSTM) neural networks. This chapter not only showcases the performance of the LSTM model but also juxtaposes it with traditional rain attenuation prediction methods, providing a clear depiction of the advancements made through this research.

The discussion delves into the interpretation of the results, drawing connections between the observed data and the theoretical framework established in earlier chapters. It seeks to provide a comprehensive understanding of the implications of these findings, both for the academic community and for practical applications in telecommunications.

As we proceed, each section will detail specific outcomes, analyze their significance, and explore the broader context of their impact on the field of rain attenuation prediction. The insights gained from this study are expected to contribute to the development of more resilient communication infrastructures, capable of withstanding the challenges posed by the natural environment.

5.2 Rain Rate Analysis

As rain rate is the primary determinator of rain attenuation over the radio wave signal, an extensive analysis has been conducted in determining anlyszing rainfall rate in the target location. As it was mentioned in the previous sections, the location of interest is Addis Ababa. Visualization and analysis for collected rainfall rate, temperature and relative humidity has been made as follow;

First, the rainfall data was collected as precipitation in mm, but recorded every 15-

minute. Usually, rain rate is expressed in mm/hr. So, the precipitation has been multiplied by 4 to make it mm/hr. the temperature and relative humidity have been kept as they were.

Visualization of the 15-min rain rate in mm/hr has been drawn using OriginPro software and it can be seen in the graph below;

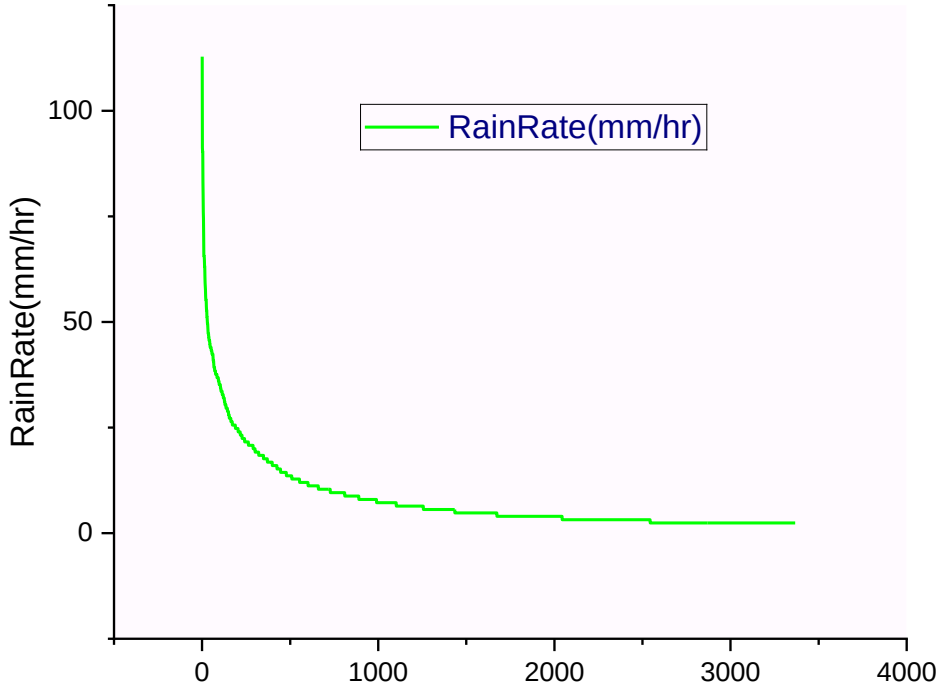

Figure 5-1 Rain Rate in mm/hr for Addis Ababa City

This graph is drawn for the statistical sorted data of the 8 years data from maximum rate(128.2 mm/hr) and minimum value of zero.

Statistical analysis has been carried out extensively to understand the nature of the metrological variables. The pdf, cdf and ccdf of the rain rate, the temperature and the relative humidity for Addis Ababa has been computed. The statistical analysis is necessary and important information for determination of the rainfall rate of $R_{0.01}$. This is because the ITU-R models are all statistics-based model and in this study, the rain attenuation data is derived from this statistical data. The $R_{0.01}$ is derived from the probability of exceedance and probability of exceedance is dependant on pdf, cdf and ccdf. The P0annual variable defined in the ITU-R P.837-7 algorithm, is the probability of exceedance that is determined by the program of the algorithm from pdf, cdf and ccdf during the compilation of the program. The whole csv data was given to the algorithm and the algorithm returns the output csv data with pdf, cdf and ccdf values. The graphs in figure 5.2 below provides visual illustration.

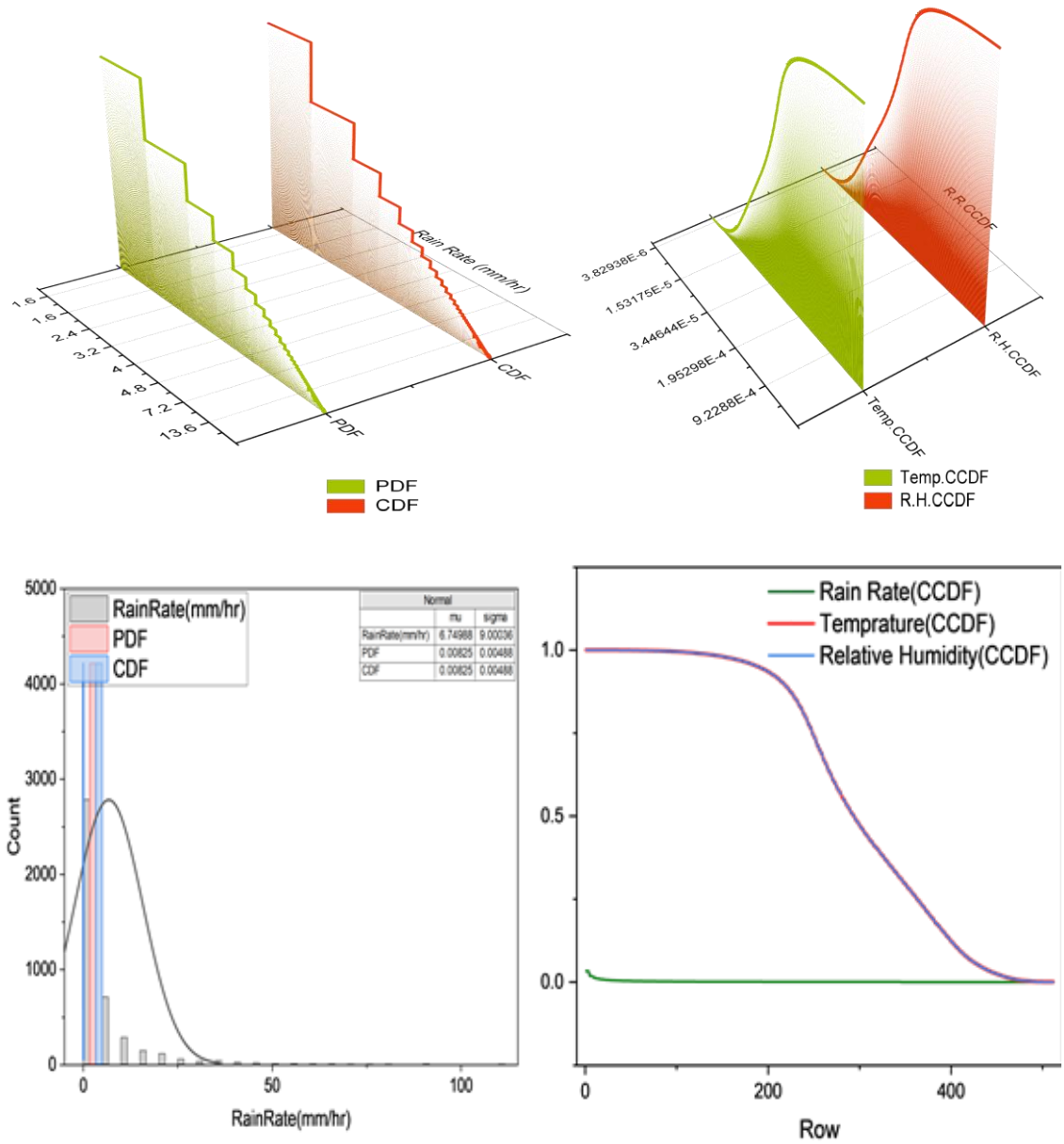

Figure 5-2 PDF, CDF and CCDF illustration

5.3 Analysis of Rainfall Rate $R_{0.01}$

As discussed in section 4.5.1 of the previous chapter, the process of determination of $R_{0.01}$ is based on ITU-R P837-7 recommendation. The detailed process has been presented in the mentioned section earlier. The algorithm has been implemented in python and the $R_{0.01}$ value for 15-min integration time as well as the 1-min integration time has been obtained. Since the data collected 8 years long and python libraries like panda has a great role in handling such big data.

Using the algorithm, the data has been used and determination of $R_{0.01}$is made and

this can be seen in the graph below;

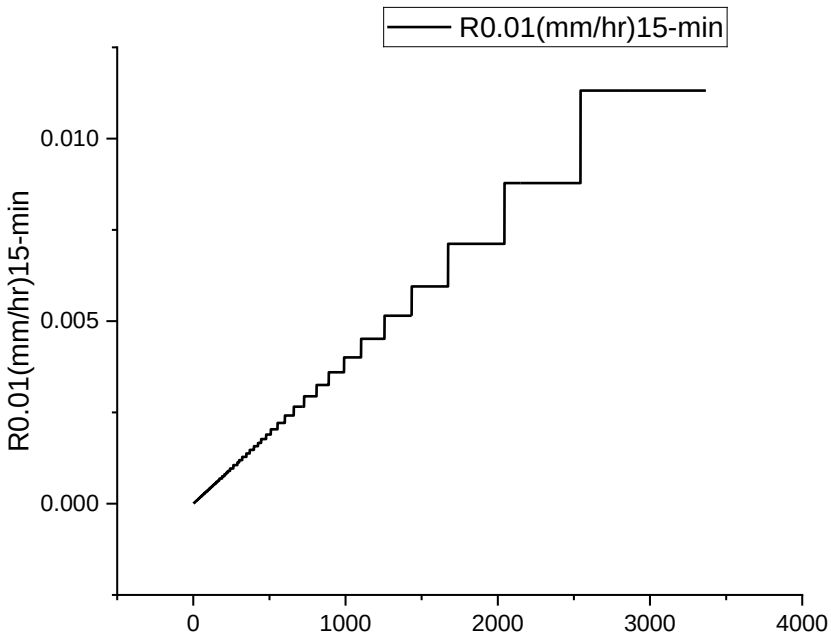

Figure 5-3 $R_{0.01}$ of 15-min integration time for Addis Ababa City

The graph illustrates the relationship between the actual rain rate and the frequency of its occurrence, specifically focusing on the rain rate that is exceeded 0.01% of the time over a 15-minute period ($R_{0.01}$). The y-axis, representing the actual rain rate in mm/hr, shows the intensity of rainfall measured during the data collection period. The x-axis, indicating $R_{0.01}$, reflects the threshold rain rate that is only exceeded in the most intense 0.01% of rain events. The step plot suggests that as the actual rain rate increases, the occurrences of rain rates exceeding the $R_{0.01}$threshold also increase, but at a diminishing rate. This indicates that while high-intensity rainfalls are less frequent, they still significantly contribute to the overall rain attenuation calculations, which are critical for designing robust communication systems that can withstand severe weather conditions. The graph provides a visual representation of the variability and distribution of rain intensities, which is essential for understanding the impact of rain on signal propagation in microwave and mmWave communication systems.

5.4 Conversion of Rain Rate Time Integration

The rain rate at a 1-minute integration time is a critical parameter for predicting rain attenuation in communication systems operating above 10 GHz. However, obtaining

accurate 1-minute rainfall data globally remains a challenge due to its limited availability. Most meteorological agencies collect data at longer integration times. Section 4.5.2 of this study provides a detailed method of converting 15-minute time integration to 1-minute time integration.

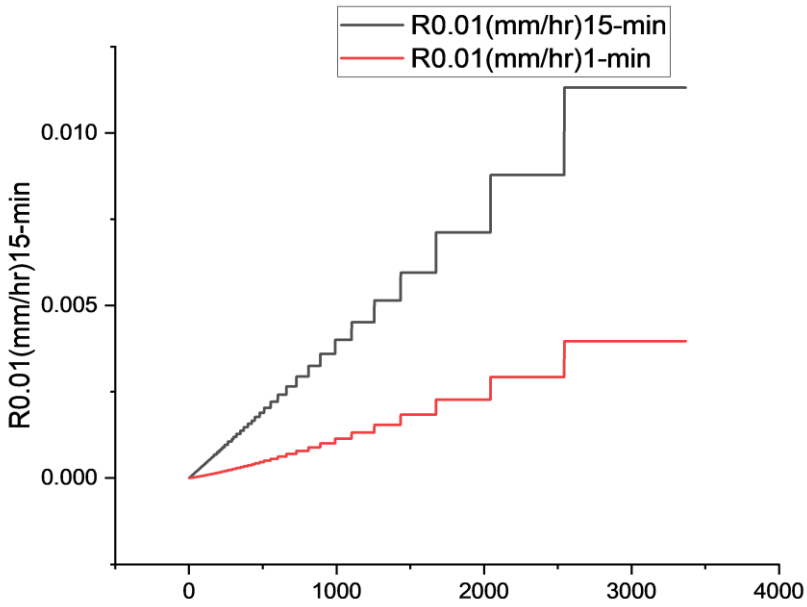

Figure 5-4 15-min Rain Rate and 1-min Rain Rate Plotting

The black line represents the $R_{0.01}$value over a 15-minute integration time, while the red line represents the $R_{0.01}$ value over a 1-minute integration time. Both lines exhibit a step-like pattern, indicating discrete increases at certain points along the x-axis. However, the red line has fewer steps and less sharp increases compared to the black line, suggesting that high-intensity rain rates are less frequent over a 1-minute period than over a 15-minute period.

Using a 1-minute rain rate instead of a 15-minute rain rate offers significant advantages for predicting rain-induced attenuation in communication systems. This higher temporal resolution provides a more granular view of rainfall intensity, crucial for systems sensitive to rapid changes, particularly those operating at higher frequencies like above 10 GHz. Accurate modeling of fading effects, such as those caused by rain attenuation in microwave and mmWave links, is facilitated by the 1-minute rain rate, capturing short-term variations impacting signal quality that may be smoothed out in longer integration times. The ITU-R recommendation supports the use of the 1-minute rate for predicting rain-induced attenuation, ensuring communication system designs

account for critical rain effects. In satellite communication, reliable links depend on precise rain rate data, with the 1-minute rate aiding in link planning and mitigation strategies. Furthermore, system losses from rain attenuation can be effectively mitigated by optimizing parameters based on the 1-minute rain rate, while its ability to capture dynamic weather conditions is particularly valuable in tropical regions with intense and fluctuating rainfall patterns.

5.5 Specific Attenuation Determination and Achieved Result

Determination of pecific attenuation was presented in detail in section 4.5.3. The section presents the method of calculating the specific attenuation using power low formula as discussed in ITU-R P.838 model in section 4.4.4. The power law says the point rainfall attenuation, which is the specific attenuation, can calculated as $kR_{0.01}{}^{\alpha}$, where the k and the α are the regration coefficient determined from the specifc frequency as presented in ITU-R P.838. The value for those coefficients has been computed for 11 GHz for this study and the final formula for specific attenuation has been obtained as $\gamma_R = 0.02\ R_{0.01}{}^{0.25}\ dB$.

This study has computed the specifc attenuation using the processed data for Addis Ababa city for both 15-minute and 1-minute $R_{0.01}$ value and has made a comparison of achieved result.

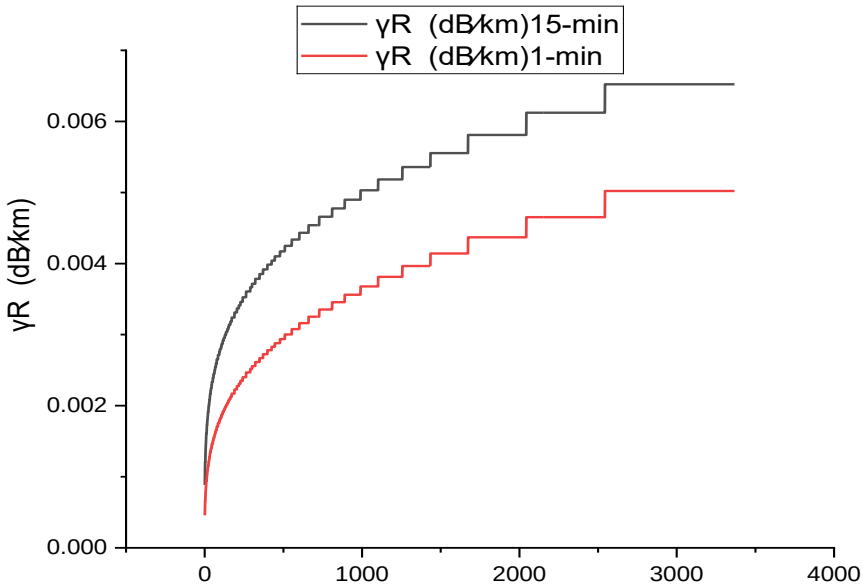

Figure 5-5 Specific Attenuation at 15-minute and 1-minute time integration

The graph's depiction of specific attenuation, with the black line representing a 15-minute integration time and the red line a 1-minute integration time, highlights the critical differences in temporal resolution between the two. The smoother curve of the black line suggests a more generalized view of attenuation, which may overlook short-term fluctuations in signal degradation due to rain. In contrast, the stepped appearance of the red line captures these rapid changes, providing a more detailed and accurate representation of the specific attenuation that communication systems might experience. For this case, the 1-min specific attenuation has a value of $6x10^{-3}$dB maximum, while the 1-min specific attenuation has $5x10^{-3}$ dB maximum, which has $1x10^{-3}$ dB estimated difference.

The importance of determining specific attenuation at a 1-minute integration time over a 15-minute period cannot be overstated. The higher temporal resolution of the 1-minute data is essential for designing and optimizing communication systems, particularly those that operate at higher frequencies and are more susceptible to rain attenuation. This finer granularity allows for a more responsive system design that can adapt to the instantaneous variations in signal strength caused by rainfall, ensuring a more reliable and consistent quality of service. Moreover, the 1-minute integration time is crucial for the development of adaptive technologies in communication systems, such as dynamic power control and adaptive modulation, which require real-time adjustments based on immediate weather conditions. By utilizing 1-minute specific attenuation data, engineers can fine-tune these systems to compensate for the effects of rain, minimizing outages and maintaining optimal performance even during adverse weather events.

5.6 Rain Attenuation Determination and Achived Results

Section 4.5.4 of this study presents a detailed explanation how to determine the total path attenuation due to rain. Using ITU-R P.838 model, the total path attenuation due to rain is the multiplicative result of the effective path length and the specific attenuation. The effective path length is related to the rain rate, as it was presented in detail in the aforementioned section. It can be expressed interms of $R_{0.01}$ as 1 devided by $(3818.99R_{0.01}^{0.018} - 10.579)$, where the coefficient 3818.99 and the power 0.018 are determined from the equation 4.36.

The total path attenuation is the result of this effective path length multiplied by the the specific attenuation. This computation is quite easy once the effective path length and

the specific attenuation is calculated. The result obtained is presented in the graph below;

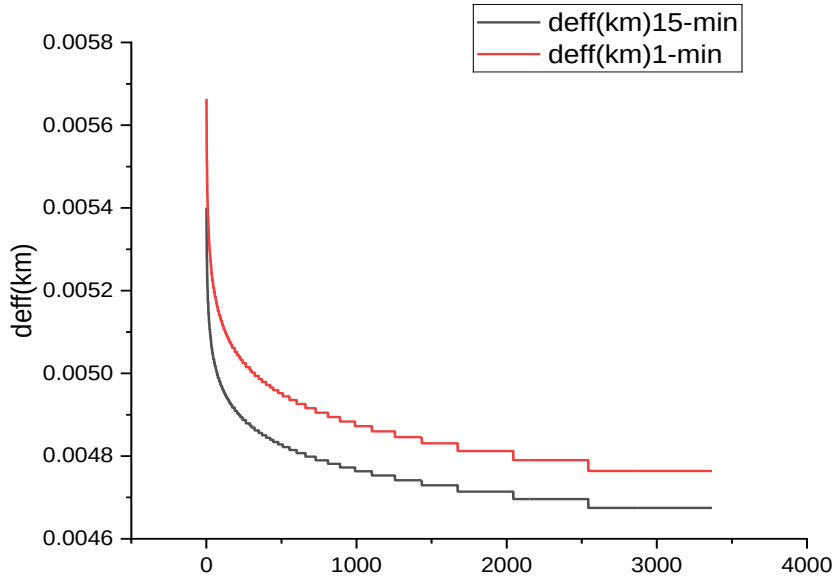

Figure 5-6 lotting of rain rate dependent effective path length for 15-min and 1-min

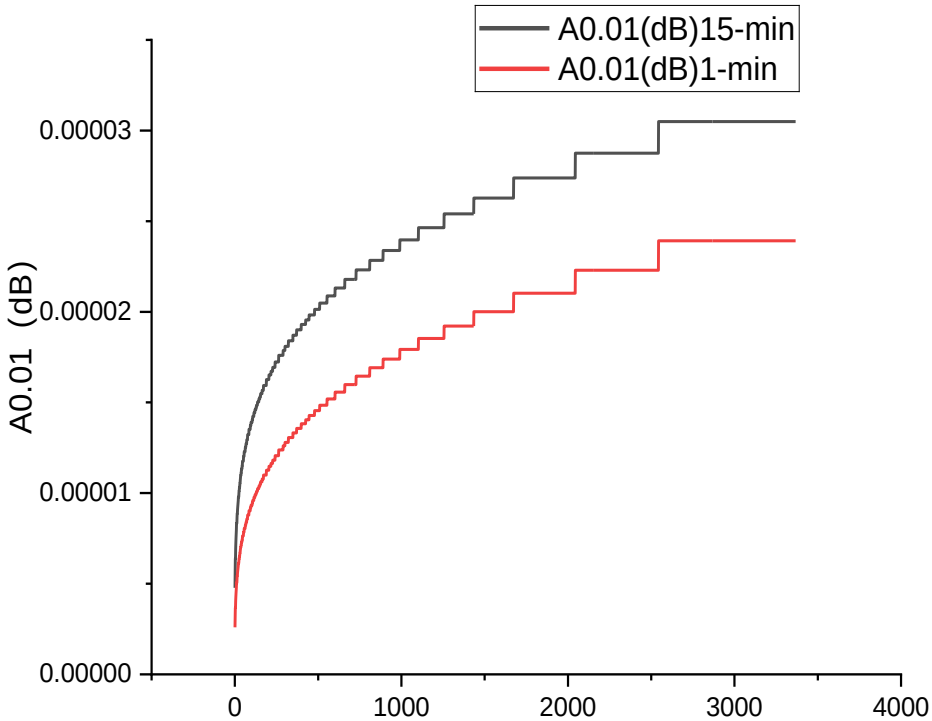

Figure 5-7 Total path attenuation due to rain for 15-min and 1-min rain rate

Determining the total path attenuation at a 1-minute integration time is crucial for

communication systems that are sensitive to short-term changes in rain intensity. It allows for a more accurate assessment of the potential impact of rain on signal quality and system performance, particularly for high-frequency links where even brief periods of intense rainfall can cause significant attenuation.

A0.01(dB)1-min, indicates the total path attenuation calculated using the rain rate exceeded for 0.01% of the time over a 1-minute period. This line starts lower on the y-axis and has a steeper slope before plateauing, suggesting a rapid increase in attenuation which then stabilizes. This behavior is indicative of the variability and intensity of rain that can occur over a short period, which is critical for systems that require high reliability and are sensitive to such rapid changes in rain intensity.

A0.01(dB)15-min graph represents the total path attenuation calculated using the rain rate exceeded for 0.01% of the time over a 15-minute period. It starts slightly higher and increases more gradually, suggesting a more averaged or smoothed representation of attenuation. This could be indicative of less variability in rain intensity over a 15-minute period compared to a 1-minute period, providing a more general view of the rain's impact over a longer duration.

Understanding the total path attenuation at a 1-minute integration time is crucial for communication systems, especially those operating at higher frequencies, where even brief periods of intense rainfall can cause significant attenuation. This data is essential for designing systems that can adapt to or compensate for these effects, ensuring consistent service during varying weather conditions. The comparison between the 1-minute and 15-minute data also allows engineers to understand the trade-offs between system responsiveness and complexity in handling weather variability, leading to more informed decisions in system design and operation.

5.7 The LSTM Prediction Model and Achied Results

The Long Short-Term Memory (LSTM) prediction model stands as a significant advancement in the realm of rain attenuation prediction for communication systems. Its architecture, designed to remember information for long periods, is particularly suited for capturing the temporal patterns and dependencies within meteorological data, which are critical for accurate rain attenuation forecasting. Unlike traditional statistical models, LSTM can process and predict complex nonlinear relationships, making it adept at handling the variability and intermittent nature of rainfall. This capability allows for more

precise predictions of signal degradation due to rain, which is paramount for the reliability and efficiency of microwave and mmWave communication links. By leveraging LSTM models, engineers can better anticipate and mitigate the adverse effects of rain on signal propagation, leading to the design of more robust communication infrastructures that maintain high-quality service even under dynamic weather conditions.

The model is presented in depth in section 4.6. The result achieved using this model are presented as follow;

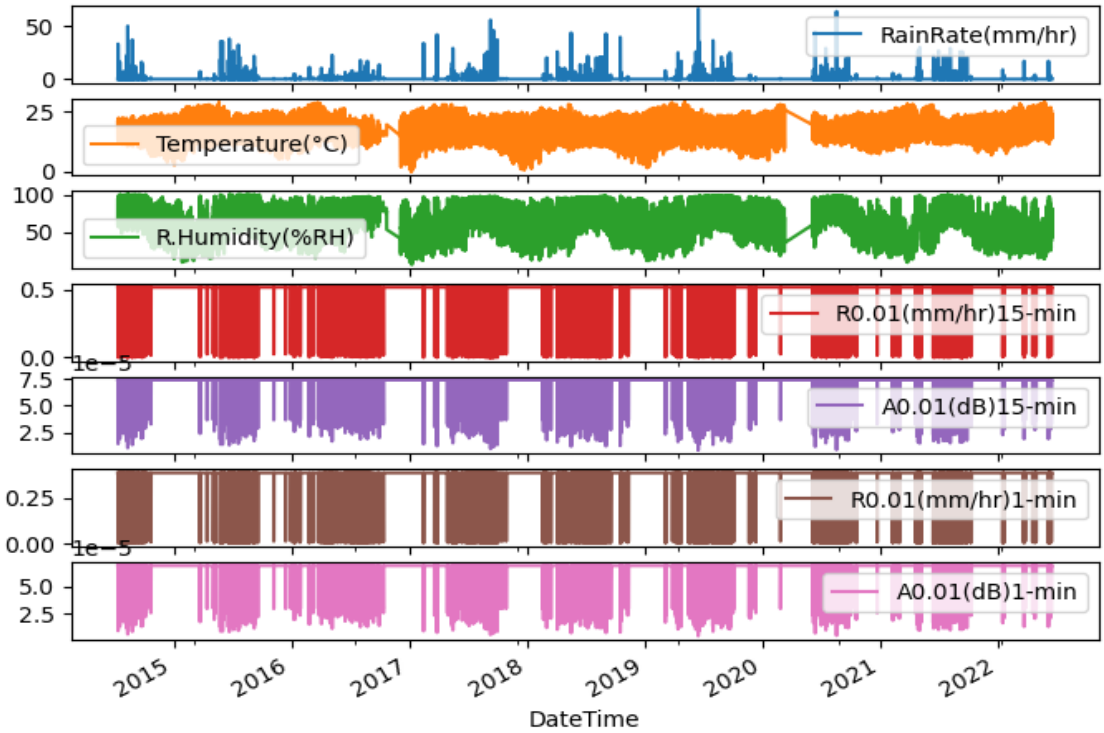

Figure 5-8 Training data visualization of the LSTM model

The model designed to take 7 input features. Those data are loaded as a csv file and visualized using python. The input variables are RainRate(mm/hr), Temperature(°C), R.Humidity(%RH), R0.01(mm/hr)15-min, A0.01(dB)15-min, R0.01(mm/hr)1-min and A0.01(dB)1-min. They are feeded to the input layer of the model and analyzed uusing the panda's data analizing library.

Figure 5.8 shows the input features historically. Remind that the rain rate, the temperature, and the relative humidity are the actual data recorded over the period. The other data are calculated for each data poin of the actual rain rate over the period. The period is quite long so, it is hard to visualize graph as in figure 5.8. The graph below in figure 5.9 show the zoomed-out version of the data for the year 2014.

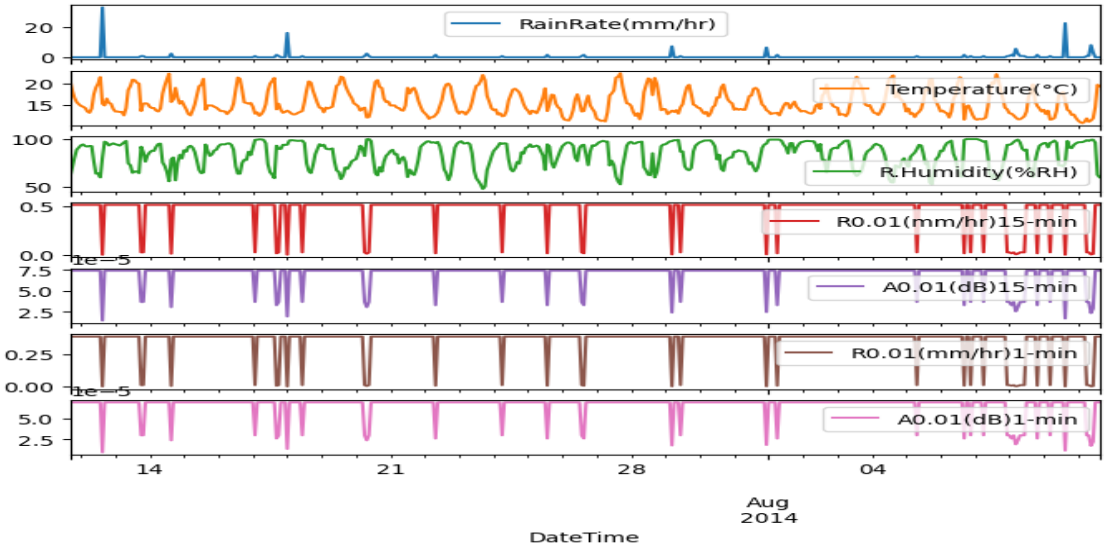

Figure 5-9 Data visualization for year 2014

Statistical discriptions are always an indicative tool in analyzing any data. The dataframe ststatement, df.describe().transpose(), gives us to look at the statistical description of the input features for the above visualized data. This is presented as follow;

[17]:

	count	mean	std	min	25%	50%	75%	max
RainRate(mm/hr)	43523.0	0.121591	1.370636	0.000000	0.000000	0.000000	0.000000	65.600000
Temperature(°C)	43523.0	16.761765	4.537377	-0.300000	13.500000	16.200000	20.300000	29.100000
R.Humidity(%RH)	43523.0	62.011870	22.335587	5.700000	43.500000	62.500000	81.900000	100.000000
R0.01(mm/hr)15-min	43523.0	0.500028	0.088322	0.000042	0.516145	0.516145	0.516145	0.516145
S.A0.01(dB/km)15-min	43523.0	0.016671	0.001818	0.001610	0.017000	0.017000	0.017000	0.017000
Deff(km)15-min	43523.0	0.004370	0.000057	0.004360	0.004360	0.004360	0.004360	0.005170
A0.01(dB)15-min	43523.0	0.000073	0.000008	0.000008	0.000074	0.000074	0.000074	0.000074
R0.01(mm/hr)1-min	43523.0	0.373761	0.067064	0.000005	0.386000	0.386000	0.386000	0.386000
S.A0.01(dB/km) 1-min	43523.0	0.015462	0.001867	0.000940	0.015800	0.015800	0.015800	0.015800
Deff(km)1-min	43523.0	0.004402	0.000067	0.004390	0.004390	0.004390	0.004390	0.005380
A0.01(dB)1-min	43523.0	0.000068	0.000008	0.000005	0.000069	0.000069	0.000069	0.000069

Figure 5-10 Statistical analysis of observed datasets

Data windowing involves segmenting the time-series data into a sequence of overlapping windows or batches that the LSTM network can process. This technique allows the network to learn from the temporal dependencies within the data, is crucial for making accurate predictions. Windowing the data correctly is crucial because it directly affects the LSTM's ability to capture the temporal patterns in the data, which are vital for tasks like predicting rain attenuation. The size of the window and the overlap can be tuned based on the specific characteristics of the dataset and the prediction task at hand.

The created WindowGenerator class is a structured approach to preparing your data

for an LSTM-based rain attenuation prediction model. It initializes with parameters defining the width of the input and label windows, as well as the shift between them, and it takes in separate dataframes for training, validation, and testing. The class methodically calculates the indices for the input and label data within each window, ensuring that the LSTM receives a consistent and correctly aligned batch of input features and corresponding labels during training. This alignment is crucial for the LSTM to learn the temporal patterns effectively. The __repr__ method provides a clear textual representation of the window configuration, which can be very helpful for debugging and understanding the windowing process. Overall, this class encapsulates the necessary functionality for windowing time-series data, making it a valuable component of your predictive modeling pipeline.

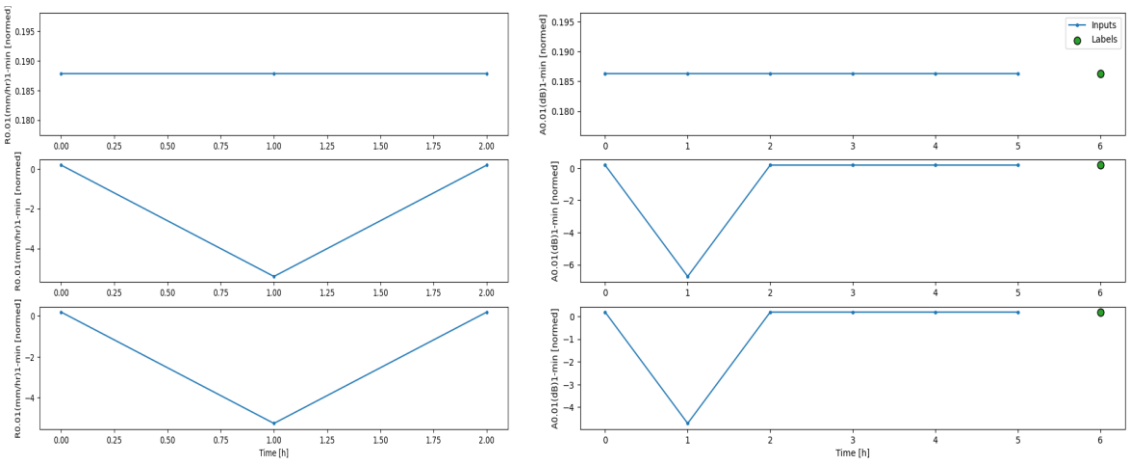

Figure 5-11 Visualization of normalized A0.01(dB)1-min

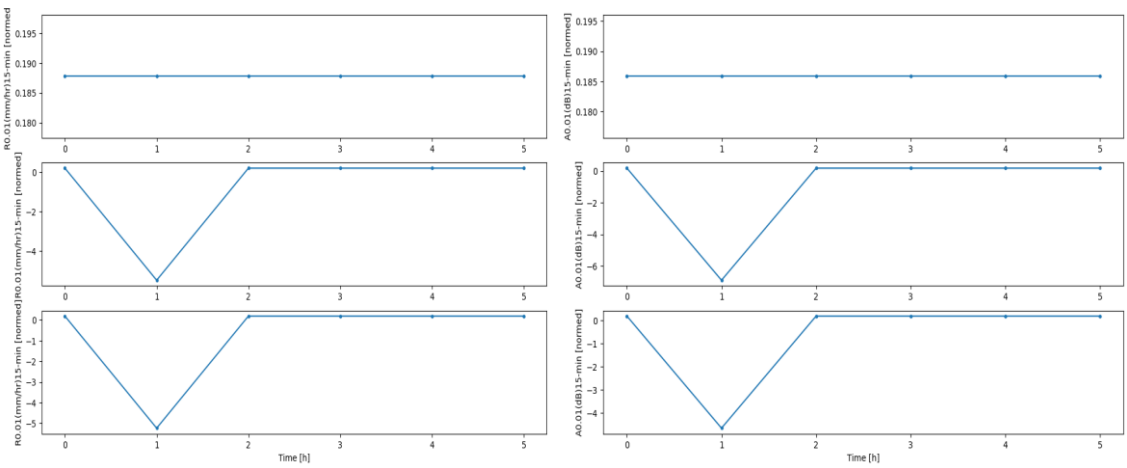

Figure 5-12 Visualization of A0.01(dB)15-min rain attenuation

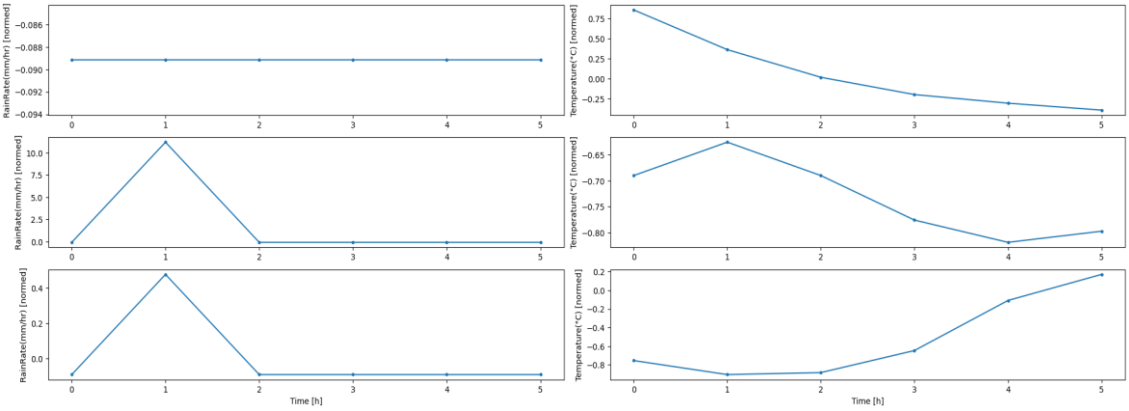

Figure 5-13 Visualization of normalized rain rate and temperature parameters

Figure 5.13 Visualization of normalized rain rate and temperature parameters

For the purpose of evaluating the performance of your LSTM model for rain attenuation prediction, it's beneficial to compare it with other models such as Baseline, Linear, Dense, and CNN. The Baseline model provides a simple reference point, while the Linear model assumes a direct relationship between inputs and outputs. The Dense model captures non-linear relationships without temporal context, and the CNN can process spatial and temporal patterns with 1D convolutions. The LSTM is specialized for sequence data and temporal dependencies. Performance metrics like accuracy, precision, recall, MSE, and MAE are crucial for comparison. These metrics help determine the most effective model by revealing each model's strengths and weaknesses in capturing the complex patterns in your time-series data. Visualizing predictions against actual values further aids in assessing model performance under various conditions. The baseline prediction is shown in the graph below for A0.001(dB)1-min.

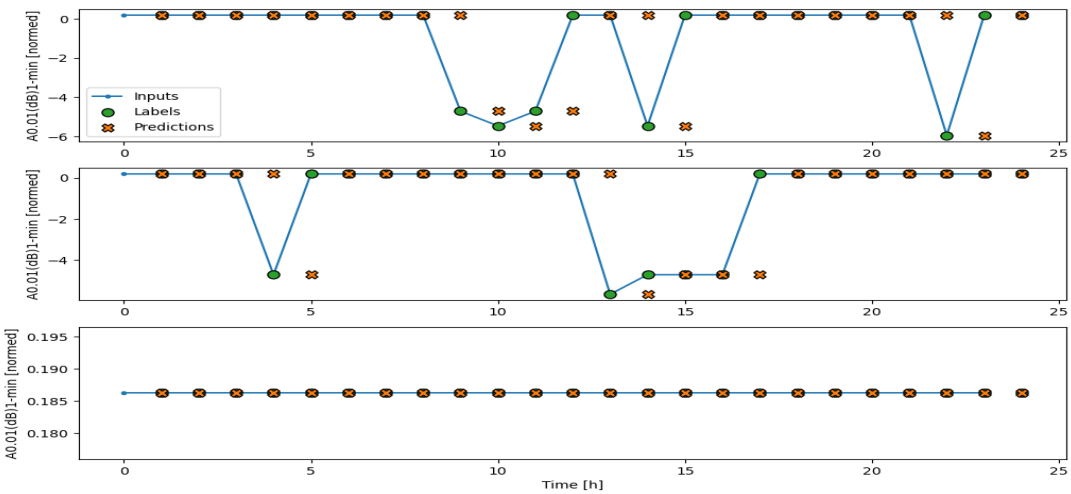

Figure 5-14 Baseline prediction

In the above plots of three examples the single step model is run over the course of 24 hours. The blue Inputs line shows the input Attenuation at each time step. The model receives all features, this plot only shows the 1-minute rain attenuation prediction, A0.01(dB)1-min. The green Labels dots show the target prediction value. These dots are shown at the prediction time, not the input time. That is why the range of labels is shifted 1 step relative to the inputs. The orange Predictions crosses are the model's predictions for each output time step. If the model were predicting perfectly the predictions would land directly on the Labels.

Linear model output is presented in the graph bellow;

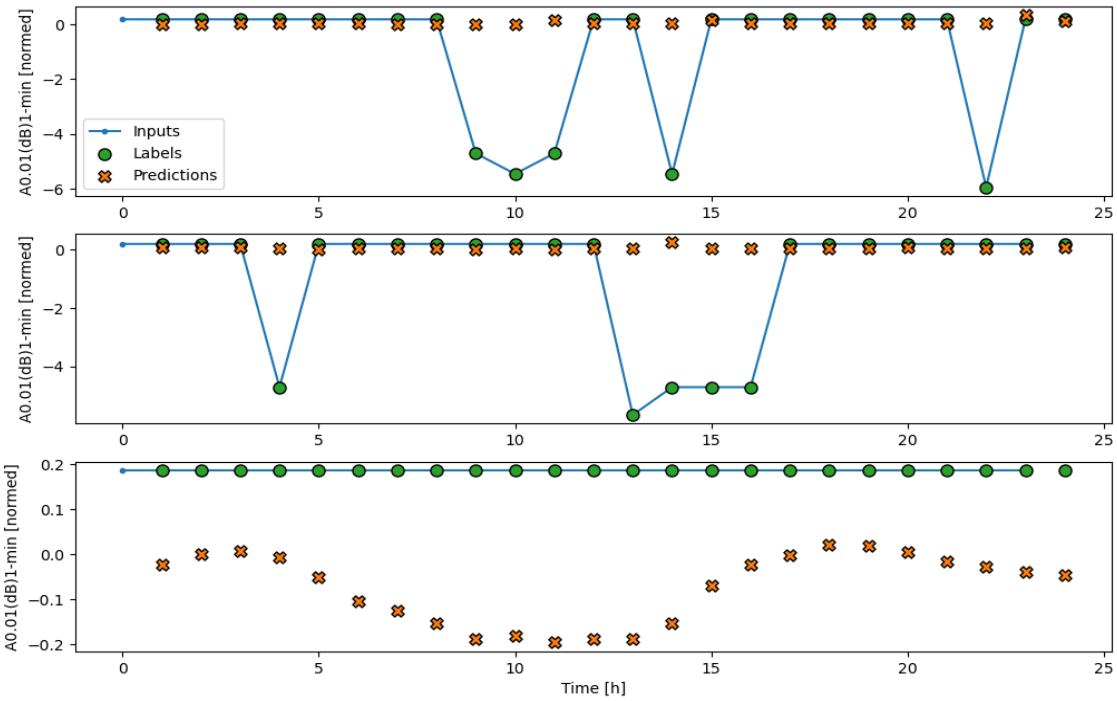

Figure 5-15 Linear model prediction

Here is the plot of its example predictions on the wide_window, note how in many cases the prediction is clearly better than just returning the input 1-minute rain attenuation prediction, A0.01(dB)1-min., but in a few cases it's worse.

one of the key advantages of linear models is their interpretability. In a linear model, each input feature is assigned a weight that represents its contribution to the output prediction. These weights can be positive or negative, indicating the direction of the relationship between the feature and the prediction. Sometimes the model doesn't even place the most weight on the input A0.01(dB)1-min. This is one of the risks of random initialization.

A convolutional layer, specifically tf.keras.layers.Conv1D in TensorFlow, is designed to handle sequential data and can process multiple time steps simultaneously. This type of layer is particularly useful in time-series analysis or any application where the temporal sequence of the data is important. The difference between this conv_model and the multi_step_dense model is that the conv_model can be run on inputs of any length. The convolutional layer is applied to a sliding window of inputs.

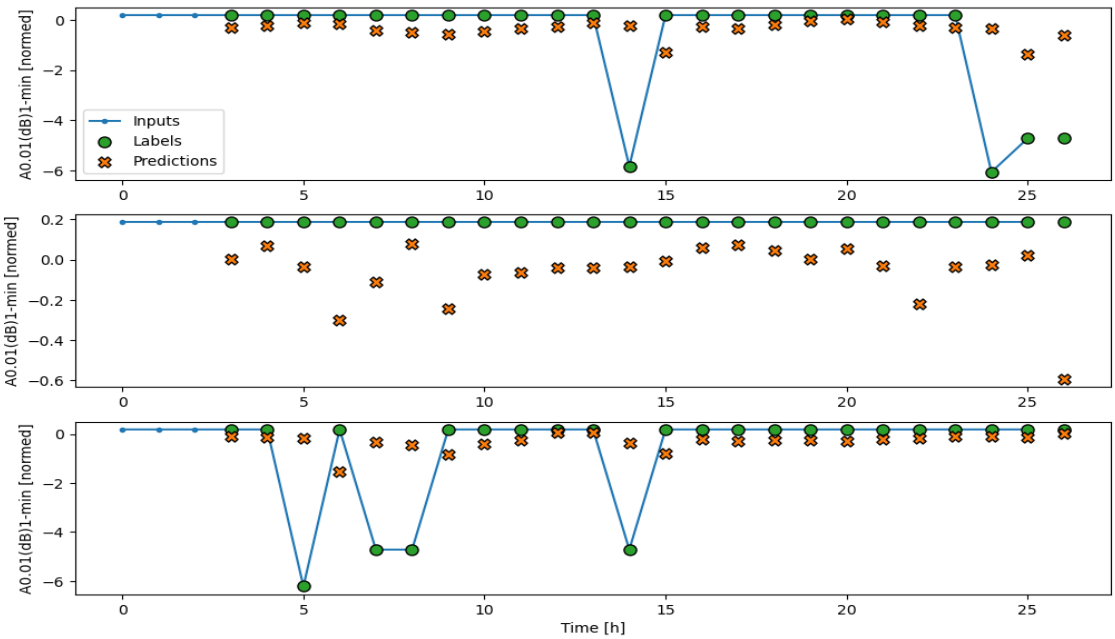

Figure 5-16 CNN Prediction Model

Recurrent Neural Networks (RNNs) are indeed a powerful class of neural networks that are designed to handle sequence data. An RNN processes sequences by iterating through the time steps and maintaining a 'memory' of the information it has seen so far using its internal state. This memory helps the RNN capture dynamic temporal behavior which is crucial for tasks like time series forecasting, natural language processing, and more.

The Long Short-Term Memory (LSTM) layer is a special kind of RNN layer that is capable of learning long-term dependencies. LSTMs have a complex architecture with gates that regulate the flow of information. These gates determine what information should be kept or discarded at each time step, which helps in mitigating issues like vanishing gradients that are common in standard RNNs.

The LSTM model utilized in this study is a sequential model designed for time series forecasting. It consists of an LSTM layer with 32 units that processes the input data while

preserving the time sequence (as indicated by return_sequences=True). This is followed by a dense layer with a single unit that outputs the prediction for each time step. The training process involves compiling the model and fitting it to the data encapsulated by wide_window, which likely represents a wider window of time steps for the LSTM to learn from. After training, the model's performance is evaluated on both the validation and test datasets, with the results stored in val_performance and performance dictionaries, respectively. The prediction result is shown in the graph below.

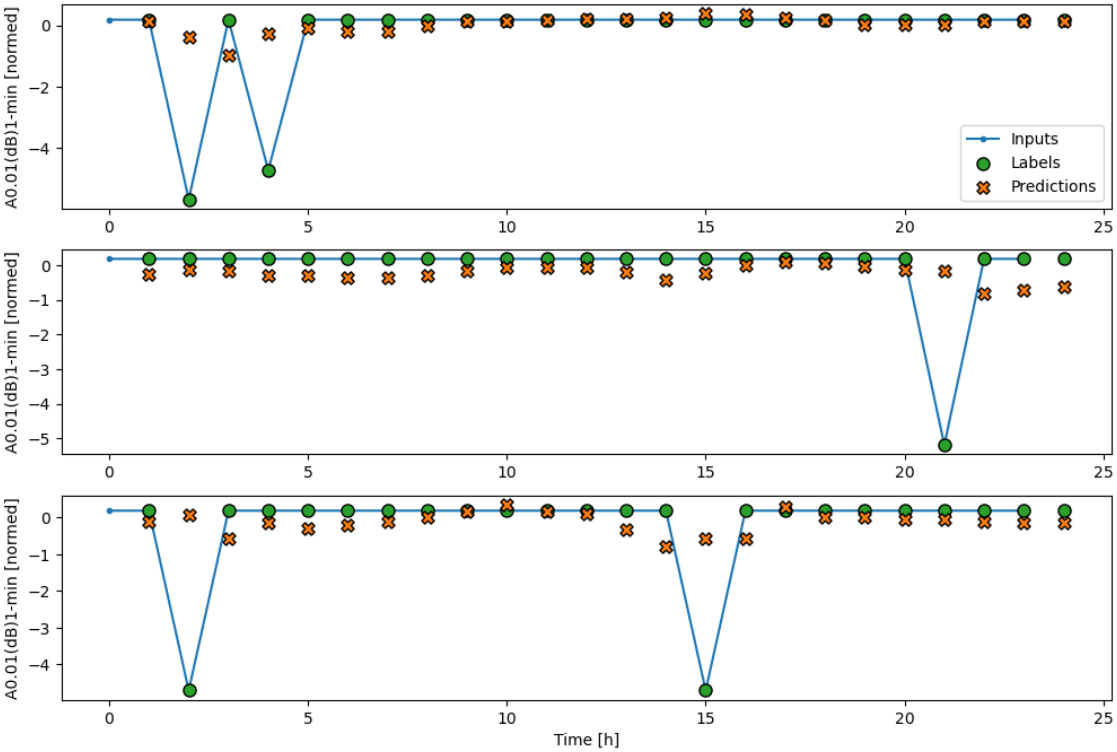

Figure 5-17 LSTM-based prediction of rain attenuation A0.01(dB)

The graph typically illustrates how closely the model's predictions align with the actual data, which is crucial for assessing the model's accuracy and effectiveness in forecasting future values. The 'Inputs' are the historical data points fed into the model, the 'Labels' are the true values that the model aims to predict, and the 'Predictions' are the model's forecasts. This prediction is a single output prediction, which in this case is the 1-min time integration rain attenuation (A0.01(dB)1-min).

If the 'Predictions' closely follow the 'Labels', it indicates that the model is performing well. However, if there are significant deviations, especially during spikes or drops, it suggests that the model may struggle to capture some aspects of the data's underlying patterns and may require further tuning or additional data for training.

The LSTM model utilized here has good prediction results, as it can be seen from the graph where the 'Prediction' and the 'Labels' line align together eventhough there is a devation at spike points. This can be modified be training the model further with more training data.

The LSTM model has outperformed all other similar models in terms of performance analysis. It shows great accuracy, having the minimum mean average error and mean absolute error. The performance of each model has been perfomed using the val_performance command and it has returned the following results.

```
{'Baseline': {'loss': 1.6426372528076172,
  'mean_absolute_error': 0.2944135367870331},
 'Linear': {'loss': 1.038765549659729,
  'mean_absolute_error': 0.37080836296081543},
 'Dense': {'loss': 1.0087255239486694,
  'mean_absolute_error': 0.3695611357688904},
 'Multi step dense': {'loss': 1.0233066082000732,
  'mean_absolute_error': 0.35461899638175964},
 'Conv': {'loss': 1.0177581310272217,
  'mean_absolute_error': 0.3572850227355957},
 'LSTM': {'loss': 1.0423932075500488,
  'mean_absolute_error': 0.38608869910240173}}
```

5.8 Summary

This chapter has presented the achived result with detailed analysis for each section and subsections. The result found in each section and subsections have been discussed in detail. The statistical analysis such as for the rain rate analysis, rainfall rate of R0.01, conversiton of 15-minute rainfall distribution in to 1-minute rainfall distribution has been carefully analyzed and discussed. The specific attenuation and the total path attenuation due rainfall for the designated microwave link has been computed and historical data has been prepared. The statistical analysis as well as graphical illustration has been made and discussed properly. The Proposed prediction model has been trained with the preprocessed data and result from the proposed model has been analysed and discussed in detail.

6 Conclution and Recommendations

6.1 Conclusion

The importance of precise estimation and forecasting of rainfall intensity, along with rain-induced signal attenuation on terrestrial line-of-sight radio connections at micro and millimeter-wave frequencies, cannot be overstated in the realm of radio communication research. Additionally, having advance knowledge about the radio link they intend to develop empowers designers to make more informed decisions and optimize communication systems effectively.

In this study, the conversion of integration time was meticulously performed using data from Addis Ababa and ITUR-P.837-7, revealing that the value obtained for R0.01 significantly deviates from what would be estimated by global prediction methods. Furhtore modere, specifc attenuation and total path attenuation has been studied and computed using ITU-R P.838-3 and P.530 on the 11 GHz microwave link. Historical rain attenuation data were compiled for 8-years rain fall data.

The LSTM model has been developed, trained and validiated using the preprocessed data of rain rate, specific attenuation, and total path attenuation. The developed model has predicted a one hour into the future rain fall attenuation with minimum absolute error of 0.053 outperfoming other forcasting algorithms. This study can be helpful, for network designers, researchrs and academicians to furthure explor an a more accurate AI model that uses locally measured data to perfectly accurate the rain attenuation event on microwave and mmWave links. The result obtained can be used in different scinarios such as for microwave designers and in real time application cases.

6.2 Recommendations

AI-models such as LSTM, should be employed in more similar prediction work, specially, for events with schochistic property, such as rainfall, because of their ability handling such events with great precision and accuracy.

Evaluating the rain rate profile is a crucial aspect of propagation research focused on rain. Without adequate rain data and processing tools, it becomes challenging to design dependable communication links. The AI prediction models can be integrated with

empirical models such as the ITU-R models to prepare data that are not measured locally such as rain attenuation in dB. The ITU-R model can help in processing data for the AI models which can be an input to predict the target variables.

Similar study should be conducted more and more in location such as Ethiopia where measured rain attenuyation is not available.

参考文献

References

1. Series, I.-R.R., *Propagation data and prediction methods required for the design of terrestrial line-of-sight systems*, in *In: Recommendation ITU-R (2015), pp. 530–12*. 2015.
2. QammerHAbbasietal, *Anovel pathloss model for angular and spatial dependency of ultra wideband off-body radio channels.* International Journal on Communications Antenna and Propagation, 2013. **3.4**: p. 206-209.
3. Otasowie, P.E.a.P.O., *Comparison of empirical path loss propa gation models with building penetration path loss model.* International Journal on Communications Antenna and Propagation (I. Re. CAP) 2016. **6.2**.
4. Itu, R., *RECOMMENDATION ITU-R P. 838-2 Specific Attenuation Model for Rain for Use in Prediction Methods; 1992199920032.* ITU: Geneva, Switzerland, 2005: p. 1-8.
5. Afullo, A.A.A.a.T.J.O., *Rainfall microstructural analysis for microwave link networks: Comparison at equatorial and subtropical Africa.* Progress In Electromagnetics Research 2014. **59**: p. 45–58.
6. Crane, R.K., *Electromagnetic wave propagation through rain. Wiley-Interscience.* 1996.
7. PA Owolawi, S.M., and TJO Afullo, *Estimation of terrestrial rain attenuation at microwave and millimeter wave signals in South Africa using the ITU-R model.* PIERS Proceedings, Kuala Lumpur, Malaysia 2012.
8. Moupfouma, F., *Improvement of a rain attenuation prediction method for terrestrial microwave links.* IEEE Transactions on Antennas and Propagation, 1984. **32**(12): p. 1368-1372.
9. Moupfouma, F. and J. Tiffon, *Raindrop size distribution from microwave scattering measurements in equatorial and tropical climates.* Electronics Letters, 1982. **23**(18): p. 1012-1014.
10. Crane, R., *Prediction of Attenuation by Rain.* IEEE Transactions on Communications, 1980. **28**(9): p. 1717-1733.
11. da Silva Mello, L.A. and M.S. Pontes. *Improved unified method for the prediction of rain attenuation in terrestrial and earth space links*. in *2009 SBMO/IEEE MTT-S International Microwave and Optoelectronics Conference (IMOC)*. 2009. IEEE.
12. Howell, R., *Terrestrial line-of-sight links: Recommendation ITU-R P. 530.* 0ROPAGATION OF, 2003: p. 385.
13. Kesavan, U., et al. *Rain Attenuation Prediction for Higher Frequencies in Microwave Communication Using Frequency Scaling Technique*. in *2014 International Conference on Computer and Communication Engineering*. 2014.
14. *MO Fashuyi, P.O., and TJ Afullo*, *Rainfall rate modelling for LoS radio systems in South Africa.* In: Trans. of South African Inst. of Elect. Engineers (SAIEE) 2006. **97**(1): p. 74–81.
15. ITU-R, *RECOMMENDATION ITU-R P. 838-3 Specific attenuation model for rain for use in prediction methods.* Rec. P. 838-3, ITU-R, 2005.
16. Abdulrahman, A.Y., et al., *Investigation of the Unified Rain Attenuation Prediction Method With Data From Tropical Climates.* IEEE Antennas and Wireless Propagation Letters, 2014. **13**: p. 1108-1111.
17. Das, D. and A. Maitra, *Time series prediction of rain attenuation from rain rate measurement using synthetic storm technique for a tropical location.* Aeu-international Journal of Electronics and Communications, 2014. **68**: p. 33-36.
18. Diba, F.D. and T.J. Afullo. *Estimation of rain attenuation over microwave and millimeter bands for terrestrial radio links in Ethiopia*. in *AFRICON 2015*. 2015. IEEE.
19. Huang, J., et al., *Rain Statistics Investigation and Rain Attenuation Modeling for Millimeter Wave Short-Range Fixed Links.* IEEE Access, 2019. **7**: p. 156110-156120.
20. Lam, H., et al. *Impact of rain attenuation on 5G millimeter wave communication systems in*

equatorial Malaysia investigated through disdrometer data. in *2017 11th European Conference on Antennas and Propagation (EUCAP)*. 2017. IEEE.
21. Series, P., *Propagation data and prediction methods required for the design of Earth-space telecommunication systems.* Recommendation ITU-R, 2015: p. 618-12.
22. Shrestha, S. and D.Y. Choi, *Rain attenuation over terrestrial microwave links in South Korea.* IET microwaves, antennas & propagation, 2017. **11**(7): p. 1031-1039.
23. Shrestha, S., et al., *Rain specific attenuation and frequency scaling approach in slant-path for Ku and Ka-band experiments in South Korea.* 대한전자공학회 학술대회, 2017: p. 625-628.
24. Sumbiri, D., T.J.O. Afullo, and A.A. Alonge, *Rain attenuation prediction for terrestrial links at microwave and millimeter bands over Rwanda.* 2016 Progress in Electromagnetic Research Symposium (PIERS), 2016: p. 4233-4236.
25. Livieratos, S.N. and P.G. Cottis, *Rain attenuation along terrestrial millimeter wave links: A new prediction method based on supervised machine learning.* IEEE Access, 2019. **7**: p. 138745-138756.
26. M. N. Ahuna, M., IEEE, T. J. Afullo, Senior Member, IEEE, and A. A. Alonge, Graduate Member, IEEE, *Rain Attenuation Prediction Using Artificial Neural Network for Dynamic Rain Fade Mitigation.* SOUTH AFRICAN INSTITUTE OF ELECTRICAL ENGINEERS, 2019. **10**.
27. Olatunde, I.D., K.O. Babatunde, and D.O. Afolabi. *Rain Attenuation Prediction in Nigeria Using Artificial Neural Network (ANN)*. 2019.
28. Samad, M.A. and D.-Y. Choi, *Learning-Assisted Rain Attenuation Prediction Models.* Applied Sciences, 2020. **10**(17).
29. Whitefield, A.F.a.D., *Deep Learning for Rain Fade Prediction in Satellite Communications.* Hughes Network Systems, LLC, 2021.
30. Yussuff, A.I.O., M.O. Ayeni, and O.E. Oreoluwa, *Adoption of Deep Neural Network Model for the Prediction of Rain Attenuation.* European Journal of Electrical Engineering and Computer Science, 2023. **7**(1): p. 70-73.
31. Crane, R.K., *Comparative evaluation of several rain attenuation prediction models.* Radio Science, 1985. **20**(4): p. 843-863.
32. Wang, L. and H. Li. *Comparative Analysis of Rain Attenuation Prediction Models for Terrestrial Links in Different Climates*. in *International Conference in Communications, Signal Processing, and Systems*. 2020. Springer.
33. Lehpamer, H., *Microwave transmission networks: planning, design, and deployment.* McGrawHill Education, 2010.
34. Joseph Ojo, E.O., Obiseye Obiyemi, et al., *Assessment of Total Attenuation and Adaptive Scheme for Quality of Service Enhancement in Tropical Weather for Satellite Networks and 5G Applications in Nigeria.* Journal of Microwaves, Optoelectronics and Electromagnetic Applications 20 2021: p. 228–24.
35. Semire, F.A., et al. *An Enhanced ITU-R 837-6 Rain Rate Prediction Model for Tropical Region*. in *The 8th International Conference on Robotic, Vision, Signal Processing & Power Applications*. 2014. Singapore: Springer Singapore.
36. Yussuff, A.I.O. and N.H.H. Khamis, *Modified ITU-R Rain Attenuation Prediction Model for a Tropical Station.* Journal of Industrial and Intelligent Information, 2013. **1**: p. 155-159.
37. Cicerone, G., et al., *Regional artificial intelligence and the geography of environmental technologies: does local AI knowledge help regional green-tech specialization?* Regional Studies, 2023. **57**(2): p. 330-343.
38. Osman, N.S. and W. Tahir. *Feature Extraction of Rain Cell Using Weather Radar Imagery in Tropical Regions*. in *2023 IEEE 13th Symposium on Computer Applications & Industrial Electronics (ISCAIE)*. 2023.
39. Singh, H., et al. *An Intelligent Model for prediction of Attenuation caused by Rain based on Machine Learning Techniques*. in *2020 International Conference on Contemporary Computing and Applications (IC3A)*. 2020.
40. Al-Saegh, A.M., et al., *AI-Based Investigation and Mitigation of Rain Effect on Channel Performance With Aid of a Novel 3D Slot Array Antenna Design for High Throughput Satellite System.* IEEE Access, 2024. **12**: p. 29926-29939.
41. Cornejo, A., et al., *Method of rain attenuation prediction based on long–short term memory network.* Neural Processing Letters, 2022. **54**(4): p. 2959-2995.
42. Diba, F.D., et al., *Wireless Telecommunication Links for Rainfall Monitoring: Deep Learning*

Approach and Experimental Results. IEEE Access, 2021. **9**: p. 66769-66780.
43. *The Earth's Atmosphere*, in *Radio Wave Propagation for Telecommunication Applications*, H. Sizun, Editor. 2005, Springer Berlin Heidelberg: Berlin, Heidelberg. p. 13-34.
44. Arto, L. and R. Antti, *Radio Engineering for Wireless Communication and Sensor Applications*. 2003: Artech. 1.
45. Barry, R.G. and R.J. Chorley, *Atmosphere, weather and climate*. 2009, Routledge London: London.
46. Nagaraj, P., *Impact of atmospheric impairments on mmWave based outdoor communication.* arXiv: Signal Processing, 2018.
47. Zahid, O., J. Huang, and S. Salous. *Long Term Rain Attenuation Measurements at Millimeter Wave Bands for Direct and Side Short-Range Fixed Links*. in *2020 XXXIIIrd General Assembly and Scientific Symposium of the International Union of Radio Science*. 2020.
48. Banday, Y., G. Mohammad Rather, and G.R. Begh, *Effect of atmospheric absorption on millimetre wave frequencies for 5G cellular networks.* IET Communications, 2019. **13**(3): p. 265-270.
49. Nyete, A.M. *Clear-air analytical and empirical K-Factor determination and characterization for terrestrial microwave LOS link applications*. 2014.
50. Freeman, R.L., *Radio System Design for Telecommunication*. 2007: Wiley.
51. *Electromagnetic Waves and Propagation Characteristics*, in *Radio Wave Propagation for Telecommunication Applications*, H. Sizun, Editor. 2005, Springer Berlin Heidelberg: Berlin, Heidelberg. p. 35-67.
52. P.527-5, I.-R. *Electrical characteristics of the surface of the Earth.* ITU-R P series 2019; Available from: https://www.itu.int/rec/R-REC-P.527/en.
53. Panter, P.F. *Communication systems design: line-of-sight and tropo-scatter systems*. 1972.
54. Shafi, M., et al., *Microwave vs. Millimeter-Wave Propagation Channels: Key Differences and Impact on 5G Cellular Systems.* IEEE Communications Magazine, 2018. **56**(12): p. 14-20.
55. Lim, N.C.Y., et al. *Review of Temperature and Humidity Impacts on RF Signals*. in *2020 13th International UNIMAS Engineering Conference (EnCon)*. 2020.
56. Houze, R., *Cloud Dynamics.* Academic, San Diego, California, 1993.
57. E.F. Nymphas, O.I., *Attenuation of millimetre wave radio signal at worst hour rainfall rate in a tropical region: A case study, Nigeria.* Scientific African, 2022.
58. Suleman K.O., B.I.T., Tijani L.O., Ogunbode A.O., Olayiwola W.A. *Effect of Temperature and Ground Water on VHF Radio Wave Propagation in Tropical Climate*. 2017. International Journal of Scientific & Engineering Research.
59. Fang, D.J.L., C. S., *Rain Effects on Radio Frequency Propagation*. 1986, MASSACHUSETTS TECHNOLOGICAL LAB BETHESDA MD WASHINGTON DIV.
60. P.341-7, R.I.-R., *The concept of transmission loss for radio links*, in *P Series Radiowave propagation*. 2019, ITU-R.
61. P.525-3, R.I.-R., *Calculation of free-space attenuation*, in *P Series*. 2016, ITU-R.
62. Mudelsee, M., *Trend analysis of climate time series: A review of methods.* Earth-Science Reviews, 2019. **190**: p. 310-322.
63. Kumar, S.A.P. and P.K. Bora. *Time series analysis and signal processing*. in *2012 2nd National Conference on Computational Intelligence and Signal Processing (CISP)*. 2012.
64. Topol, E.J., *High-performance medicine: the convergence of human and artificial intelligence.* Nature Medicine, 2019. **25**(1): p. 44-56.
65. Böse, J.-H., et al., *Probabilistic demand forecasting at scale.* Proceedings of the VLDB Endowment, 2017. **10**(12): p. 1694-1705.
66. Tong Y, L.J., Yu L, Zhang L, Sun L, Li W, Ning X, Xu J, Qin H, Cai Q., *Technology investigation on time series classification and prediction. 8:e982 https://doi.org/10.7717/peerj-cs.982.* PeerJ Computer Science, 2022.
67. Kadous MW, S.C., *Classification of multivariate time series and structured data using constructive induction.* . 2005.
68. Lopez BJ, S.C., Antonio G., *Interrupted time series regression for the evaluation of public health interventions: a tutorial. International Journal of Epidemiology* 2017.
69. Box, G.E., et al., *Time series analysis: forecasting and control*. 2015: John Wiley & Sons.
70. Gardner Jr, E.S., *Exponential smoothing: The state of the art—Part II.* International journal of forecasting, 2006. **22**(4): p. 637-666.

71. Harvey, A.C., *Forecasting, structural time series models and the Kalman filter.* 1990.
72. Casolaro, A., et al., *Deep Learning for Time Series Forecasting: Advances and Open Problems.* Information, 2023. **14**(11): p. 598.
73. Diba, F.D., *Radio wave propagation modeling under precipitation and clear-air at microwave and millimetric bands over wireless links in the horn of Africa.* 2017.
74. Project, T.N.O., *Map of Ethiopia*, M.o. Ethiopia, Editor. 2020.
75. S. Walkerand, Y.E., K. Tesfaye, E. Bekele, A. Yeshana, and G. Mamo. *THE USE OF AGROCLIMATIC ZONES AS A BASIS FOR TAILORED SEASONAL RAINFALL FORECASTS FOR THE CROPPING SYSTEMS IN THE CENTRAL RIFT VALLEY OF ETHIOPIA*. 2003.
76. Belda, M., et al., *Climate classification revisited: from Köppen to Trewartha.* Climate Research, 2014. **59**: p. 1-13.
77. Berhanu, B., A. Melesse, and Y. Seleshi, *GIS Based Hydrological Zones of Ethiopia*. 2012.
78. P.618-14, R.I.-R., *Propagation data and prediction methods required for the design of Earth-space telecommunication systems*, ITU-R, Editor. 2023, ITU.
79. P.837-7, R.I.-R., *Characteristics of precipitation for propagation modelling*, ITU-R, Editor. 2017.
80. P.311-16, R.I.-R., *Acquisition, presentation and analysis of data in studies of radiowave propagation*, in *Radiowave propagation*, ITU-R, Editor. 2016.
81. ITU-R, *ITU-R P.1510-1, Mean surface temperature*, in *P Series Radiowave propagation*, ITU-R, Editor. 2017.
82. ITU-R, *Guide to the application of the propagation methods of Radiocommunication Study Group 3*, in *Recommendation ITU-R P.1144-12*, P.S.R. propagation, Editor. 2023.
83. Emiliani, L.D., L. Luini, and C. Capsoni, *Analysis and Parameterization of Methodologies for the Conversion of Rain-Rate Cumulative Distributions from Various Integration Times to One Minute.* IEEE Antennas and Propagation Magazine, 2009. **51**(3): p. 70-84.
84. AlKhedhairi, K.I. and J. Din. *Conversion of 15-minutes to 1-minute rain attenuation derived from tropical rain attenuation measurement*. in *2011 IEEE International RF & Microwave Conference*. 2011.
85. Mandeep, J.S., et al., *The Study of Rain Specific Attenuation for the Prediction of Satellite Propagation in Malaysia.* Journal of Infrared, Millimeter, and Terahertz Waves, 2010. **31**(6): p. 681-689.
86. ITU-R, *ITU-R P.530-18:Propagation data and prediction methods required for the design of terrestrial line-of-sight systems*, in *Recommendation ITU-R P.530-18*, ITU-R, Editor. 2021, ITU.

独创性声明

本人声明所呈交的学位论文是本人在导师指导下进行的研究工作和取得的研究成果，除了文中特别加以标注和致谢之处外，论文中不包含其他人已经发表或撰写过的研究成果，也不包含为获得北京交通大学或其他教育机构的学位或证书而使用过的材料。与我一同工作的同志对本研究所做的任何贡献均已在论文中作了明确的说明并表示了谢意。

学位论文作者签名： 签字日期： 年 月 日